NTNU – Trondheim
Norwegian University of
Science and Technology

Index Tests and Their Applications

Determining Rock Strength and
Strength-anisotropy as a Function of
Inclination by use of Index Testing and
Mathematical Modelling

Tor Andre Rugland

Petroleum Geoscience and Engineering
Submission date: June 2015
Supervisor: Erling Fjær, IPT

Norwegian University of Science and Technology
Department of Petroleum Engineering and Applied Geophysics

Abstract

Drilling problems in shale continue to be an expensive problem in the petroleum industry due to lack of information concerning rock mechanical parameters. Conventional laboratory tests are expensive and time consuming, as shale is a difficult material to test. Index testing on shale material is an easy, in-expensive and effective alternative. Index testing has previously been performed in order to obtain this information, but the truth is that more testing have been needed in order to fully understand the value of these tests. This thesis has enhanced the knowledge and application area for some of the index tests. Four index tests, respectively CWT, Shale Puncher, Scratch Test and Brazilian Test, has been investigated and compared to both modeled data with the patchy weakness model and other published results. A wide collection of data has been used in order to enhance the understanding of these tests.

In general measured results correlate well with expected theoretical results. Also the UCS estimations from the index tests correlate with other UCS data. A large comparison of strength data shows that a solid estimation with respect to UCS may be determined by use of the index tests presented. By looking at maximum and minimum readings of presented results, and strength as a function of inclination, degree of strength anisotropy may be determined. Index testing has also proved to provide information concerning heterogeneity.

Index test results confirm previous published findings, but some deviations are seen for the interpretation of punch results due to geometrical difficulties. Also the area of application of the scratch test is investigated, and a unique finding is presented where strength anisotropy may be determined as a function of scratch direction.

Overall this thesis contributes with important discussion and results regarding shale mechanical parameters and strength anisotropy.

Sammendrag

Boreproblemer i skifer fortsetter å være et kostbart problem for petroleumsindustrien, grunnet mangel på informasjon om bergmekaniske parametere. Standard laboratorietester er kostbare og tidkrevende, da skifer er et vanskelig materiale å teste. Index testing har tidligere blitt utført for å få tak i denne informasjonen, men sannheten er at mer testing har vært nødvendig for å fullt ut forstå verdien av disse testene. Denne masteroppgaven har forbedret kunnskap og bruksområdet for noen av disse index testene. Fire tester, henholdsvis CWT, Shale Puncher, Scratch Test og Brazilian Test har blitt undersøkt og sammenlignet med både modellerte data med hjelp av patchy weakness modellen og andre publiserte resultater. Et bredt utvalg av data har blitt brukt for å øke forståelsen av disse testene.

Generelt korrelerer målte resultater godt med forventede teoretiske resultater. Også UCS beregninger fra index testene korrelerer med andre UCS data. En stor sammenligning av styrkedata viser at et solid estimat med hensyn til UCS kan bestemmes ved anvendelse av de presenterte index testene. Ved å se på maksimum og minimum malinger, og styrke som en funksjon av inklinasjon, av presenterte resultater, kan graden av styrke anisotropi bestemmes. Index testing har også vist seg å gi opplysninger om heterogenitet.

Resultater fra index testene bekrefter tidligere publiserte funn, med et avvik angående tolkning av Shale Puncher resultatene grunnet geometriske problemer. Anvendelses-området for Scratch Testen har blitt utvidet, og et unikt funn er presentert der styrke anisotropien kan enkelt bestemmes som en funksjon av test-retning.

Totalt sett bidrar denne masteroppgaven med viktig diskusjon og resultater vedrørende bergmekaniske parametere og styrke anisotropi i skifer.

Acknowledgements

I would like to extend my sincere thanks to several people at SINTEF Petroleum for support and assistance of this thesis. Foremost, I would like to thank Erling Fjær for supervising, guiding, discussion and always making time for a technical conversation.

In the laboratory I would like to express my gratitude to several key individuals for advising me with their technical abilities.

Eyvind Søstebø for critical discussion on index test results and general discussion on rock testing, and also instructions regarding the CWT analysis.

Lars Eirik Walle for Scratch Test apparatus guidance, and support if (when) a problem occurred with the setup.

Anna Stroisz for basic CWT training, sample preparation, Brazilian test introduction and discussion of results.

Idar Larsen for discussion on previous measured scratch results, and other UCS measurements.

Jørn Stenebråten for direction on interpretation of scratch results.

Hans Lund for core preparation and general support in the rock formation laboratory. Including his intelligent sense of humor.

Andreas Bauer and Alexandre Lavrov for discussing the opportunities with existing and new design of index tests.

Trondheim
June 2015
Tor Andre Rugland

Table of Contents

List of Tables

List of figures

Nomenclature

v_p	Phase velocity, P-wave velocity
α	Attenuation
f, f_n	Frequency, resonant frequency
n	Standing wave resonances, integer
Q	Quality factor
λ	Wave length
CWT	Continuous Wave Technique
D, d	Diameter
L	Sample length
C_0, S_0	Cohesion, Cohesion Point, Inherent Shear strength
E	Young's Modulus, Intrinsic Specific Energy
E_s	Specific Energy
G	Shear Modulus
r	Correlation coefficient, radius
S	Standard error of estimate
ϕ	Porosity
σ_{peak}	Measured peak force
τ	Shear Stress
μ	Coefficient of internal friction
F_{peak}	Measured peak force
A_s	Shear area
t	Thickness
φ	Friction angle
β	Failure angle
UCS	Unconfined/Uniaxial compressive strength
F_t	Horizontal force
F_n	Vertical Force
ζ	Ratio between the vertical and horizontal force action on the cutter
w	Width
A	Cross sectional area

σ_1	Maximum principal stress
σ_2	Intermediate principal stress
σ_3	Minimum principal stress
AE	Acoustic Emission
$\sigma_t = T_0$	Tensile strength
σ_v	Compressional stress
Specimen	Disk shapes small rock sample
Sample	Either core plug or disk shaped rock sample, dependent of the test.
θ	Inclination angle
η	Free Patchiness parameter
x	Total angle of failure in punch
ψ, psi	Punch fracture angle

1 Introduction

1.1 Project context

Over 75% of the drilled formations consist of shale, and shale instability makes up for about 70% of the borehole problems. Problems can mainly be divided into two sections: chemical and mechanical stability (Skalle 2014). Shale drilling problems continue to be a costly challenge for the oil and gas industry (Stenebråten, et al. 2008). In order to reduce the shale related problems, more knowledge of rock-mechanical properties are required. Both concerning optimization of drilling parameters and other applications including: hydraulic fracturing, sand production and reservoir compaction (Schei, et al. 2000). In many applications mechanical properties are required in the overburden formations of the reservoir. But core sampling and formation/reservoir tests are typically done along the reservoir or potential pay-zones. Access to research and data from the overlaying formations are consequently restricted. Additional problems emerge if a shale core-sample is drilled. Often the core is damaged in terms of fracturing, and further testing of the sample is impossible (or very limited). Regular measure shale-cores are therefore unusual. If such a core is retrieved without damage, testing is then extremely time-consuming since the low permeability of shales, and is not cost efficient. As indicated the reality is that very few (or none) of these tests exist (Stenebråten, et al. 2008). Core testing yields direct measurements concerning rock mechanical parameters. wireline logs (e.g. sonic, porosity, density etc.) is used to retrieve data, as these are continuous and standard procedure while drilling a well, but the disadvantage with this data is that the measurements are indirect, and parameters are calculated from correlations.

Increased knowledge and data of shale and shale mechanical properties are clearly needed. Drill cuttings and cavings serves as a possible source of this information. They can be collected directly from the shale-shaker, giving real-time data, and preserves the in-situ properties (to some extent) as they are covered with mud. As these rock parts are relatively small, standard testing cannot be performed. Index testing is an alternative to these, and many of the tests are relatively simple and require little rock material (Nes, et al. 1996).

Already mentioned shale makes up for the larger part of drilled formations. Therefore shale strength anisotropy is an important matter when drilling. In order to truly understand how this impact the strength and stability of the rock, experimental work has to be carried out. As conventional test are too expensive or time consuming another alternative is index testing. Index testing is defined as different types of easy accessible tests done cheap, fast, simple and requires a small amount of material (Stenebråten, et al. 2008). Several such tests already exist and will be investigated in this thesis. The truth is that some of these tests are relatively new, and thus they have already been studied, for some tests, confusion exists and uncertainties of measured parameters are the case.

1.2 Project outline

The scope of this thesis will in the first part examine four such tests. Trying to answer questions related to actual measured parameters and applications. This is done by both a study on published literature and experimental work. Some of the experimental work was done in relation to my previous project-assignment (Rugland 2014) completed at NTNU autumn 2014. These chapters also look into in what degree these test may indicate information about the strength anisotropy of shale, and a comparison study on this. In all four existing index tests are investigated, and one new test technique is introduced.

CWT (Continuous Wave Technique) is an ultrasonic measurement. Using acoustic transducers to measure acoustic phase velocities on rock samples. Test setup requires little rock material, hence cuttings are a good fit. The test is a non-damage test, and rock mechanical properties may be estimated by use of existing correlations (Nes, et al. 1996).

The Shale Puncher is a relatively new test, using the punch device and a loading frame to measure cohesion from small samples. Cuttings may also be used in this test (Stenebråten, et al. 2008). Measured data from the puncher may be used as input or in conjunction with other tests and mathematical modeling (Stenebråten, et al. 2008).

The Scratch Test cuts the surface of a core plug with a knife, monitoring forces in x and y direction to measure strength and elastic properties (Schei, et al. 2000). The test needs more rock material, and cores are necessary. This test gives a good understanding of the strength anisotropy, and serves as the main test on this matter.

The Brazilian Test is a metal frame using a loading frame to provoke tensile break in the presented sample. This is a common test, and a better alternative to the point load test. Tensile strength is easily calculated from the measured results, and results tend to be reproducible and consistent (Claesson and Bohloli 2002). The test will be investigated based on existing literature, as a lot of experimental work already exists.

With use of these four index tests, both existing experimental results and obtained results will be investigated. A comparison study between rock mechanical parameters will be presented. Mathematical modeling and correlations concerning these parameters are also integrated. Concerning strength anisotropy, a study of what information that can actually be obtained by the different tests is provided. Looking at if a test provides only information about maximum and minimum readings, at what inclination a minimum reading occurs or if the test can provide a complete description of strength as a function of inclination. These are topics this thesis will discuss and study.

2 Previous work

Autumn 2015 I wrote the project assignment: *Index Testing, A study of the effect of inclination in relation to bedding on rock mechanical parameters.* This was done in the supervision of Erling Fjær for NTNU at SINTEF Petroleum AS. This project assignment serves as an introduction for this master thesis. Some of the research and experimental work is used as the foundation, where further research and result interpretation is continued in this thesis. Therefore it is often referred to, although it has not been published outside NTNU.

Experimental work performed and investigated in this thesis has been examined in several papers, but new applications and use of equipment and results including comparison of results is unique (as I am aware of). A lot of sources has been needed in this thesis, but some papers serves of greater importance concerning the index tests and theoretical explanations, and are presented below.

Index Tests papers which constitute the theoretical base of my work, presented in the first part of the thesis:

- CWT (Nes, et al. 1996).
- Shale Puncher (Stenebråten, et al. 2008).
- Scratch Test (Schei, et al. 2000)
- Brazilian Test (Simpson, et al. 2014).

Other sources of great importance:
The book (Fjær, et al. 2008) has also served as a rock mechanical encyclopedia throughout the writing period, and has been to great support concerning the majority of themes and problems presented in this thesis.

The paper (Horsrud 2001) presents the correlation between acoustic phase velocity and rock mechanical properties.
Previous Shale Punching results from (Rademakers 2010).
Previous Vp vs. inclination results from (Torsæter, Nes and Rinna 2012).

3 Literature study

In this chapter theory behind shale are presented. This is to give a better understanding of how shale may impact measured data and create problems with the testing.

3.1 Introduction to Shales

As presented in the introduction, shale makes up for 75% of the drilled formations, and over 70% of borehole problems (Skalle 2014). Shale is not just a subject when drilling wells. Another aspect of shales is the shale gas and shale oil, which is highly on today's agenda. Therefore understanding and defining is of great importance. In the next sections and subchapters (3.1.1-3.2.3) general information concerning shales are given, as well as a more specific presentation concerning properties of the tested shales.

3.1.1 Shale mineralogy

Shale is a general term used for sedimentary rock containing a large percentage of clay. The definition varies with different publications. In (Fjær, et al. 2008) shale is defined as a rock where clay-minerals make up the load-bearing framework. Therefore the clay content has to be over ~40%. While in (The James Hutton Institute 2006) shales are defined containing 50-60% clay-minerals. Clearly there are detailed variations, but similarities are present. When it comes to specific mineral content of shales two "average" estimates from (The James Hutton Institute 2006) is presented below in Table 3-1. Content is determined by x-ray powder diffraction analysis.

	Shaw and Weaver (1965)	Hillier (2006)
	[%]	[%]
Quartz	30.8	23.9
Feldspar	4.5	3.7 (K-spar) 2.4 (Plag.)
Carbonate	3.6	7.5 (Calcite) 1.3 (Dolomite) 0.5 (Siderite
Fe-oxides	0.5	0.8
Clay minerals	60.9	47.7 (Di-clay) 7.5 (Tri-clay)
Other minerals	2	0.5 (Pyrite)
Organic matter	1	Not determined

Table 3-1 Average estimation of shale composition (The James Hutton Institute 2006)

As shale is a sedimentary rock it consists of several layers, this makes the rock highly anisotropic. This behavior is along the planes, where it is introduced a plane of weakness where the shale splits easily between to layers. All shales exhibit some degree of anisotropy. This fact is often neglected in rock mechanical analysis, and is partly a portion of the drilling problems encountered in the industry. As shale contains a lot of compact clay minerals, corresponding pore sizes is very small. Characteristically pore-size is in the range of 5 to 25 nm. From the natural behavior of clay it attracts water (ionic attraction) (Skalle 2014), and therefore shale holds a lot of bound water. Defining and measuring the elastic properties of the solid shale is therefore difficult (Fjær, et al. 2008).

The layered structure of shale is illustrated in Figure 3-1 and Figure 3-2. These pictures are taken with a technique called scanning electron microscopy, SEM. In Figure 3-1 a young shale is shown. Layering can easily be seen, and indicating the large anisotropy in shale. On the right in Figure 3-2 an older, more brittle shale is seen. Also here the layering is clear. Figure 3-3 shows an example of the complex structure in shale, which helps explains the strong anisotropy and heterogeneity.

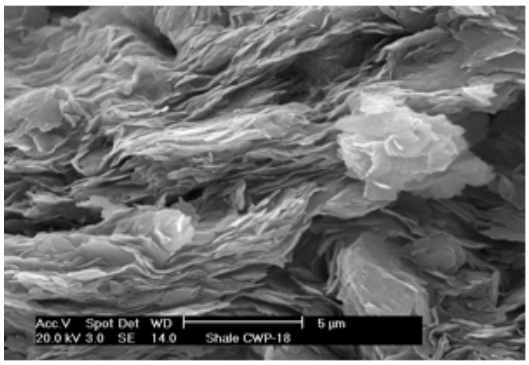

Figure 3-1 SEM Young shale (The James Hutton Institute 2006)

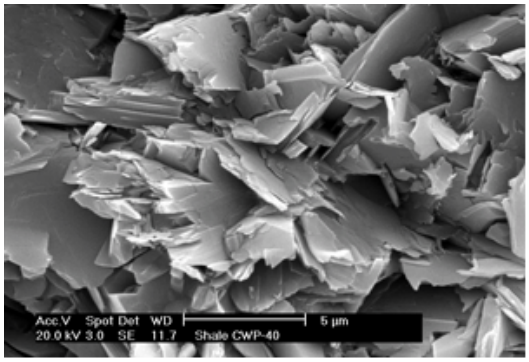

Figure 3-2 SEM Old shale (The James Hutton Institute 2006)

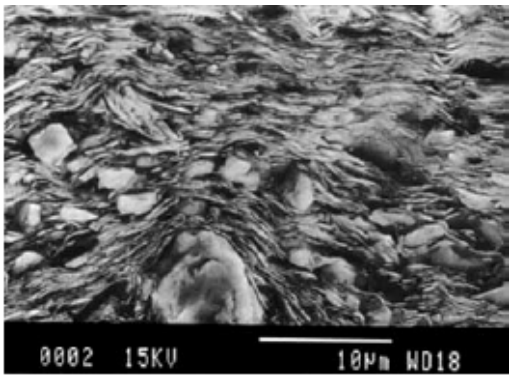

Figure 3-3 SEM Complex Shale (Fjær, et al. 2008)

3.1.2 Shale properties

3.1.2.1 Porosity and Permeability (Fjær, et al. 2008)

Shale porosity is highly variable and can be as small as a 1-5% up to high porosity shale in the 70% range. Despite the highest porosity ranges, shale permeability is always very low. As previously explained due to the nano-meter pore-size, permeabilities are in the range of nano-meters as well. This is measured by laboratory permeability test. When in-situ stresses are taken into account modelled in-situ permeability is expected to be even lower. Mentioned in the introduction is the fact that shale testing is time-consuming. The low permeabilities effect the time to establish pore pressure equilibrium and becomes a very expensive rock to test with concern to the standard rock mechanical tests. It was also mentioned in the introduction the difficulties of retrieving a rock core from the specific formation. Tensile failure during retrieval of the core is to be expected, as overpressure is established inside the core, because of the high sampling rate. Consequently the collected core sample is not fully saturated, and do not represent an in-situ situation when tested. Capillary forces would lead to more damage of the sample if attempting to resaturate the core sample. In-situ information is therefore extremely difficult to measure exact. Mathematical models and surface condition testing (simulated in-situ conditions as far as it is possible) is therefore the best alternative to try to make an understanding of shale.

3.1.2.2 Mechanical properties (Fjær, et al. 2008)

As shale varies in the extreme, mechanical properties also is dependent of rock type, composition and fluid content. Shale data has been collected, to make an estimate or "standard" measures for shale. Some typical numbers are presented bellow:

Bulk Modulus: 5-25 GPa

Shear Modulus: 4-10GPa

Friction Angle: 10°-20°

Clearly numbers are dependent of which type of clay mineral is (kaolinite, smectite, illite) dominant, and in particular on the adsorbed or bound water present within minerals and on mineral surfaces.

Lashkaripour and Dusseault 1993, presented in (Fjær, et al. 2008) describe a large set of shale data from published literature and in house studies, where majority of shale is less than 20% porosity. An important finding was that strength and stiffness is related to some extent. Two relations were presented: Ratio between young's modulus and unconfined strength $\frac{E}{C_0} \sim 200$. Compressive strength is typically 10-15 times higher than the tensile strength (C_0/T_0). (Horsrud 2001) confirmed the ratio with a North Sea shale study where the same ratio was estimated to be around 150.

3.1.3 Mancos and Pierre Shale

The Mancos Shale alternatively the Mancos group is a late Cretaceous formation, found throughout main parts of the western US. Deposited in Western Cretaceous Interior Seaway. Previously it has been seen as a source-rock of oil and gas, and as a sealrock for conventional reservoirs. Mostly containing accumulated mudrock with a very high content of quarts (Broadhead 2013). The tested shale is an outcrop from TerraTek Inc, Salt Lake City. A more specific rock content is presented in (Simpson, et al. 2014), the described rock is close to the tested rock in this thesis, when not taking into the account of local heterogeneity of Mancos. The composition of Mancos shale is presented in Table 3-2. Other parameters of importance are: porosity about 6-8%. Bulk density around 2.57 g/cm^3. In (Rugland 2014) wet density was measured to be 2.65g/cm^3.

As presented above in section 3.1.1, Mancos fails to classify as shale in geological context, because of its low clay content (less than 40%). Yet it is commonly used for testing, as it is seen as an equivalent to gas shale, and is easy accessible. Mancos shale exhibits many of the features observed in other shales (Simpson, et al. 2014).

Quartz	40-50%
Clay	20-25%
Carbonates	20%
Organic material	<1%

Table 3-2 Mancos Shale composition

The Pierre Shale is a late Cretaceous formation. It is mainly found in the Great Plains. The formation can be divided into two main parts, East Dakota where the formation consist of several hundred feet of offshore marine shale and minor marl. And in west Montana, which is seen as the sediment source, the shale is built of numerous thousand feet of volcanic rich and non-marine sediments (Schultz, et al. 1980). Samples used in the project originating from Wyoming. In (Bøe 2005) Pierre 1 (sample ID: ML 192-1) specific data is presented. The Pierre shale used in this thesis is similar to the one described in the report. This was also confirmed by conversation with Idar Larsen at SINTEF Petroleum. Pierre mineralogical composition was determined by interpretation of characteristic reflections on the x-ray diffractogram and is presented in Table 3-3. Porosity was determined by the buoyancy method, which is a simple method using displaced water and density of displaced water. Porosity is presented in table Table 3-4. The dry bulk density is also presented in Table 3-4. Also wet density was measured in (Rugland 2014) and water content is presented in the same table.

Test	ID	Qtz	K-fsp	Plag	Chl	Kaol	Mic/Ill	ML	Smect	Calc	Sid	Dol	Pyr
Bulk	ML 192-1	20.1	0.7	15.7	2.2	6.8	16.6	0.3	31.5	1.8	0.7	1.8	2.0
Fine fraction <4 µm	ML 192-1	7.4	0.3	1.8	7.9	8.7	15.2	0.0	57.8	0.2	0.1	0.1	0.5

Table 3-3 Pierre Shale 1 composition. Abbr: Qtz = Quartz, K-fsp = potassium feldspar, Plag = plagioclase feldspar, Chl = chlorite, Kaol = kaolinite, Mic/Ill = mica and illite, ML = mixed layer clay, Smect = smectite, Calc = calcite, Sid = siderite, Dol = dolomite/ankerite, Pyr = pyrite (Bøe 2005).

Bulk dry density	2.209 g/cm^3
Wet density	2.38 g/cm^3
Porosity	19.2%
Water content	8%

Table 3-4 Pierre Shale 1 measured parameters (Bøe 2005) and (Rugland 2014).

3.1.4 Heterogeneity

Rocks natural contain heterogeneity, distinctly nonuniform. Especially shale can contain a lot of heterogeneity and complex structure. Local heterogeneity is sometimes visible and can easily be observed. Heterogeneity on the microscopic level has to be studied in a microscope or by testing. The visible heterogeneity is showed throughout Figure 3-4 to Figure 3-9. The white colour in the rocks presented are quartz, and the black mainly clay. Quartz implies a greater strength compared to clay, and it is therefore expected for the samples containing a lot of quartz to yield a higher strength. The impact of heterogeneity in shale testing, calculations and modelling is often neglected. Shale is handled as an isotropic- and homogenous medium to simplify. Consequently understanding the effect of heterogeneity is neglected, and may be overseen. Heterogeneity is therefore of great importance. Even with relatively easy laboratory work, a need for understanding how the heterogeneity may affect the result is present. An example from (Fjær, et al. 2008) is given: As a normal uniaxial compressive strength test is carried out, it fails with the weakest plane or crack in the sample. Therefore UCS measurements are sensitive to the degree of heterogeneity of the rock sample. Weaker cracks or flaws in the sample yield a lower UCS measurement in the specific sample, compared to the formation. Particularly this effect is seen in weaker rocks. The local heterogeneity obscures the total results for the formation, as the sample represents a larger scale rock. Variation in UCS measurements may therefore be expected. To reduce the effect of heterogeneity of testing, introducing several methods for testing the same parameters will yield a greater reliability of the results. UCS is an important parameter in many applications, and is often relied on concerning large decisions during drilling. By collecting as

much data as possible from the material available or analogue material, safe and stable drilling, and reduction in borehole problems may be the case.

In micro scale heterogeneity may “disturb” or give inconsistent measurements from laboratory results. But in larger reservoir scale it can impact borehole stability. As a specific example: in (Khan, et al. 2012) it is presented that the heterogeneity was not accounted for and wrong mudweight where chosen. This decision lead to borehole collapse, as anisotropic horizontal stresses were not considered.

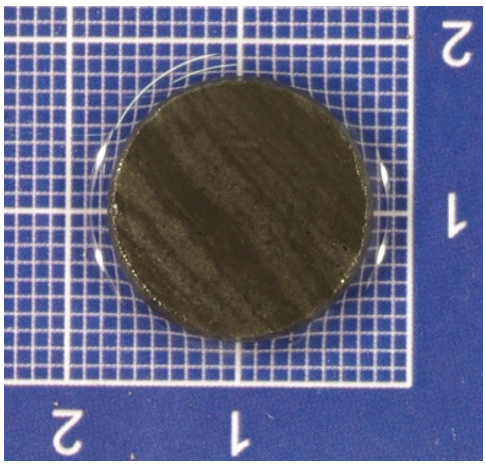

Figure 3-4 Heterogenity of Mancos Disk Shaped Sample, saturated with Marcol Oil (Rugland 2014)

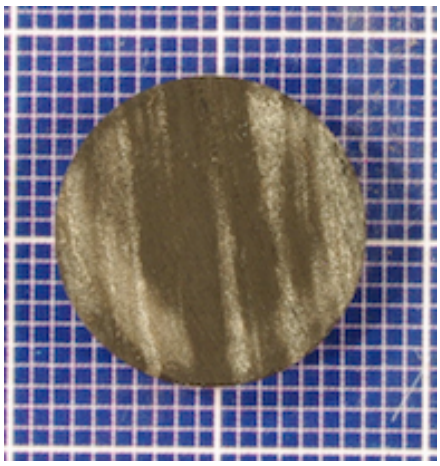

Figure 3-5 Heterogeniyu of Mancos Disk Shaped Sample, dried with alcohol (Rugland 2014)

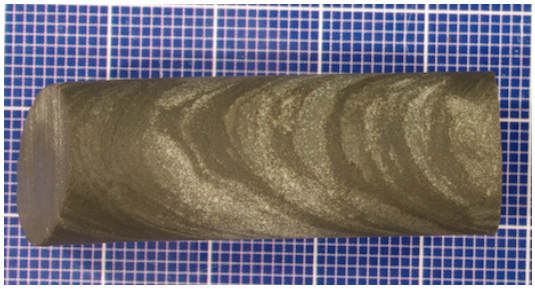

Figure 3-6 Heterogeniety of Mancos core plug ex. 1, dried with alcohol (Rugland 2014)

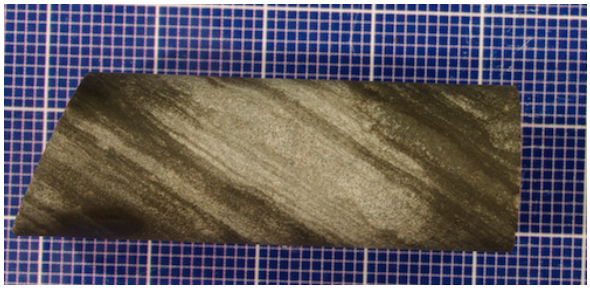

Figure 3-7 Heterogeniety of Mancos core plug ex. 2, dried with alcohol (Rugland 2014)

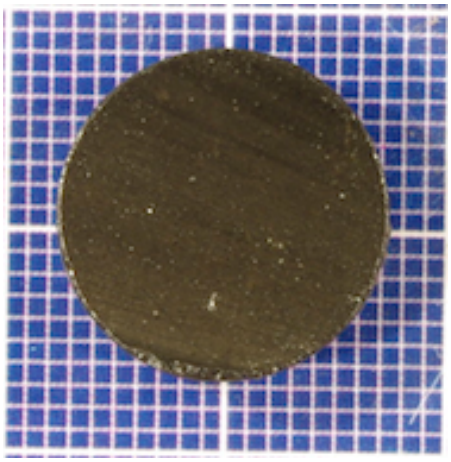

Figure 3-8 Layering of Pierre Disk Shaped Sample. Layering can be spotted, and also a small degree of heterogeneity (Rugland 2014).

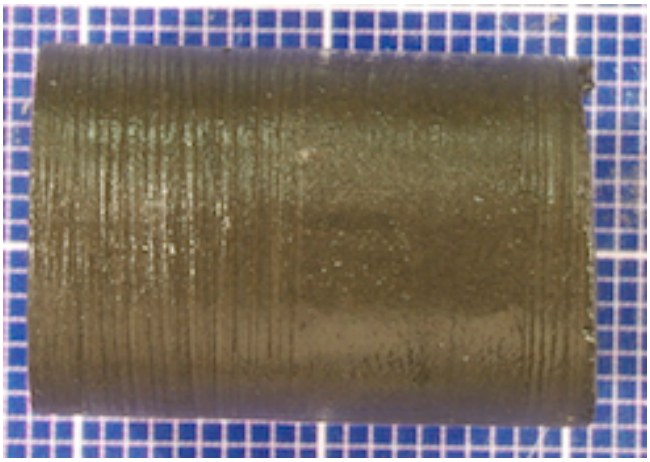

Figure 3-9 Pierre Core Plug Example. Layering is hard to spot, and heterogeneity is not visible. (Rugland 2014)

3.2 Strength Anisotropy

To shortly summarize the above: Shales are sedimentary rocks deposited mainly of compact flat clay particles. These particles are parallel to each other, and make up the layering in the rock, and leads to the high anisotropy in shales. Where some planes are weaker than others. To some degree the intrinsic anisotropy of the clay minerals make up for the anisotropy in the rock (elastic properties). The other part, which can be considered to be on the macroscopic scale where layering or existing oriented fractures in the rock implies anisotropy. Fractures along the weak planes, reduce the strength along that plane. (Fjær, et al. 2008).

Strength anisotropy indicates the rock strength to vary with the orientation of the bedding of the sample to the principal stresses. All rocks contain a degree of strength anisotropy as it is not an isotropic and homogenous material, but shale is in the larger range (Fjær and Nes, 2014).

3.2.1 Models

As strength anisotropy continue to be a problematic topic, several models to explain rock mechanical issues concerning strength anisotropy have been made. In this section a choice of common models are presented. An in-house study at SINTEF Petroleum comparing mainly Mancos shale (but also other shale types) with measured UCS from uniaxial and triaxial test, with modelled data is used. The models themselves, comparison and some results to show the strength anisotropy are presented bellow.

3.2.1.1 Griffith cracks (Fjær and Nes 2014)

The model assumes that the weak planes can be seen as a set of parallel elliptical cracks. When a crack is induced and starts growing failure occurs. This is basically the theory behind the failure criterion used (Griffith criterion):

$$\sigma_1' cos^2\theta + \sigma_3' sin^2\theta - \left[\sigma_1^{2'} cos^2\theta + \sigma_3^{2'} sin^2\theta\right]^{\frac{1}{2}} + 2T_0^* = 0 \qquad [1.]$$

The cracks are (as explained above in section 3.2) assumed to be oriented along the weak bedding planes, the inclination angle θ is defined as in Figure 3-10. T_0^* is the minimum tensile strength of the rock, which occurs for $\theta = 90°$, when the cracks are angled normal to the minimum principal stress. For uniaxial compressive stress ($\sigma_1' > 0;\ \sigma_2' = \sigma_3' = 0$), the criterion is reduced to:

$$\sigma_1' = \frac{2T_0^*}{cos\theta(1 - cos\theta)} \qquad [2.]$$

For uniaxial tensile stress ($\sigma_3' < 0;\ \sigma_1' = \sigma_2' = 0$), the criterion becomes

$$\sigma_3' = -\frac{2T_0^*}{sin\theta(1 + sin\theta)} \qquad [3.]$$

Figure 3-11 shows the Griffith Crack model applied to a set of measured data. This is plotted with the results from a standard uniaxial compressive strength test. As explained in 3.2.1 Mancos is the tested rock. Clearly there is a fit between the model and actual measurements. From 15° to about 60° the model is a bit off compared to the measured datapoints.

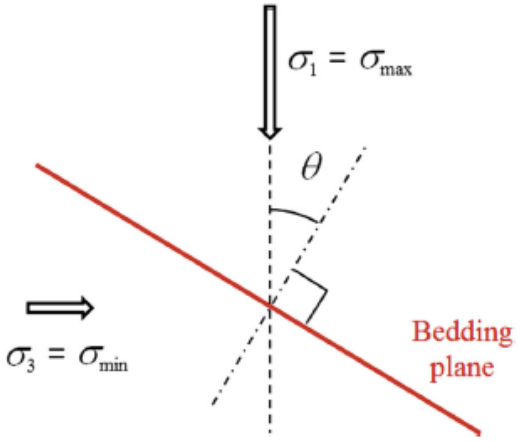

Figure 3-10 Definition of the inclination angle θ (Fjær and Nes, 2013)

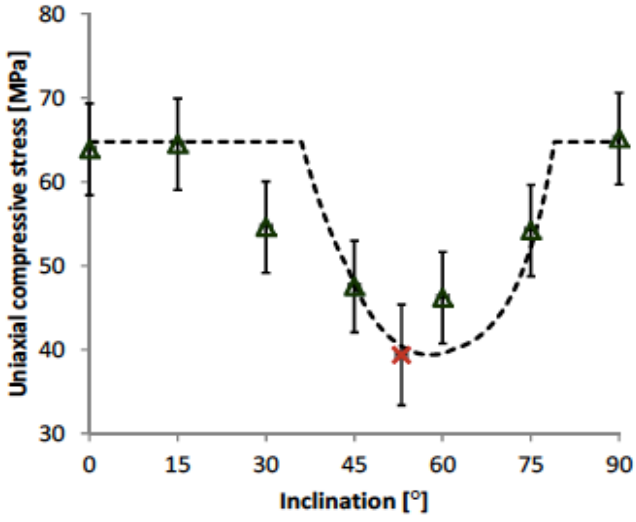

Figure 3-11 Mancos UCS results vs. inclination as calculated with the Griffith Crack model. Triangles are measured UCS datapoints. The red cross is extrapolated from CID tests. Dashed line is Griffith Cracks model calculations. (Fjær and Nes 2013).

3.2.1.2 Plane of weakness (Fjær, Stenebråten, et al. 2014)

This model is the most common and simplest when modelling anisotropic strength. The rock is seen as transversely isotropic, consisting of layers where the planes between the layers are parallel to each other with reduced strength. Failure is assumed along a random plane, outside the planes of weakness. This is determined by the Mohr-Coulomb criterion:

$$\sigma_1' - \sigma_3' = 2\frac{S_0 cos\varphi + \sigma_3' sin\varphi}{1 - sin\varphi} \quad [4.]$$

Where σ_1' and σ_3' are respectively the maximum and minimum effective principal stresses, φ is the inherent friction angle, and S_0 is the corresponding cohesion. The model is combined by failure along and outside the weak planes and the second part, which is failure along one of the weak planes, is given by the criterion:

$$\sigma_1' - \sigma_3' = 2\frac{S_{0w} cos\varphi_w + \sigma_3' sin\varphi_w}{sin2\theta cos\varphi_w - (cos2\theta + 1) sin\varphi_w)} \quad [5.]$$

S_{0w} and φ_w are respectively the cohesion and friction angle for the weak planes, while θ is the angle between the major principal stress and the normal to the weak planes as described in Figure 3-10.

As in Figure 3-11 the same measured data points where applied to the plane of weakness model showed bellow in Figure 3-12. Similarities can clearly be seen. Same problems occur between 15° and 50°. In Figure 3-12 and Figure 3-13 the plane of weakness model and the Griffith Cracks model are plotted with the UCS measured data. Results are clearly similar.

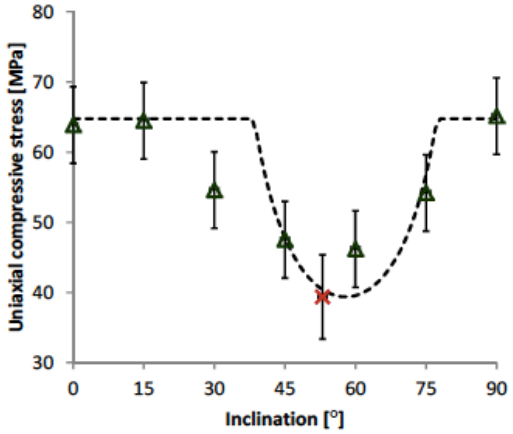

Figure 3-12 UCS vs. inclination, modelled by the plane of weakness model. Triangles are measured datapoints, the red cross is extrapolated from CID tests. Dashed line is the plane of weakness model (Fjær and Nes 2013).

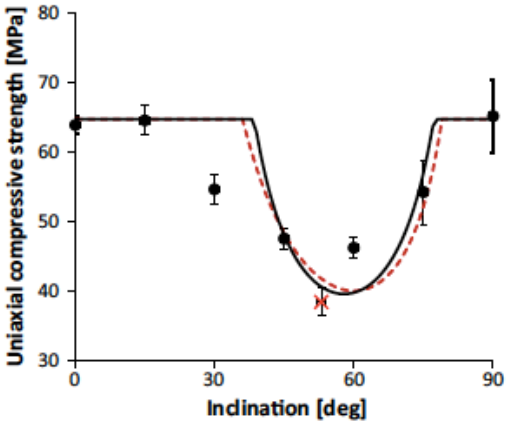

Figure 3-13 UCS vs. inclination as modelled by both the plane of weakness model (Black line) Griffith crack model (red dashed line). Filled circles are measured datapoints, the red cross is extrapolated from CID tests. (Fjær and Nes 2014)

3.2.1.3 Patchy weakness (Fjær, Stenebråten, et al. 2014)

This model is a development based on the weak plane model. The patchy weakness model assumes a set of weak planes, which are highly parallel to each other. Within these sets of weak planes, it is assumed that weaker spots is present and may induce failure more easily. As for the plane of weakness model, this model is built from two parts. Failure along, and outside the weak planes. This is described by two criterions. Assuming uniaxial conditions, and including the patchiness parameter the criterion outside the weak planes become:

$$\sigma_1' - \sigma_3' = 2(1 - \eta sin^2 2\theta)\frac{S_0 cos\varphi + \sigma_3' sin\varphi}{1 - sin\varphi} \qquad [6.]$$

The criterion along the weak planes including the patchiness parameter along the weak planes is described by:

$$\sigma_1' - \sigma_3' = 2\frac{(1 - \eta sin^2 2\theta)(S_{0w} cos\varphi_w + \sigma_3' sin\varphi_w)}{sin2\theta cos\varphi_w - (cos2\theta + 1)sin\varphi_w)} \qquad [7.]$$

The patchiness parameter η is assumed to be a measure of how many of these weak spots existing in the rock within a weak plane. An estimation of this parameter can be

found experimentally, and the parameter may be described as a free parameter. Clearly the criterion describing failure outside the weak planes are affected by the patchiness parameter. This can be explained as the stress is redistributed, where the stress is greater at some other point, affecting the failure outside the weak planes. The situation where $\eta = 0$, the patchy weakness model becomes the same as the plane of weakness model. This may be described as the limit for the patchy weakness model.

Figure 3-14 shows the measured UCS datapoints from the uniaxial tests on Mancos, plotted by use of the patchy weakness model. A really good fit of the model and actual measured data is the case. Mancos parameters are presented in Table 3-5. Compared to Figure 3-13 datapoints and modelling are much more corresponding. In the Mancos case it is clear that the Patchy weakness model best describes the real mechanical parameters in the rock.

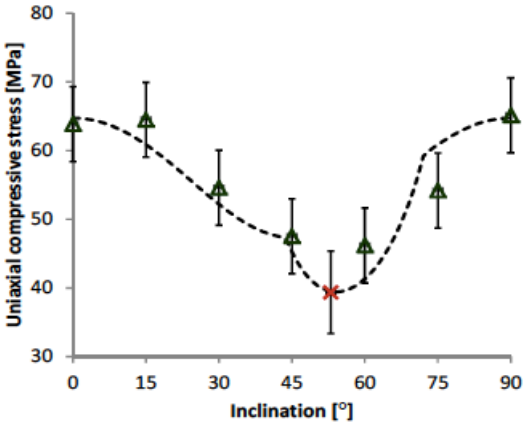

Figure 3-14 UCS vs. inclination for Mancos. The black dashed line is the patchy weakness model, where n=0.26. Filled triangles are measured UCS datapoints, and rex cross is extrapolated from CID test (Fjær and Nes 2013).

In Figure 3-15 and Figure 3-16 two North Sea shales are applied to the patchy weakness model for different confining stresses. This is to show the sensitivity of the model with respect to shale parameters (Table 3-5). The figures respectively presents shale S1 and shale S2. Note that in Figure 3-15 $\eta = 0$, therefore this is an equivalent to the weak plane model. For Figure 3-16 $\eta > 0$, and the characteristic double dip can be seen for the situation of 0 Mpa confining pressure.

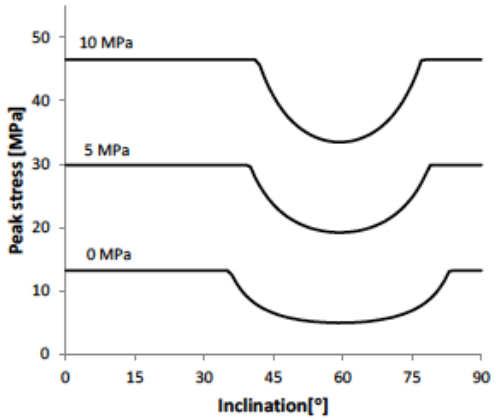

Figure 3-15 Peak effective stress vs. inclination at different confining pressures denoted in the plot. Parameters for shale S1 are showed in Table 3-5 (Fjær and Nes 2013).

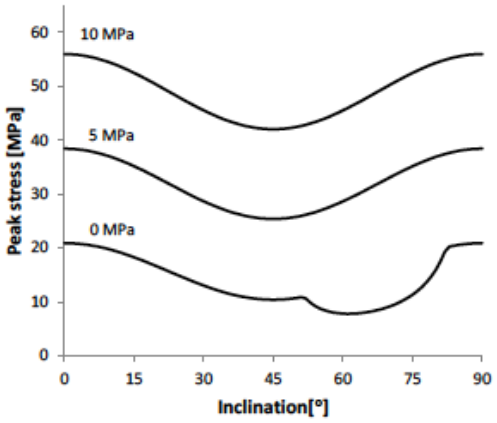

Figure 3-16 Peak effective stress vs. inclination at different confining pressures denoted in the plot. Parameters for shale S2 are showed in Table 3-5 (Fjær and Nes 2013).

Parameter	Mancos	S1	S2
$S_0[MPa]$	18.3	3.6	5.6
$\varphi[°]$	31.0	32.5	33.8
$S_{0w}[MPa]$	16.8	1.5	2.4
$\varphi_w[°]$	25.8	28.7	44.0
$\eta[-]$	0.26	0	0.5
$\sigma_c[MPa]$	>>12	-	20

Table 3-5 Best fit parameters for patchy weakness model used in Mancos, S1 and S2 calculations (Fjær and Nes 2013).

3.2.2 Experimental Strength Anisotropy

From the section above clearly the strength varies with inclination. With a minimum somewhere between 30° and 60° which is typical for anisotropic rocks (Fjær and Nes 2014).

In Figure 3-17 an example of two samples loaded to failure are given. When $\sigma_3 = 0$ (no confining pressure) this is a classic uniaxial test. The figure shows one sample with the largest principal stress direction normal to the bedding (Left) and one parallel to the bedding (Right). The black thick lines across indicate the failure cracks. The bedding planes represent the possible planes of weakness, and this determines failure of the sample. Therefore is it to expect that the sample with maximum load parallel to the bedding have a higher failure angle compared to the sample with maximum load normal to the bedding. A micro-crack is initiated at one of the weak planes, and grows rapidly until failure. Also the sample with maximum load normal to the bedding needs a higher load before failure. This is also explained by the bedding of the rock, which constitute possible planes of weakness. Layers are stronger in the case of normal to the load, compared to parallel. From this interpretation the effect of strength anisotropy is clear. This is a good example of how a deviated well may be impacted of the strength anisotropy.

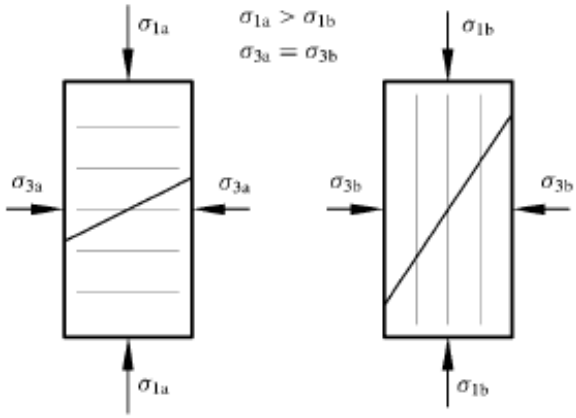

Figure 3-17 Samples load to failure: Left: Maximum load normal to bedding; Right: Maximum load parallel with bedding (Fjær, et al. 2008)

Applying the theory explained above, calculations for a specific drilling case can be made. A general example of such calculation is shown in Figure 3-18. The parameters

used in this calculation is not of importance, but the main point with this figure is to show the effect of weak planes present in the formation (as such a model will change depending on the case). From Figure 3-18 calculation with regards only to the isotropic model, stable drilling may take place. Comparing the formation with weak planes included in the model, in this specific example an increase of mud density of about from 1.65g/cm^3 to 1.8 g/cm^3 is the case. In a stability matter the mud density corresponding, would for inclinations >30° exceed the fracture gradient, and yield that stable drilling is impossible. For other cases this may be the case and could lead to unstable drilling and possible damage or kill the well, as seen in this example.

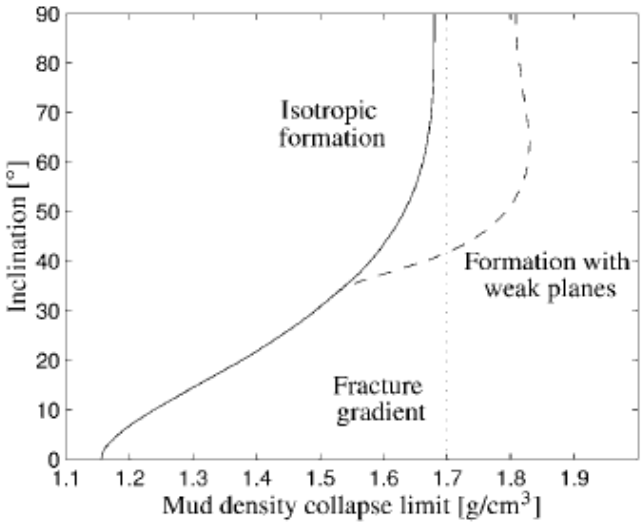

Figure 3-18 Stability Analysis for deviated well (Fjær, et al. 2008)

3.2.3 Real life example of strength anisotropy (Khan, et al. 2012)

From section 3.2.2 it is likely to expect an effect of the strength anisotropy when drilling wells, or operating in wells. Especially deviated wells, where the force distribution is changed both by the natural inclination of the well and drilling of the hole (disturbance of force balance as formations are drilled).

(Khan, et al. 2012) presents a real case where 15 wells are investigated. The well data are collected from the Horn River Basin, which is the largest shale gas field in Canada. Within these 15 wells, a lot of problems were the case, ranging from mud loss or lost circulation to tight hole/stuck pipe and several lost BHA. The conclusion of the investigation was that the problems were an effect of heterogeneity and strength

anisotropy, which were not accounted for in modelling before drilling. In retrospect calculated data were compared to new modelling including these factors. Bellow one example of such calculations is presented. In Figure 3-19 the original mud window calculations are shown. These calculations were used for choice of mud weight during drilling of the specific well. A quite wide mud window was the case, and stable drilling was assumed. Figure 3-20 shows the new, updated calculations were the anisotropy affects the stresses and narrows the mud window. As the original mudweight calculations were used, clearly the wrong mudweight was chosen, and lead to stability problems. These results showed to be consistent and correlated with breakout and induce fractures seen from the image- and caliper logs. This study also gave information about the extent of the heterogeneity of the Horn River Basin, as the wells were located a long distance from each other.

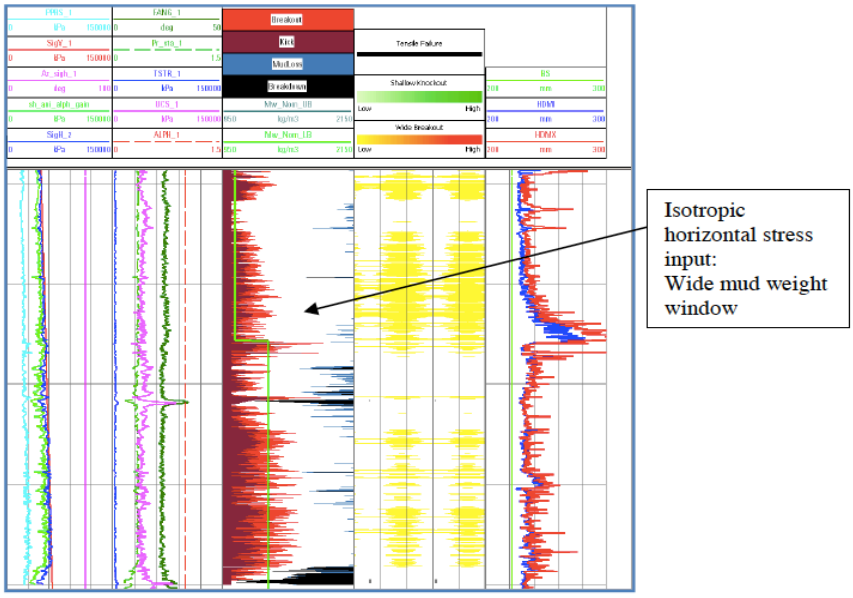

Figure 3-19 Original mud window calculations without heterogeneity and strength anisotropy. Wide mud-weight window.

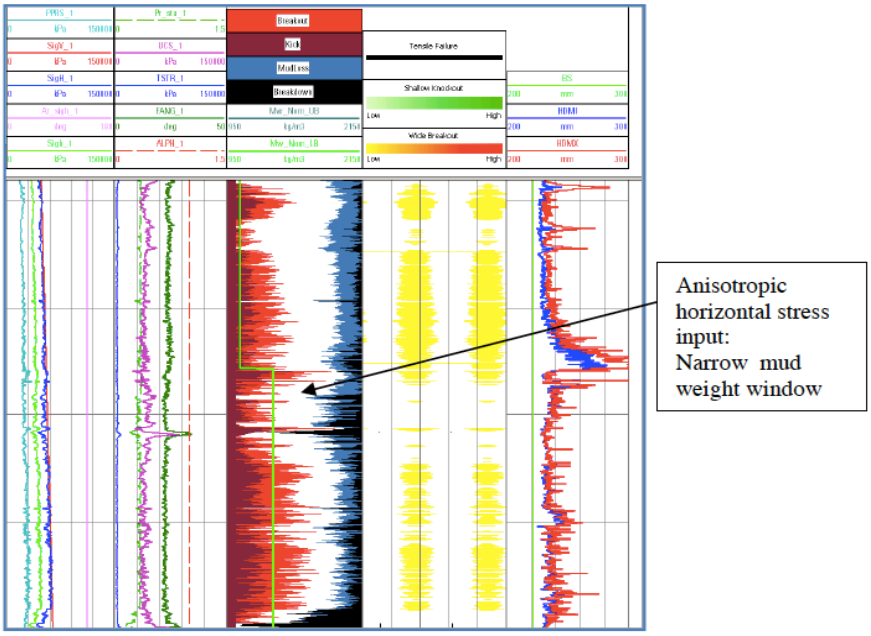

Figure 3-20 New mud window calculations including heterogeneity and strength anisotropy. Narrow mud-weight window.

4 Test descriptions

In this section a detailed presentation concerning the theoretical aspect of the investigated Index Tests will be presented. Also tests setup and applications.

4.1 Continuous Wave Technique (Nes, et al. 1996)

4.1.1 Introduction

The Continuous Wave Technique (CWT) is a test to measure acoustic phase velocities on rock samples. Since the equipment used is relatively small it is exceptionally suitable for measuring on small fine-grained samples (e.g. cuttings and cavings). Also sub-mm cuttings can be tested. The test setup is inexpensive (approx. 20.000$). Equipment is movable, small and simple in use. This introduces the opportunity to measure quasi real-time data at wanted location (e.g. rig-site, lab). Since the test-setup needs only small rock specimen the reaction time is low within the sample. Data measured is applicable in several areas including estimation of mechanical properties (mechanical parameters-correlations exist), consequence on fluid effects in the sample, estimation of data in non-logged formations and pore pressure results.

4.1.2 Theoretical background

The essential measures gathered from the continuous wave technique are the phase velocity, denoted v. With the right sample handling and sample quality (grinding process, equipment calibration etc.), correct equipment and spectrometer analysis, variations as small as $\Delta v/v \sim 10^{-7}$ and $\Delta\alpha/\alpha \sim 10^{-5}$ may be measured. Where v is the velocity and α the attenuation. Described in next section the main equipment consists of two acoustic transducers oppositely parallel mounted, making up a resonator. The CWT measures by use of ultrasonic standing waves resonances, and sweeps over a given frequency range f. Where f consist of numerous standing wave resonances. Measured resonances are contained within the amplitude-modulated signal received by the opposite transducer. Every standing wave resonance, n, will be described by a resonant frequency f_n and a quality factor $Q \equiv f_n/\Delta f_n$, where Δf_n is the linewidth at

the half-power points. Commonly, Q^{-1} represented the internal friction, for the situation of plane waves, Q^{-1} is related to the acoustic attenuation α as $Q^{-1} = v \cdot \alpha/(\pi \cdot f_n)$. For the measurement, plane waves are assumed, giving that λ/D is adequately small, where λ is the acoustic wavelength and D equals the diameter. Principally, resonances will result each time $\lambda = v/f$ fulfills $L = n \cdot \lambda/2$, where L, is the sample thickness and n, an integer. The acoustic phase velocity for P-waves or S-waves, can therefore be described as:

$$v = 2 \cdot L \cdot \Delta f \qquad [8.]$$

Where $\Delta f \equiv f_{n+1} - f_n$ = the difference in frequency between two continuously resonances. A characteristic example is shown in Figure 4-1, where Plexiglas is used, as it forms a more or less perfect spectrometer. To compare a shale with $v_p = 2000 m/s$ and $L = 1.5\ mm$ would display $\Delta f = 0.67\ MHz$ and the useable frequency would range from $1\ to\ 10\ MHz$.

4.1.3 Test setup and procedure

Figure 4-3 and Figure 4-2 indicate the actual test setup, which is explained in this part. The setup is made up of a sample holder consisting of two transducers parallel to each other. The specimen is fastened between these with the application of a micrometer. A direct measure of the sample thickness may be noted from the micrometer when the sample is fastened in place, reducing the uncertainty of sample thickness when applied in the same way to all the tested specimens. The top transducer is attached to a signal generator, which applies the computed frequency sweeps. The bottom transducer is attached to a detector (see Figure 4-3) and identifies and amplifies the received signal. To synchronize, a cable between the generator and the detector is required. The full setup is connected to a computer to gain easy access to measurements and analysis.

Procedure for performing a CWT measurement can be described in these steps:

1. Place the sample between the opposite located transducers, and fasten specimen until clicking sound is heard (meaning the specimen is in correct place). Using the fine calibration screw for smaller tightening steps. Sample

thickness is noted from the micrometer. Performing this step several time enhances the thickness certainty, as the sample may exhibit local thickness variations.

2. Enter the required input on the computer. Frequency range, f, is decided by a trial run, where the spectrometer easily indicates the useable range for the specific sample. As an example Pierre shale exhibit a frequency range from 1 MHz to 7 MHz. Excitation voltage used was 10V and amplification 50dB. Sample length about 2.80mm (dependent of sample).
3. Test is run and corresponding resonance spectrum is showed on the computer screen. Note if useable frequency is not sufficient, a new test is run immediately with new values for the frequency range.
4. Remove background noise from the raw-results by choosing bottom peaks with use of the computer program.
5. Top peaks are chosen in the same way in the computer program.
6. For each Δf, corresponding velocities are calculated by the program. Mean velocity for the sample is also calculated. The program calculates the velocities for each Δf together with the mean velocities. Results are saved to the computer and noted for further interpretation.

Approximately 15-20 minutes is used for each sample measurement, including sample preparation.

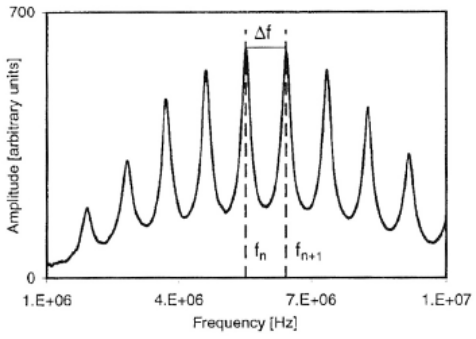

Figure 4-1 CWT resonance spectrum in a 1.5mm plexigalss sample, P-wave. (P-wave). Two resonances are marked to describe Δf. The measured P-wave phase velocity is ($2725 \mp 6\ m/s$) (Nes, et al. 1996).

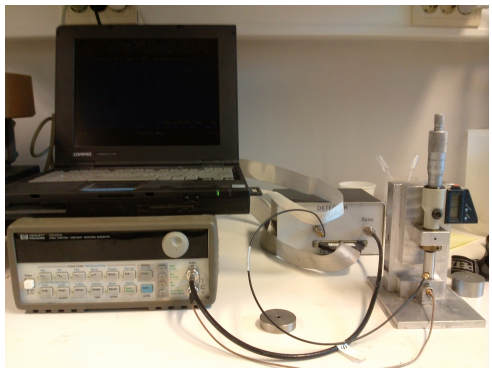

Figure 4-2 Actual setup used in project assignment (Rugland 2014).

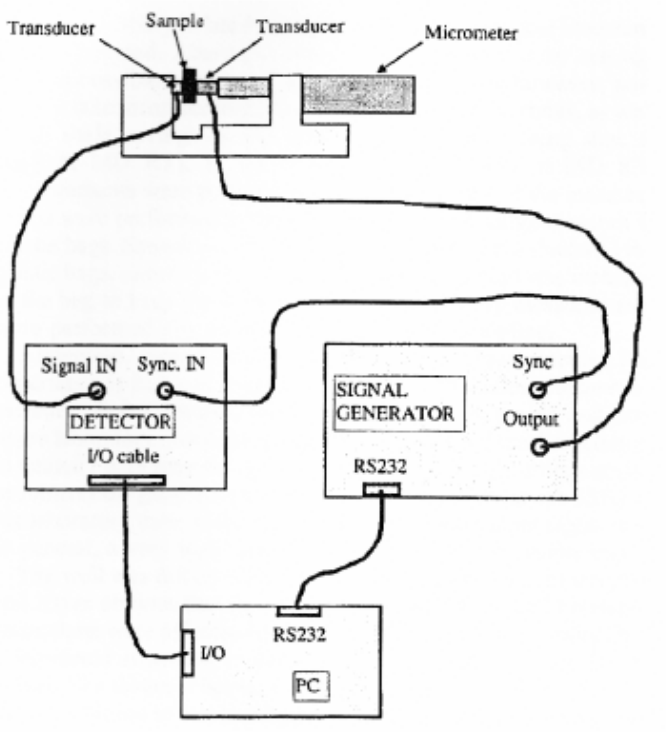

Figure 4-3 CWT Test setup sketch (Nes, et al. 1996).

4.1.4 Applications

Explained in section 4.1.1 CWT is a cheap, quick and simple way to determine rock mechanical data. The movability of the equipment also represents a positive point. Since the method is non-destructive more testing on the samples may take place, which means that a lot of information can be extracted from one single small sample. A study on use of the measured velocities has been carried out and is presented in (Horsrud 2001). Results show that several of the key parameters concerning rock mechanics can be calculated based on correlations between velocity measurements and the corresponding parameter. The most significant findings is given in Table 4-1:

Correlation	r^2	S
$C_0 = 0.77 v_p^{2.93}$	0.99	3.4MPa
$C_0 = 243.6 \varphi^{-0.96}$	0.98	3.7MPa
$E = 0.076 v_p^{3.23}$	0.99	0.4GPa
$G = 0.03 v_p^{3.30}$	0.99	0.2GPa

Table 4-1 Correlations for predicting static mechanical properties of shales. (Horsrud 2001)

Where C_0 is the uniaxial compressive strength, E is the Young's modulus, G the Shear Modulus and v_p the measured velocity. r is the correlation coefficient and S the standard error of estimate. Also a porosity correlations was presented in (Horsrud 2001) giving a good and easy estimation of the porosity based on acoustic velocity measurements:

$$\varphi = 227.8 v_p^{-2.37} \quad [9.]$$

Here φ is given as percent-porosity and v_p is the acoustic velocity given in km/s.

The correlations in Table 4-1 are studied in the discussion of results part. Looking at how these correlations correspond with calculations and measurements from the other index tests.

4.1.5 CWT Sample preparation and inclination definition

Samples tested in the CWT apparatus are first drilled out as cores from a block of the specific rock type. Cores are drilled for every 15°, from 0° to 90°. The rock cores respectively measures diameter about 15mm and length 5-10cm. A typical core can be seen in Figure 4-4.

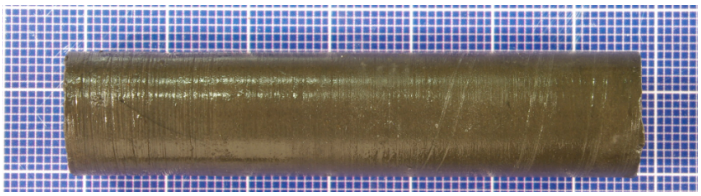

Figure 4-4 Typical drilled core, Pierre (Rugland 2014)

After the core has been drilled, specimens are cut along the core by hand, with use of a handsaw. Cut specimens measure a bit over 3mm in thickness. The cutting process is quite time-consuming for harder rock types. The two tested rock types are as explained Mancos and Pierre. The Pierre is cut relatively easily, while Mancos requires more work, and wears down the saw blade, and often a new blade is required for each cut of Mancos, compared to Pierre where 4-7 samples may be cut with one blade. This is illustrated in Figure 4-5. When specimens are cut with a thickness of 3mm, a manual grinding process takes place to ensure parallel surfaces of the sample. This is done by hand in a customized metal mold. The mold is placed on a metal plate, which is levelled to ensure parallel surfaces. Fine abrasive paper is used to grind the specimen. The mold consists of several steps, where each step gradually makes the specimen thinner, before reaching target thickness of 2.80mm. The target thickness where chosen to get several specimens from one core. In the discussion part, a study of the thickness effect is presented. Each step is approximately 0.03mm less than the previous. With these small steps the specimen is not as easily damaged, and equality between all the tested samples are the case. This gives uniformity in the tested samples, to easy compare measured data. Figure 4-6 shows the grinding system, which consists of the metal mold and the abrasive paper-montage. It is important to grind slowly to ensure as little damage to the sample as possible. Turning and rotating the sample within each step to get the perpendicular surfaces needed to

get reliable measurements. Figure 4-7 shows a finished disk sample after the grinding process, ready for testing.

Figure 4-5 Sawblade after (top) and before (bottom) cutting of Mancos sample (Rugland 2014).

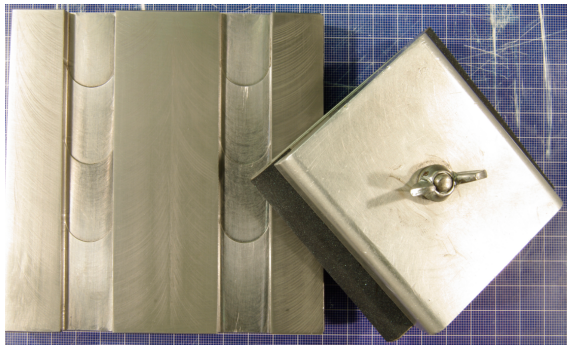

Figure 4-6 Grinding system (Rugland 2014).

When cores are drilled they are stored in marked containers, containing Marcol Oil to keep the samples wet. During sawing and grinding, a pipette is used to apply Marcol Oil, to ensure some degree of wettability of the samples during work. After grinding process is completed, samples are put back into smaller containers with Marcol Oil. As the process takes place a sample should be exposed as little as possible in air. Shale dries out quickly, and may impact the test results as properties may change or samples induce micro fractures (Rademakers 2010).

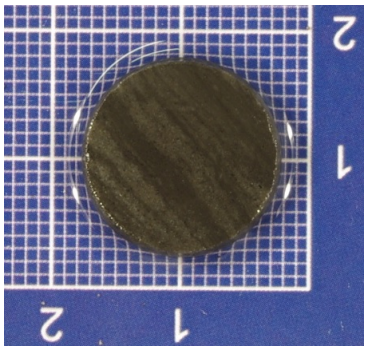

Figure 4-7 Typical disk sample ready to be tested (Rugland 2014).

Definition of the inclination is presented in Figure 4-8. The cores where drilled as explained every 15°. Where 0° represents the bedding normal to the acoustic transducers, and 90° bedding parallel to the acoustic transducers.

Figure 4-8 Orientation of drilled samples. Angle measured between the sample axis and the bedding plane normal. 0° is situated normal to bedding plane, and 90° is situated parallel to bedding plane (SINTEFPetroleum 2014).

4.2 The shale puncher (Stenebråten, et al. 2008)

4.2.1 Introduction

The shale puncher is a compact mechanical device to measure cohesion from small rock samples. The puncher requires the same type of samples as the CWT, and is normally used in conjunction with the CWT apparatus. The device is easy to use, and measurements are consistent. Cohesion serves as an important parameter when describing other mechanical parameters (e.g. rock strength, patchy weakness model). The puncher is a shear test, where strength is easily calculated. Shear strength is in practice useful when optimizing drilling parameters. With the puncher device strength is calculated from small samples compared to normal testing where large core plugs are required. This makes this technique very attractive.

4.2.2 Theoretical background

The Puncher device monitors the force used to punch a hole through a small disk-shaped sample with a moving piston set. This is done efficiently by use of the compact device and a loading frame with pre-set test settings. The shear strength is easily calculated as the applied force divided by the area of the tested sample (constant with respect to pistons). The puncher is defined as a shear test, which means that volume change is very small. As explained in the CWT section, small samples require low reaction time, and involved pore pressure gradients are small. Therefore such a test is relatively quick to run.

The specific sample is installed into the device. When working with small shale samples, it is important to keep the samples wet to ensure as little damage of the sample as possible. The device can therefore be filled with a test fluid to ensure wet conditions of the sample when testing. The tested samples used in this thesis are kept wet by applying Marcol oil to the installed sample by use of a pipette. The device is fixed together and the axial force is applied. The pre-set settings where set to a displacement-rate of 0.15mm/min. Two typical test plots of axial force versus axial displacement from the test are showed in Figure 4-9.

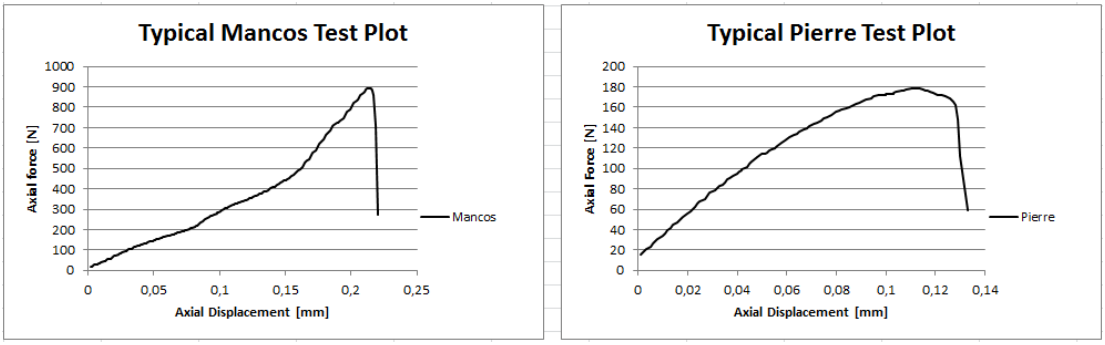

Figure 4-9 Typical punch test plots for Mancos and Pierre (Rugland 2014).

Further in this theoretical background some explanation about shear strength is required to fully understand the puncher as a shear test, and the shear condition.

4.2.2.1 The Mohr coulomb failure criterion (Fjær, et al. 2008)

Shear failure in a sample is expected along a plane when the shear failure is sufficiently high. Along the failure plane, a fault zone will be the case, where the to sides opposite situated of the fault zone will move in opposite direction described by a frictional process. This process is depending of the force, which is pressing the two sides of the fault-zone together. Critical shear stress can therefore be described as dependent of the normal stress, σ' (e.g. a function of the normal stress). This assumption is called the Mohr's hypothesis. This is shown in Figure 4-10.

$$|\tau_{max}| = f(\sigma') \qquad [10.]$$

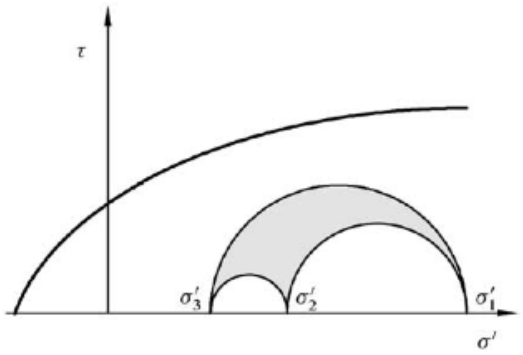

Figure 4-10 Failure line by use of Mohr's hypothesis. After (Fjær, et al. 2008)

Clearly from Figure 4-10, the explained assumption above is simply affected by change in both minimum and maximum principal stresses, and the intermediate stress my be neglected. The Mohr-coulomb failure criterion can be written more applicable where normal stress, $f(\sigma')$, is a linear function of σ':

$$|\tau| = S_0 + \mu\sigma' \qquad [11.]$$

Where $|\tau|$ is the absolute value of the shear stress, S_0 is the cohesion and μ is the coefficient of internal friction. Figure 4-11 is a case of the Mohr-Coulomb criterion where the Mohr circle is touching the failure line. The failure line intersects the shear axis, with the friction angle φ. For the case described in the shale puncher the Mohr-circle is shifted to the left, with symmetrical to the shear axis (y-axis). Assuming only pure shear stress condition.

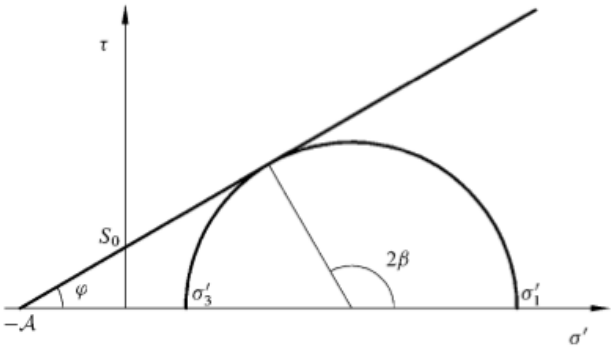

Figure 4-11 Mohr-Coulomb failure criterion with Mohr circle. After (Fjær, et al. 2008)

The monitored maximum force (given by Figure 4-9) is used to estimate the shear strength of the sample. By introducing the Mohr-coulomb failure criterion the cohesion point S_0 can be calculated from the resulting equation:

$$S_0 = \frac{\sigma_{peak}}{cos(\varphi)} \qquad [12.]$$

Where σ_{peak} is the measured peak stress from the test plot, and φ is the angle of internal friction (Fjær, et al. 2008). σ_{peak} is calculated by dividing measured peak (maximum) force by the area of the shear surface. Shear surface is purely a function of the constant piston diameter and the thickness for the specific sample. Figure 4-12 indicates the measured peak stress from the punch test. Note the minimum and

maximum stress are equal but oppositely directed. This is the condition of pure stress. S_0 is the cohesion point where the Mohr-Coulomb failure criterion intersects with the shear strength axis. The friction angle makes up the last section from σ_{peak} to the cohesion point.

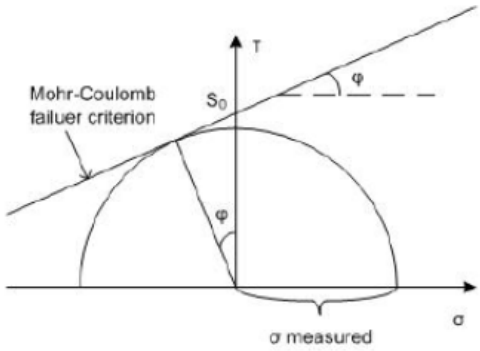

Figure 4-12 Minimum and maximum principal stress equal and opposite. Pure shear. After (Stenebråten, et al. 2008).

The stress condition presented above is assumed when testing. The previous few paragraphs have been used to evaluate this assumption. Probably the presented shear state in a sample is questionable homogenous. Heterogeneity exists to some degree in a rock sample, and heterogenic applied force is to be expected. Yet the possibility of pure stress at some region in the sample cannot be excluded. At some specific region in a certain direction, pure shear stress conditions exist, described as zero normal stress along the shear axis in the Mohr-Coulomb diagram. The thesis (Rademakers 2010) investigated this on a large scale, with the same conclusion.

Given that pure shear state is assumed in this thesis and applied to the measured data from (Rugland 2014), $\sigma_{measured}$ is therefore calculated as explained above, by dividing the measured peak stress by the shear surface. Previous work (Stenebråten, et al. 2008) evaluated the assumed condition by simulations in Abaqus, and pure shear stress condition has been assumed for the results presented in the same paper. As this assumption may not correlate fully with the real situation, it may in fact be close or at least a reasonable estimation. By applying the assumption to the results in this thesis the described shear surface becomes a function of the piston diameter and thickness of the presented sample. The fracture surface is assumed to be a perfect cone with maximum length at top piston and narrower part at the bottom piston. Typical fracture

surfaces are presented in Figure 4-13, where the structure to the left represents the perfect cone (assumed). The middle and the right structure is often the realistic case. Figure 4-14 shows to the left a mounted sample before testing, and to the right where break is detected and how the cone structure propagates.

Figure 4-13 Typical fracture surfaces after punch test. (Rademakers 2010).

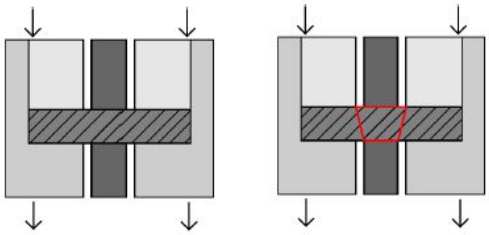

Figure 4-14 Typical break inside shale puncher. (Rademakers 2010).

σ_{peak} can be written as:

$$\sigma_{measured} = \sigma_{peak} = \frac{F_{peak}}{A_s} \quad [13.]$$

And the shear surface is estimated by use of the equations:

$$A_s = \pi(r_1 + r_2)s \quad [14.]$$

$$s = \sqrt{t^2 + (r_2 - r_1)^2} \quad [15.]$$

Where r_1 and r_2 is respectively top and bottom punching piston diameter (illustrated by Figure 4-18) and t the thickness of the specific sample.

4.2.2.2 Failure and friction angles

By use of the definition from (Fjær, et al. 2008), the internal friction angle may be calculated from the failure angle β, by the equation:

$$\varphi = 2\beta - \frac{\pi}{2} \quad [16.]$$

As mentioned several times, data from the CWT is of great interest in the punch test. The failure angle cannot be measured directly in the test, but by use of the acoustic wave velocity measurements (P-wave) of the same sample, correlations exist and friction angle may be estimated. UCS may also be calculated from an existing correlation. Following correlations are used for interpretation of data:

$$UCS = 0.77 \cdot V_p^{2.93} \quad [17.]$$

$$\beta = 49.8° + 0.3 \cdot UCS \quad [18.]$$

$$\beta = 39.9° + 5.5 \cdot V_p \quad [19.]$$

Where V_p is computed in km/s, UCS in MPa and angle in degrees. Using these equations, following relation for cohesion can be written:

$$S_0 = \frac{UCS}{2 \cdot tan(\beta)} \quad [20.]$$

4.2.2.3 Punch results in the patchy weakness model

Measurements from the shale puncher may be used to estimate the cohesion for use in the patchy weakness model, for strong and weak layers. Cohesion from the punch results is to assume a maximum measurement at 0° inclination and a minimum at 90° inclination. Where inclination definition is the same as explained for the CWT in section 4.1.5, further explained in section 4.2.4. This assumption is expected based on section 3.2.2. Where the sample requires a higher applied axial force when bedding is situated normal to the axial force compared to bedding parallel to the axial force. In

the puncher all the layers has to be broken in order to get failure. Therefore the cohesion for the strong layers and cohesion for the weaker layer may be calculated, where σ_0 is the intrinsic cohesion. These parameters can be used to estimate UCS according to the patchy weakness model described in section 3.2.1.3. The assumption explained is illustrated in Figure 4-15. From the figure, following equations can be written:

$$\sigma_{90} = x \cdot \sigma_{wp} + (1 - x) \cdot \sigma_i \quad [21.]$$

Rearranging:

$$\sigma_{wp} = \frac{\sigma_{90} - (1 - x)\sigma_i}{x} \quad [22.]$$

Where σ_{wp} is the cohesion at the weak plane, σ_{90} is the minimum cohesion from the puncher result, σ_i the intrinsic cohesion from the puncher result and x the angle of failure induced by the puncher. An expression for x can be written as (according to Figure 4-15):

$$x = \frac{2 \cdot \psi}{360} \quad [23.]$$

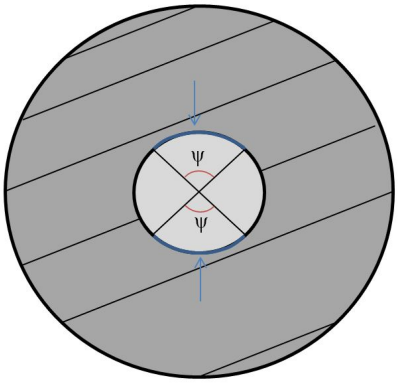

Figure 4-15 Disk shaped sample illustrating how to estimate friction angle from punch test. ψ indicating the failure angle of the punch sample, showed by the blue arrows.

4.2.2.4 Uniaxial Compressive Strength (UCS) (Fjær, et al. 2008)

Uniaxial compressive strength also written unconfined compressive strength is by definition a measure of the rock or material capability to withstand deformation, when a force is applied. Uniaxial, means that zero confining pressure is applied to the core. A UCS test is a standard test in rock mechanics and an important parameter. In practice such a test can shortly be explained by a pair of pistons applies axial stress to a cylindrical sample, and the force applied and deformation is monitored, until failure. Figure 4-16 shows a typical test-plot, and Figure 4-17 shows the axial force applied with zero confining pressure. Definition of inclination angle for a standard UCS test is as described in Figure 3-10.

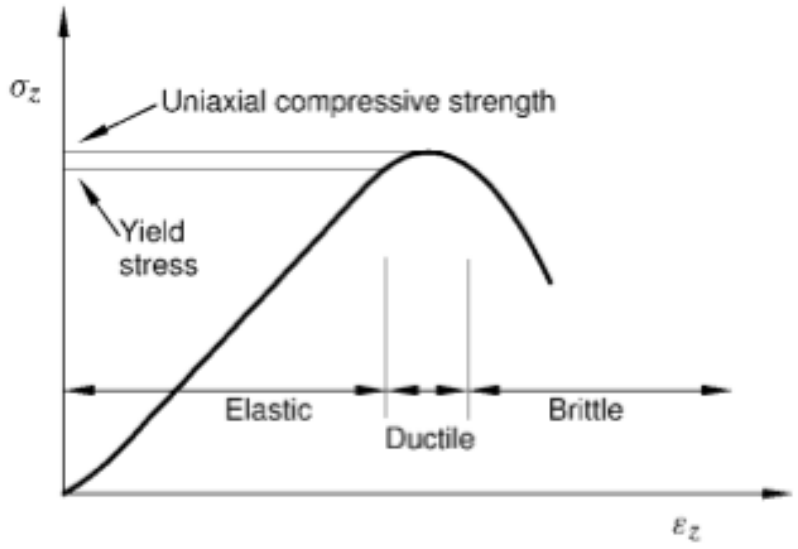

Figure 4-16 A typical uniaxial test-plot, explaining the modes in a UCS test (Fjær, et al. 2008).

Figure 4-17 Axial Force applied. Zero confining pressure. Modified from (Fjær, et al. 2008)

4.2.3 Equipment and procedure

The shale puncher device consists of six separate parts. Figure 4-18 is a technical drawing of the parts. Figure 4-19 shows the parts mounted together, making up the shale puncher. Figure 4-20 shows the genuine design and size of the puncher used for the test results presented in this thesis. Essentially, the puncher can be split into two larger parts, making up the top puncher piston and bottom puncher piston.

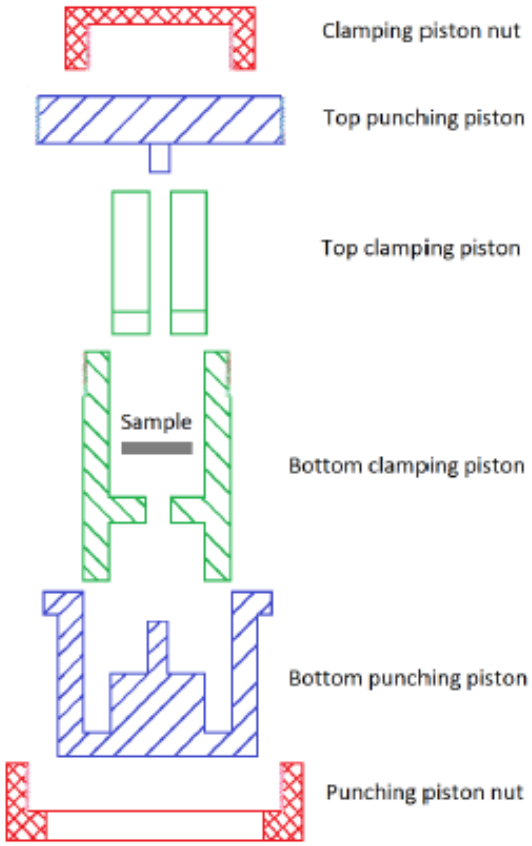

Figure 4-18 Technical drawing of the Shale puncher design. (Stenebråten, et al. 2008)

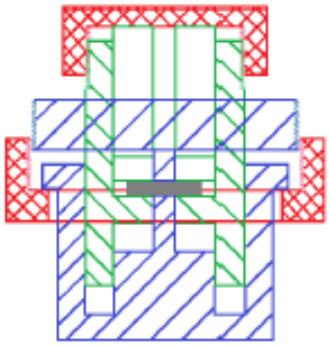

Figure 4-19 Technical drawing of the mounted Shale Puncher (Stenebråten, et al. 2008)

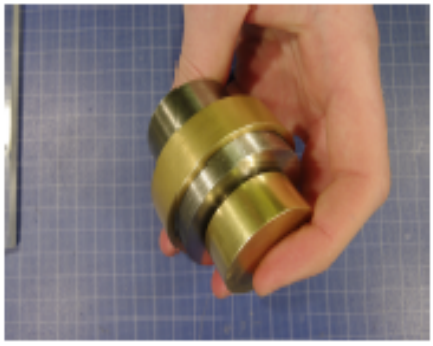

Figure 4-20 Used shale puncher, size and design. (Rademakers 2010)

Shale Puncher assembling

Sample is prepared as described and placed onto the bottom clamping piston. Top clamping piston and top punching piston is put into place, and the clamping piston nut is tightened with a special made wrench, which has a constant measure momentum spring attached to it. This procedure is repeated for the bottom part of the device. By using a more or less constant momentum, all the samples are mounted the same way, to decrease the possibility of an external factor concerning damage from the fastening process.

Mounting of the load frame.

When puncher device is mounted, it is centred onto the bottom of the MTS load frame. A nut is put onto the device and the top of the loading frame to prevent possible damage to the frame (steel vs. steel). The load frame is manually brought down, as close as >1mm from the puncher device. The test is then carried out with the computer program with the pre-set settings. Figure 4-21 shows the total setup for the punch test including the loading frame, and Figure 4-22 shows the mounted puncher device in place in the load frame.

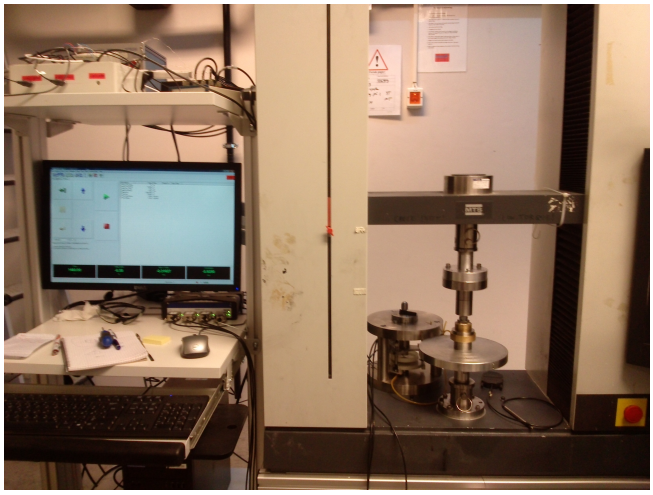

Figure 4-21 Full Shale Puncher Setup (Rugland 2014).

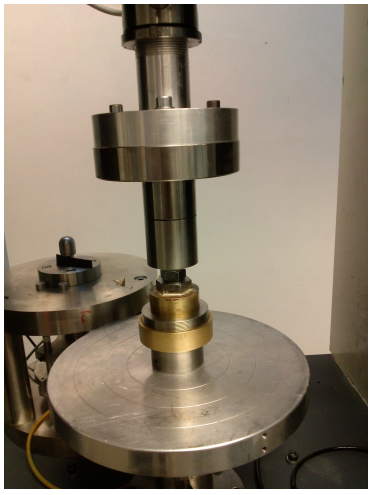

Figure 4-22 Shale Puncher mounted in MTS Load Frame (Rugland 2014).

The initial input from the program running the test are presented in Table 4-2 below. Except the pre-set settings manual input of sample diameter and sample thickness is entered before test is run. Normally a test plot as shown in Figure 4-9 are obtained, and test data are saved to the computer for later analysis.

Panel Input	Value	Units
Break Sensitivity	75	%
Break Threshold	20.000	N
Data Acq. Rate	2.00	Hz
Max Crosshead	1.00	mm
Max Load	5000.000	N
Pre-Load	10.000	N
Pre-Load Speed	0.500	mm/min
Test Speed	0.150	mm/min

Table 4-2 Default Input of Shale Puncher Test (Rugland 2014).

From Table 4-2 a pre-load is applied, where the load frame connects with the punch device. This is done to ensure the punch device is correct mounted and the test can be run further without complications, this also works as a safety device for the load frame. Pre-load speed is set to 0.500mm/min until a force of 10 N is detected. This is sufficient for the load frame to be well connected to the puncher device without any irreversible effects on the sample.

The actual testing, which can be described as part two, is continued with a speed of 0.150 mm/min. This caries on until one of the following scenarios occur: 1) break is detected by drop over 75% of axial force (break detected). 2) Maximum load of 5000 N is reached. 3) Maximum axial displacement of 1 mm is reached. For the data described in the thesis, break was always detected (as expected). Typical tested samples are presented in Figure 4-23 and Figure 4-24.

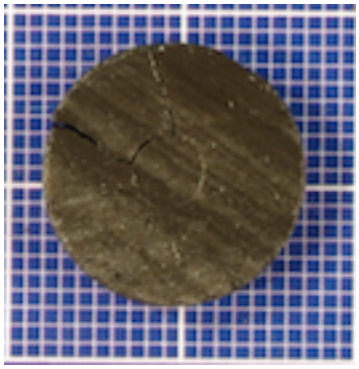

Figure 4-23 Typical Tested Sample Ex1 (Rugland 2014).

Figure 4-24 Typical Tested Sample Ex2 (Rugland 2014).

4.2.4 Shale Puncher sample preparation and inclination definition.

The same sample preparation and inclination definition as for the CWT explained in section 4.1.5 applies for the shale puncher. Also explained in the CWT section, acoustic velocity measurements do not damage the samples. Therefore they are first tested in the CWT apparatus, then in the shale puncher. In this way two tests and lot of information from each small sample can be measured.

After sample preparation and CWT measurement are completed, testing in the puncher takes place right away. This is to ensure small or none property change, as the small samples is exposed with a higher surface area to thickness ratio then the original cores, both to air and fluid.

4.3 The scratch test (Schei, et al. 2000)

4.3.1 Introduction

The scratch test is performed by use of a sharp mechanical nail (cutter knife), scratching the surface of the rock, while monitoring forces in the x and y direction. Typical depth of scratch is less than 1mm, and is constant for each measurement. Scratch results may be further analysed and serves an important role when estimating mechanical parameters. The test is quick, and easy to perform. The measurement is a direct measure of the presented core sample, and the measurement is continuous along the whole core. Mainly the test results may be used in UCS estimation and Young's modulus estimation. The test has been widely investigated, and strong correlations between scratch measurements and material strength and stiffness exists.

4.3.2 Theoretical background

While testing, the cutter scratches at the given depth, and two modes (failure mechanisms) may occur. 1) Ductile mode or 2) Brittle mode. Ductile mode may also be called plastic flow, occur at small depths, where the depth is larger than grain size. The mode can be described as a flow of rock in front of the cutter. Brittle mode occurs when scratch depth exceeds the threshold depth; this depth is strongly dependent on UCS and toughness of the rock. Brittle mode may be described as chipping, where small cracks are initiated at the front of the cutter and propagate upwards. When a crack reaches the surface of the rock, the described chipping movement from the cutter removes it. Usually this depth is somewhere between 0.5-2mm. The two modes described can easily be identified in Figure 4-25 and Figure 4-26.

Figure 4-25 Ductile mode (Schei, et al. 2000).

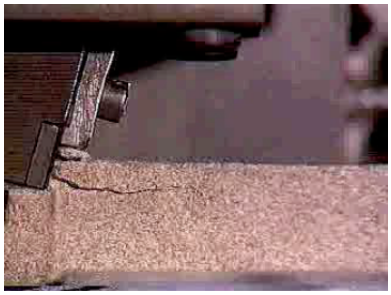

Figure 4-26 Brittle mode (Schei, et al. 2000).

The different failure mechanisms explained, represents two different relationships between the horizontal cutting force F_t and the depth of cut d. For the ductile mode, F_t is proportional to the cross sectional area of the cut, and consequently to the depth of cut, d, where cutter width is constant. For brittle mode, F_t rises at a lower rate than d, because the energy required to form a chip is correlated to the surface of the crack, and not the volume of rock removed. Accordingly, lower depths require less force to initiate the cut (ductile mode), and larger depths require larger force to initiate the cut. This explanation describes the transition zone between the two cutting-modes, and the depth which chipping appear. Knowing that the intrinsic energy is a good correlation with the UCS of the rock, scratching has to be performed in the ductile regime. Ductile mode is clearly the mode, which would yield the most consistent and reliable measurements. This regime can be said to be where the range of cut is described by a constant intrinsic specific energy. Experimental results shows that the horizontal force, F_t, averaged over the scratch length is varying proportionally to the depth of cut. The vertical component, F_n, is also proportional to the depth. Equations for the horizontal and vertical directions can therefore be expressed as:

$$F_t = EA \qquad [24.]$$

$$F_n = \zeta \cdot EA \qquad [25.]$$

Where E is defined as the intrinsic specific energy, ζ the ratio of the vertical to the horizontal force action on the cutting face, and $A = wd$ ($w = witdh, d = depth$) the cross-sectional area of the cut.

4.3.3 Equipment and procedure

The full scratch setup consists of three parts. The metal frame, which constitutes the scratch device, a motor connected to the scratch device, and a computer where measurements are controlled and monitored. The full setup is shown in Figure 4-27. The main components of the scratch device are a changeable sample holder (depending of core sizes), a moving cart containing the vertical positioning system, the load cell and the cutting element. The load cell used in this thesis is capable of

4000N, which is over the practical area. Approximately 200N would be maximum force needed for the cores in this thesis. The cutting element is a PDC cutter, which can be changed to several different sizes to best fit the sample. Larger sample = larger cutter, dependent on the diameter of the core. Figure 4-28 shows a typical core mounted in the scratch device.

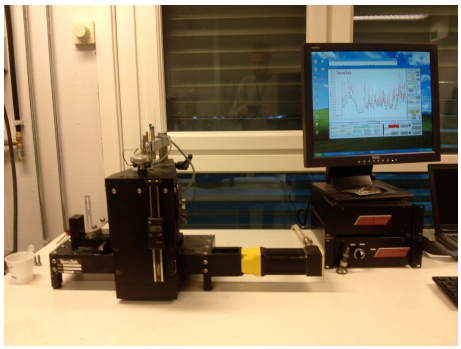

Figure 4-27 Full scratch setup

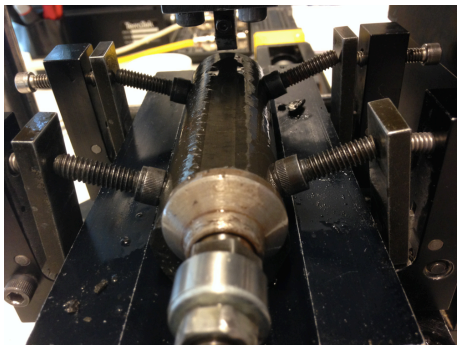

Figure 4-28 Scratch test, Mounted Sample

The scratch test is kinematically controlled. Cutter speed and cut depth is manual input in the program and depth is adjusted by lowering the cutter-knife manually to requested depth. This is controlled both by a micrometer and a LVDT to ensure correct depth. Typical depth is as explained 0.1-2mm. Standard speed is also around a few mm/s.

As the test is run, both the horizontal force component, along the motion of the cutter F_t, and the vertical force normal to the scratch surface, F_n, is monitored and plotted along length direction of the core. A ratio F_n/F_t around 6N indicated sharp cutter, and may be used as a measure of the wear on the cutter. Test plot is obtained (Figure 4-29) and stored to the computer. Data are further analyses in a pre-made excel sheet from SINTEF Petroleum.

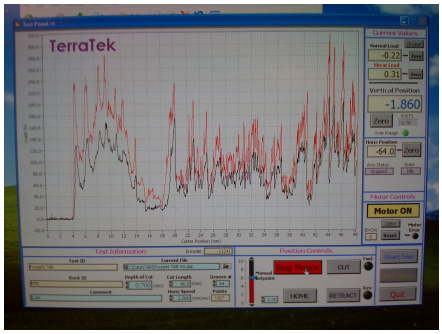

Figure 4-29 Typical scratch test plot (Rugland 2014).

A normal test procedure is described stepwise below:

1. **Mounting of sample**. Core sample is mounted to the scratch device. Depending on core diameter different fastening equipment is used. Brackets, clamps and bolts are used to tighten the sample in place. The diversity of the mounting process makes the scratch test suitable for all sizes of rock cores.
2. **Initial Input.** Initial input is decided, as the depth series, typical three cuts of different depths. Cutter speed is set to a constant speed throughout the testing. Although depth is manually controlled, it is also saved as input to the computer program for easy access when analysis of the data takes place. Note to zero the depth for each scratch, to control the depth with respect to the micrometer and LVDT.
3. **Pre Scratch.** Or pre-cut is done to make sure the sample surface is smooth and linear along the length direction of the sample. In order to make this surface, several pre-cuts of small depths may be necessary. Too large pre-cut depths may induce cracks in the sample. Typically pre-cut 0.1-0.3 mm for each scratch.
4. **Test Scratching.** The same practice as for the pre scratch in performed. A scratch series is chosen, normally three scratch series of given depths. In this thesis scratch series were in mm: 0.2, 0.3, 0.5 or 0.3, 0.5, 0.7.
5. **Interpretation of data.** Results from the scratch test are saved to the computer and analysed in an excel sheet.

4.3.4 Scratch Applications

Results from the scratch test may be used in estimating several mechanical properties. Correlations and equations are shown in this subchapter. Actual measured data are presented in the Results chapter.

4.3.4.1 Rock Strength

Results from the scratch test show a respectable correlation between the specific energy, denoted E, and UCS of the rock. This is shown in

Figure 4-30. The presented plot is dry sandstone (Castlegate). This correlation is also expected to exist for shales according to (Schei, et al. 2000). Slope of the presented curve may vary for different types of rock. Conversation with Idar Larsen at SINTEF Petroleum confirms the slope presented may be used for interpretation of tested shales in this thesis.

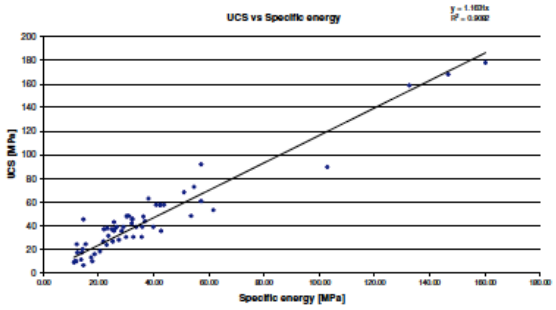

Figure 4-30 Example of Correlation between UCS and specific Energy for dry sandstone materials. (Schei, et al. 2000)

4.3.4.2 Strength anisotropy with scratch device

Section 4.3.6 explains the scratch direction and inclination of tested samples. It is expected that a sample would yield different strength when scratching with or against layers. This is also expected for the case where scratching is performed parallel to the bedding and across the bedding. This is illustrated by Figure 4-31. The arrows at the top and bottom of the sample show the direction where the scratching is performed parallel to the bedding. In this direction it is expected to be easier to cut. While the arrows on the sided (right and left) of the sample indicates scratching across the bedding planes. This is expected to yield a higher strength, as bedding has to be

broken continuously along the core. This assumption is tested and presented in the results chapter.

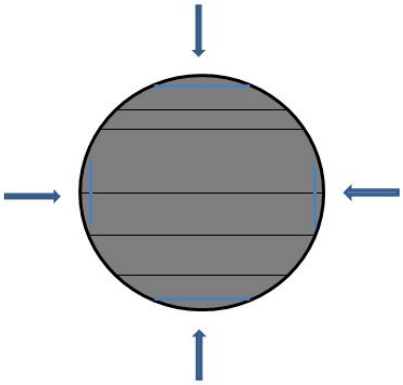

Figure 4-31 Expected strength anisotropy of scratch results.

4.3.4.3 Rock Stiffness

Presented in (Schei, et al. 2000) is the correlation between Young's modulus and specific energy. This relation is not as strong as the UCS correlation, and exists probably because of the relation between strength and stiffness. It may however represent a respectable estimation of Young's modulus. Based on the assumption that the force variations in a scratch test characterize a series of small stress build-up drop-tests equivalent to UCS-tests, where this can be written as the peak values of the derivative of the force:

$$\frac{dF_t}{ds} \qquad [26.]$$

Where F_t is the tangential force, and s is the displacement of the cutter lengthwise the surface of the rock. Experimental data from (Schei, et al. 2000) express that the mean value of the positive peaks of the dF_t/ds curve correlates with measurements from of the Young's modulus. This is shown in Figure 4-32. A parameter named M_{slab} is introduced and described as:

$$M_{slab} = \frac{Mean\ value\ of\ positive\ peaks\ of\ \frac{dF_s}{ds}\ curve}{(Cutter\ width) \cdot (Scratch\ depth)} \qquad [27.]$$

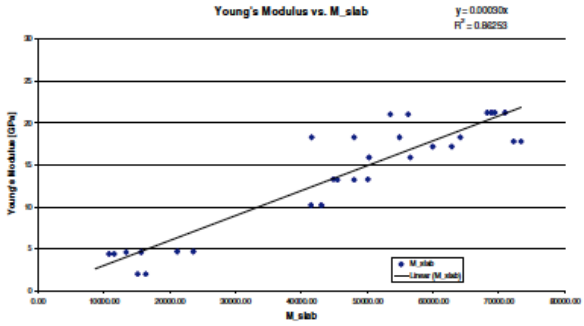

Figure 4-32 Example of correlation between Youngs's modulus and Mslab parameter. (Schei, et al. 2000)

Compared data in Figure 4-32 clearly correlates to some degree. And show the diversity of the scratch test. From a series of scratch tests a lot of rock mechanical data may be extracted.

4.3.4.4 Specific Energy calculations

The Specific energy is computed with theory presented in (TerraTek 2005). By use of an excel sheet, recorded data are used to calculate Es by the equation:

$$E_s = \frac{Average\ Shear\ Force}{(Cut\ Width) \cdot (Cut\ Depth)} \quad [28.]$$

4.3.4.5 UCS Calculations

With further analysis on the specific energy, the Uniaxial Compressive Strength may be calculated as a correlation to Es presented in (TerraTek 2005). The correlation coefficient between Es and UCS is presented in Figure 4-30. Expression for the UCS may be written as the correlation factor times the Es:

$$UCS = 1.163 * \left(\frac{1}{Cut\ Witdh}\right)\left(\frac{\Delta Average\ Shear\ Force}{\Delta Depth\ of\ cut}\right) \quad [29.]$$

4.3.5 Sources of error

- **Instability**. The main source of error in the scratch test is stability issued concerning the core sample. If the core is not properly mounted into place: vibration, sliding, shifting of the sample may occur, and measured results cannot be used. Results are highly reliant on this issue.

- **Cutter sharpness.** The cutter needs to be sharp for the cutting process to be as smooth as possible, in the ductile regime. Weak cutter may induce fracturing as chipping along the surface. Wear of the cutter is presented in section 4.3.3.

- **Depth of cut.** Cut series, including pre-cut should never exceed the threshold. This is to exclude brittle mode, and damage of the sample. Too large depths can also split the sample.

- **Length of cut.** Scratch should stop a few cm before reaching the end of the sample. And for each cut or pre-cut, length should be shortened by approximately 2mm. This is to avoid accumulation of rock sediments, which could lead to sample splitting at the end.

- **Sample saturation.** For shale, a saturated sample would give a different result than a dry sample. Shale weakens when drying out. Therefore samples may be mounted in a vessel filled with fluid. Another option is to wrap a wet core with thin cling film, and use a pipette to apply fluid for each scratch. (Schei, et al. 2000) presents a saturation effect in sandstone of 25%, and it is expected that this would be even higher for shale.

4.3.6 Scratch sample preparation, inclination definition and scratch direction.

Cores are drilled out as for the CWT cores presented in section 4.1.5, but with different measures. The scratch-cores are drilled out for every 30°, from 0° to 90°. Diameter and length is respectively 1.5" and 5-10cm. A larger core than the CWT and Shale Puncher is the case. The reason is explained in the discussion part, because the cutter size and wall thickness effects the measurement. Also the cores needs to be larger in order to do the amount of scratches required to investigate the anisotropy. Scratch directions are presented later in this subchapter.

Cores are drilled according to the Figure 4-8 presented in section 4.1.5.

Direction of scratch varies with the inclination. This is presented in the figures below. For core with 0° where bedding is normal to the scratch direction, measurements are performed both on the sides, top and bottom. This is more clearly indicated in Figure 4-33 and Figure 4-34. Sample is scratched in the direction indicated by the arrows and numbers. Rotated and scratched for every 90°.

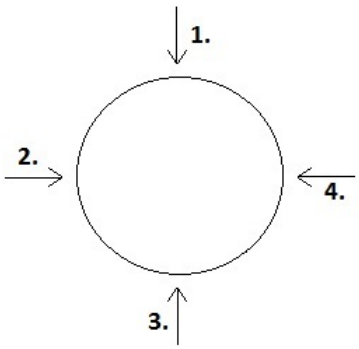

Figure 4-33 Scratch direction 0°, front.

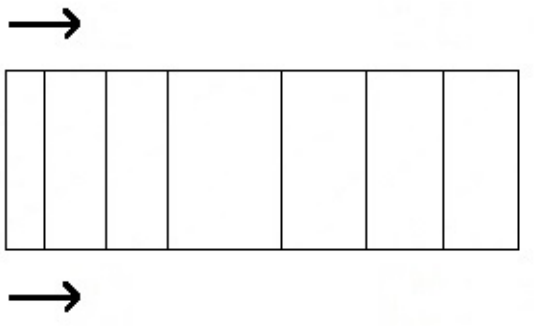

Figure 4-34 Scratch direction 0°, lengthwise.

For cores with inclinations between 0° and 90° (in this case 30° and 60°) scratching is performed both with and against bedding, respectively two measurements are performed for each direction. This is indicated by Figure 4-35.

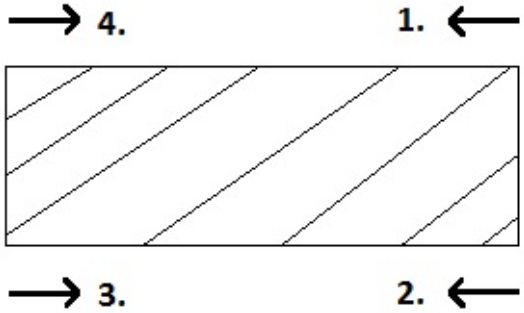

Figure 4-35 Scratch direction for 30° and 60°.

For cores 90°, parallel to the bedding, the same procedure as for 0° is performed. This is indicated by Figure 4-36 and Figure 4-37

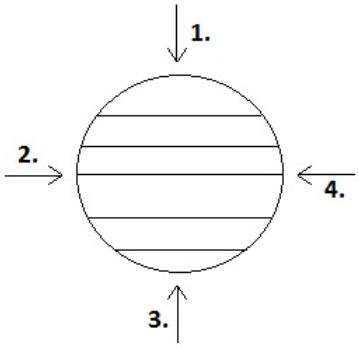

Figure 4-36 Scratch direction 90°, front.

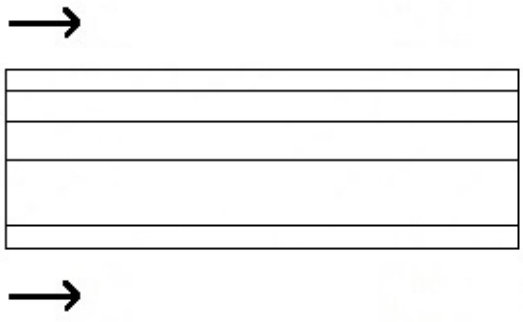

Figure 4-37 Scratch direction 90°, lengthwise.

4.4 The Brazilian Test (Simpson, et al. 2014), (Claesson and Bohloli 2002)

4.4.1 Introduction

Brazilian Testing is frequently used in the petroleum industry. The test is an indirect measure of the rock tensile strength. The test is easy to perform, and requires only standard rock mechanical laboratory equipment. Samples need little or no preparation, and can be tested quickly. Assuming isotropic material properties, an equation is used to calculate the tensile strength from test results. The test may also give valuable information concerning fracture growth within the sample. Which can translate into larger scale explanations as hydraulic fracturing inside a reservoir and fracture growth when drilling a well.

4.4.2 Theoretical background

Simply, the Brazilian Test is carried out by use of two oppositely directed metal plates compressing the sample. This is seen in Figure 4-38. Note the curvature in the metal plates, for a wider contact surface on the sample. The core sample is usually shorter or equal in thickness, L, to the diameter of the sample, D.

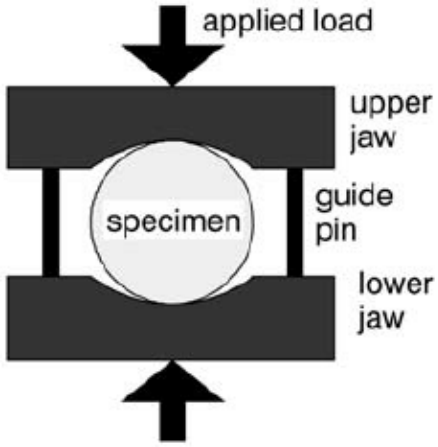

Figure 4-38 Simple sketch of the Brazilian Test equipment (Fjær, et al. 2008).

Failure in the sample takes place by an extension fracture, in- or close to the middle plane of the sample. Three failure modes may be described, dependent on the loading type. 1) Tension and opening. 2) Shear and sliding. 3) Shear and tearing (Fjær, et al.

2008). A crack may propagate according to the described modes or in a combination of them. Using this model it is assumed that the sample is continuous, homogenous and isotropic. When applying a line load to the circular sample, it is expected to behave in the linear elastic domain. When one of the assumptions is not fulfilled the stress distribution changes. What makes the Brazilian Test attractive is that the theoretical solution to the test indicates a constant tensile stress on the plane between the two load lines. Indirect tensile strength, $\sigma_t = \sigma_h$, perpendicular to the loaded diameter may therefore be described as:

$$\sigma_t = \frac{2F}{\pi DL} = \frac{F}{\pi RL} = T_0 = 0.636\frac{F}{DL} \quad [30.]$$

$$\sigma_v = \frac{6F}{\pi DL} = \frac{3F}{\pi RL} \quad [31.]$$

Where σ_t is the tensile strength, F is measured force at which the sample fails, D is the diameter, L is the length (thickness of the sample). As seen in Figure 4-40 the maximum principal stress is compressive from the point load of the sample, while along the plane between both loading lines the stress is tensile (double arrow in the middle). The maximum compressive stress is about three times the absolute value (eq. 31.) of the tensile stress in the central part of the loaded diameter. In fact close to the loading line. Hence this is the theoretical solution, where the end points of the loaded diameter are described as singular points in the applied stress. Based on the plane stress assumption the intermediate stress can be neglected. Further from the centre of the sample, tensile strength is the case but in a smaller degree, decreasing magnitude. At half the radius from the centre of the load line, the tensile strength is assumed to be half the maximum tensile strength from the centre. In Figure 4-39 (Claesson and Bohloli 2002) mathematically models the ratio between principal tensile stress to compressive stress in accordance to distance from the centre of the specimen. This shows a respectable estimation of previous explained theoretical assumptions.

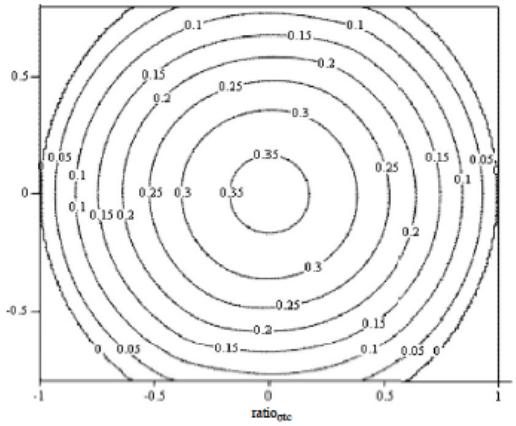

Figure 4-39 Modelling of Ratio between principal tensile stress to compressive stress (Claesson and Bohloli 2002)

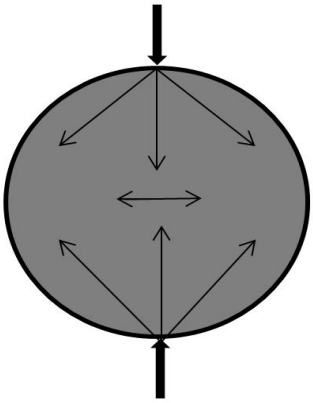

Figure 4-40 General stress distribution in Brazilian test. Double arrow in the middle indicates the tensile stress.

Figure 4-41 shows applied pressure to the specimen, where P is the applied force, L the length of the specimen and R the radius.

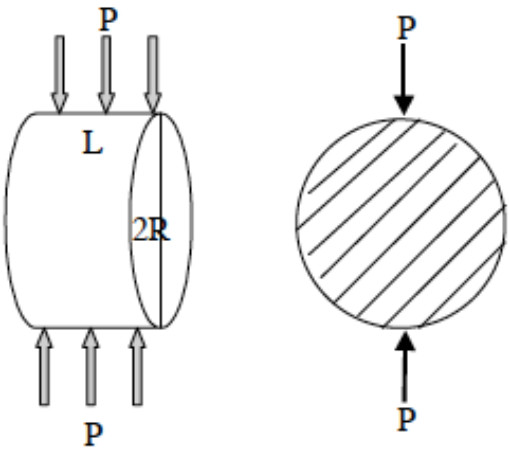

Figure 4-41 Sketch of applied force in Brazilian test (Claesson and Bohloli 2002)

The explained stress state where a point load line can be assumed, should lead to a diametrical splitting of the sample. Where a micro-crack is induced and propagates, between both loading lines. In practice various fracturing may be the case. As maximum stress concentration in positioned in the centre of the sample, shear failure may occur and introduce a v-type of fracturing close to the loading lines. A set of parallel fractures may also be seen.

Indicated above the Brazilian Test theory is in practice much more complex than assuming a perfect loading line between two points, with zero thickness. Studies on this concern has been made and published. These works can be found from (Claesson and Bohloli 2002). The principal problem is as explained in section 3.1.4 and 3.2, connected to rock as a material. Rock is a heterogenic material and exhibit anisotropy. Therefore simplified mathematical models may not always cover the realistic case. Also existing micro-cracks in the sample may change the stress distribution, and influence the local stress at a (or several) point in the sample. In (Simpson, et al. 2014) this is investigated by measuring the acoustic emission hits while testing. Forming of a crack in the sample is connected to existing micro-cracks. These cracks emit energy in the form of elastic waves. Which can be described as acoustic emission, and can be measured. Measuring at the start of a Brazilian Test would expect to yield scattered emission results across the surface of the sample. When the rock strength is approached, and a larger scale fracture is induced, acoustic emission activity is expected to increase and be situated in the critical region. Figure 4-42 shows an example, presented in (Simpson, et al. 2014) of such an acoustic emission measurements while testing. Expectations of how the activity counts will change during testing are clear from the figure.

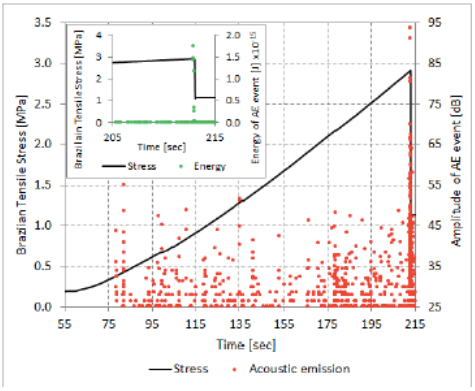

Figure 4-42 Acoustic Emission example (Simpson, et al. 2014)

The details in Figure 4-42 are explained. The Y-axis is the Brazilian Tensile Stress in MPa, and the X-axis is the time in sec. Amplitude in dB of the AE is measured at the far right Y-axis. From the graph it is clear that the AE increases when the specimen forms a crack and fails. The smaller graph in the left corner represents the energy of the AE in $J \cdot 10^{-15}$. The same can be noticed here.

4.4.3 Equipment and procedure

The actual equipment explained above can be seen in Figure 4-43 bellow.

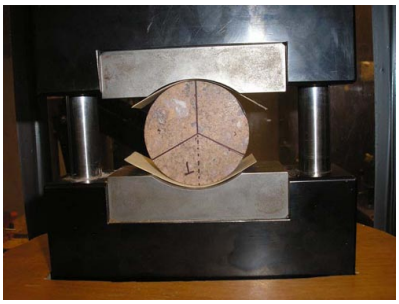

Figure 4-43 Brazilian test frame (Simpson, et al. 2014).

The test procedure is as described quite simple. Samples are cored in required diameter. In (Simpson, et al. 2014) the dimensions used were 24mm length (thickness) and 48mm diameter, giving a thickness-to-diameter ratio (t/D) of 0.5. Some manual investigation of the samples takes place, to mark bedding and layers. This is done so that the sample may be adjusted in the Brazilian metal frame so the wanted inclination to the principal stress applied may be carried out. How the angle is configured is presented in section 4.4.4.

The Brazilian metal frame is fixed into the loading frame, with the specimen already in place. To soften the contact between the sample and the frame, a thin layer of paper masking tape is wrapped around the sample. Then a premade testing program is applied. The loading frame applies the pressure computed, continuous until the sample fails, and the computer register failure of sample. After, data is collected and processed. With use of eq. 30, tensile strength of the sample is calculated.

For further investigation of the crack initiation acoustic emissions may be recorded, as explained above in section 4.4.2. This is explained in detail in (Simpson, et al. 2014). But it mainly consists of acoustic emission sensors mounted in place to record the elastic waves generated during testing and propagation of fractures.

A greater investigation of the fracturing can be performed, by applying recording by a high-speed camera, mounted in place before testing. This information can as explained be useful in several areas of research. This is further discussed in (Simpson, et al. 2014).

4.4.4 Brazilian Test sample preparation and inclination definition

As the cores are drilled out parallel to the bedding, rotation of the samples is the only thing required to investigate the given inclination to bedding (Figure 4-44). Where 0° is load parallel to the bedding and 90° is load normal to bedding. This means that several specimen can be tested from one single core, and hence give more accurate measurements, compared to if the cores had to be drilled for each of the needed angles.

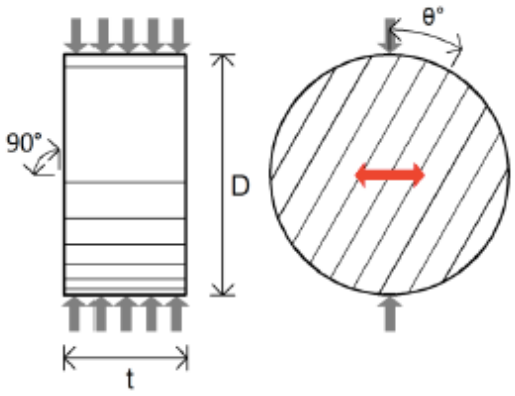

Figure 4-44 Definition of how inclination to bedding of disk shaped sample is determined in Brazilian testing (Simpson, et al. 2014).

4.5 Design of new Index Test.

Investigation of the index tests explained above, lead to ideas of how to improve or create a test to more specific measure strength anisotropy, with the challenges present, e.g. rock material, inclination, equipment and preparation. Several ideas where discussed with scientists at SINTEF Petroleum AS. One of them appeared to be quite interesting. Designing such a test could take a lifetime of knowledge, and as Alexandre Lavrov at SINTEF Petroleum said it: this would make a good PhD. An outline of this test and possible validation is presented in this section.

4.5.1 Test outline

The test is a modification of the Brazilian test and a std. UCS test, where contact surface of the sample is modified, in order to provoke shear failure in the tested sample. The equipment is illustrated in Figure 4-46 and is made up by a metal frame, consisting of two oppositely metal rectangles. Similar to a Brazilian test, but where the frame is straight rather than bent with an angle. A prepared sample as seen in Figure 4-45 where top and bottom is cut off to get a larger contact surface, is placed inside the frame and force is applied. Test conditions are shown in Figure 4-48.

What is unique with this test is that sample preparation decides the test rather than the equipment itself. By cutting of a section of the circular sample parallel on each side, as in Figure 4-45 the contact surface becomes larger, and stress distribution changes, compared to Brazilian test. In a std. UCS test, force is applied to a vertical standing core, and failure occurs at a weak plane. This means the sample choose the plane of failure. Same principal is assumed here. Force is applied to the enlarged surface, and failure occurs at a weak plane. A factor $\sigma_{measured}$ is introduced. Where this can be written as:

$$\sigma_{measured} = \frac{F}{A_{cs}} \qquad [32.]$$

Where F is measured maximum force, and A_{cs} is the contact surface area. It is assumed that this factor is dependent with inclination of the sample. Definition of sample inclination is as described in 4.4.4. Consequently a larger force has to be applied when largest principal stress is situated normal to bedding, and minimum when bedding is situated parallel to maximum principal stress.

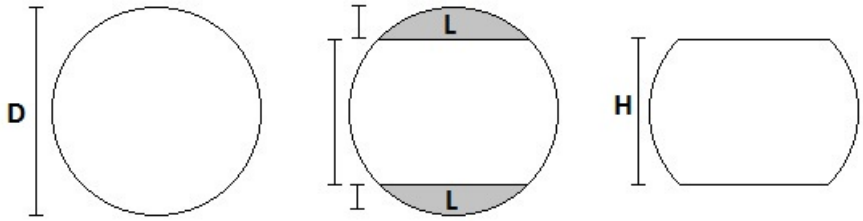

Figure 4-45 Prepared sample explanation.

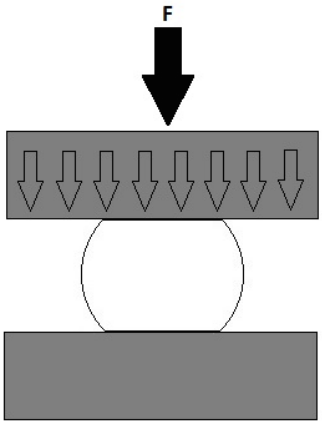

Figure 4-46 Illustrated test description.

4.5.2 Pre-testing and test validation

In order to validate such as test, modelling and mathematical estimates should be carried out. Several uncertainties and problems have to be considered. Making a mathematical estimate of stress distribution in such a test may be done by the following explanation.

Assuming:

$$\sigma_1 \propto F \quad [33.]$$

$$\sigma_2 \propto 0 \quad [34.]$$

$$\sigma_3 \propto -n \cdot \sigma_1, where\ n < 1 \quad [35.]$$

Where σ_1 is maximum principal stress, proportional to applied force, and σ_3 is minimum principal stress proportional to σ_1 and a negative factor n less than 1, which can be determined geometrical. Assuming shear failure, failure may occur according to the patchy weakness model or at the weak plane. It can be written:

Intrinsic:

$$\sigma_1 - \sigma_3 = f(\varphi) \quad [36.]$$

Weak plane:

$$\sigma_1 - \sigma_3 = f(\theta) \quad [37.]$$

Where intrinsic failure is a function of friction angle according to the patchy weakness model, and failure outside the weak plane according to inclination of bedding as seen from inclination definition in Figure 4-47. Indicated in Figure 4-48, by assuming a simple stress distribution and decomposing the forces, an estimate may be calculated. From the figure it can be interpreted:

$$F_n = F_0 = cos\beta \cdot F \quad [38.]$$

$$F_p = sin\beta \cdot F \quad [39.]$$

Where forces are illustrated as in Figure 4-48, F_n the y-component and F_p the x-component. β is the angle between F_n and F.

Assuming this is true, principal stresses may be calculated by:

$$\sigma_3 \propto 2F_p = 2sin\beta \cdot \frac{F_0}{cos\beta} \quad [40.]$$

$$\sigma_1 \propto F_0 \quad [41.]$$

These equations may be used to give a rough estimate of required force, and stress distribution is assumed highly simplified. It may however serve as important information regarding force range in the test.

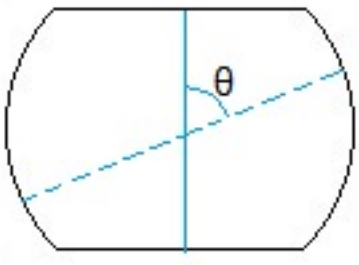

Figure 4-47 Inclination definition.

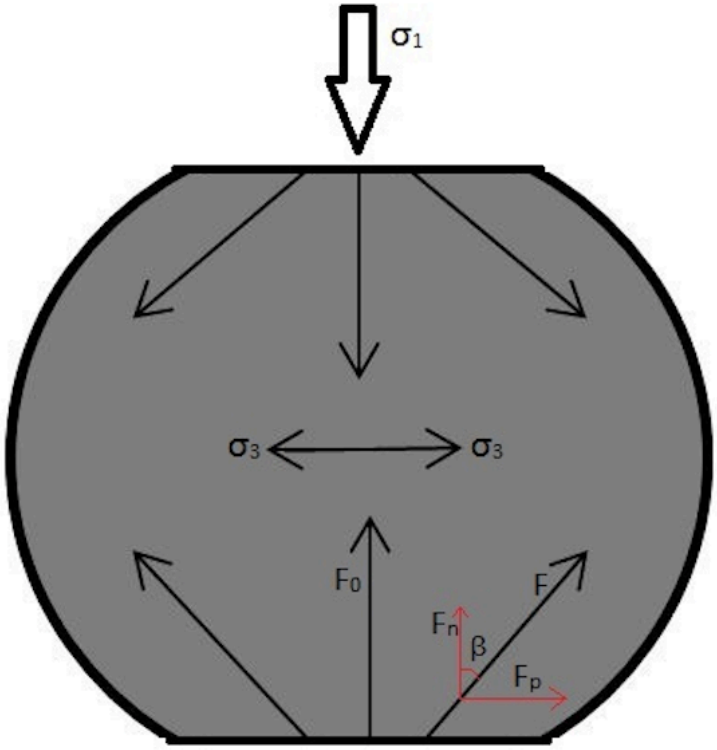

Figure 4-48 Decomposing of forces. Red arrows indicate decomposing of F in x and y direction.

Another method to validate and extract information is to make a data model to see what could be expected from such a test, and how parameters will affect the measurement. This should be done in a finite element program (e.g. Abaqus, Comsol, Flac). Simulations should be performed according to a test matrix introducing a range of input parameters to see how expected results would change in accordance to these. Conversation with Alexandre Lavrov suggested to introduce an angle as seen in Figure 4-49, and the relation between width and length of the sample. By running such a test matrix, a good estimation of what to expect from such a test would be presented. Suggested matrix is illustrated in Table 4-3. Also running the matrix for a variation of Poisson's ratio, 0.2, 0.3, 0.4.

	φ	10	20	30	…
W/D					
D/2					
D/4					
D					
2D					
…					

Table 4-3 Finite element simulation matrix.

By performing these calculations and simulations information regarding what to expect form such a test would be obtained. As the test is relatively easy to perform a homogeneous material (example castlegate rock) could be tested, to some degree exclude the heterogenic factor. This would show if shear failure would be the case, and give answers to questions regarding the simple stress distribution assumption.

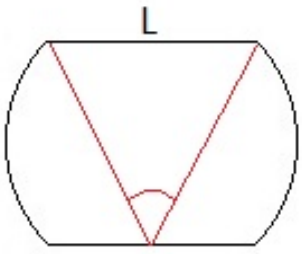

Figure 4-49 Length and angle definition for use in finite element simulation.

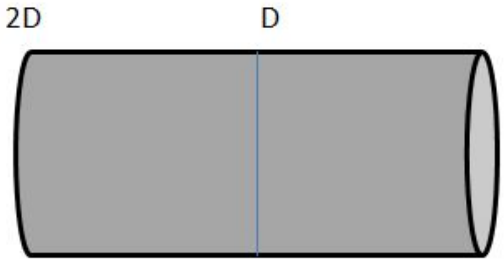

Figure 4-50 Example of W/D relations.

A third method can be shortly mentioned: photo elasticity. This method records stress distribution in a transparent medium, which exhibits colours when applied a special light. Running this test on such a medium and record the stress distribution change as the test run, would be interesting, and helpful to understand the expected complex stress distribution. Conversations with professors at Material Science and Engineering department indicated that this would be possible to perform with the suitable equipment, and of great interest concerning stress change.

4.5.3 Test strengths and weaknesses

Strengths

From one drilled core, several samples could be prepared. Meaning that from the same core tested in a UCS test, more measurements could be performed for one core in this test. This number would depend on the factor how the W/D relation affects the measurement.

From the same inclination definition as for Brazilian test, it is easy to determine inclination. For a core parallel to bedding, only turning of the sample would be required to test for the specific inclination, see section 4.4.4. Investigating the full inclination range is therefore easily performed, and strength as a function of inclination may be obtained.

Each sample requires little or no preparation. Cutting the core in suited lengths are the only preparation needed.

The test would also help understand how the contact surface in a Brazilian test is affected. The Brazilian test is as explained highly complex, considering the stress distribution.

Weaknesses

The test is similar to a UCS test, and exhibits many of the same features. But a problem occurs where the sides of the sample is curved, and makes the stress distribution more complex.

The largest problem with this test would be due to sample preparation. How to prepare the sample with two oppositely placed surfaces with the same depths would be a challenge. Cutting and grinding the rock surface could damage the sample and affect the measurement. A similar preparation-technique as for the CWT and Punch samples would be preferred. In theory L in Figure 4-45, would be equal, but in practice this would not be the case. How this difference would affect the stress distribution and the corresponding results, would be investigated by the finite element simulations.

Actual stress situation is complex. For strength anisotropy to be measured, pure shear failure has to occur. If tensile strength is to large, this would affect the measurement. Calculations and finite element simulations would assist in determining this ratio.

5 Experimental results

In this chapter results from the performed tests will be presented. Only measured data is presented here, while computed and calculated data are presented in Chapter 6.

5.1 CWT Results

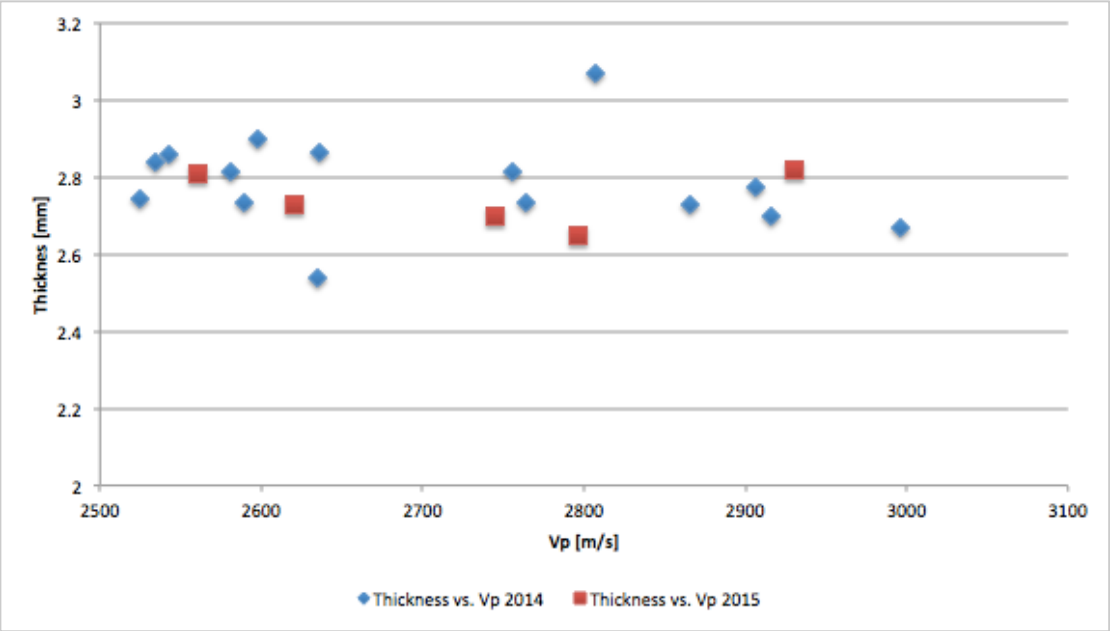

Figure 5-1 Pierre, Thickness vs. Vp. Blue squares are results from (Rugland 2014), and red squares are new results.

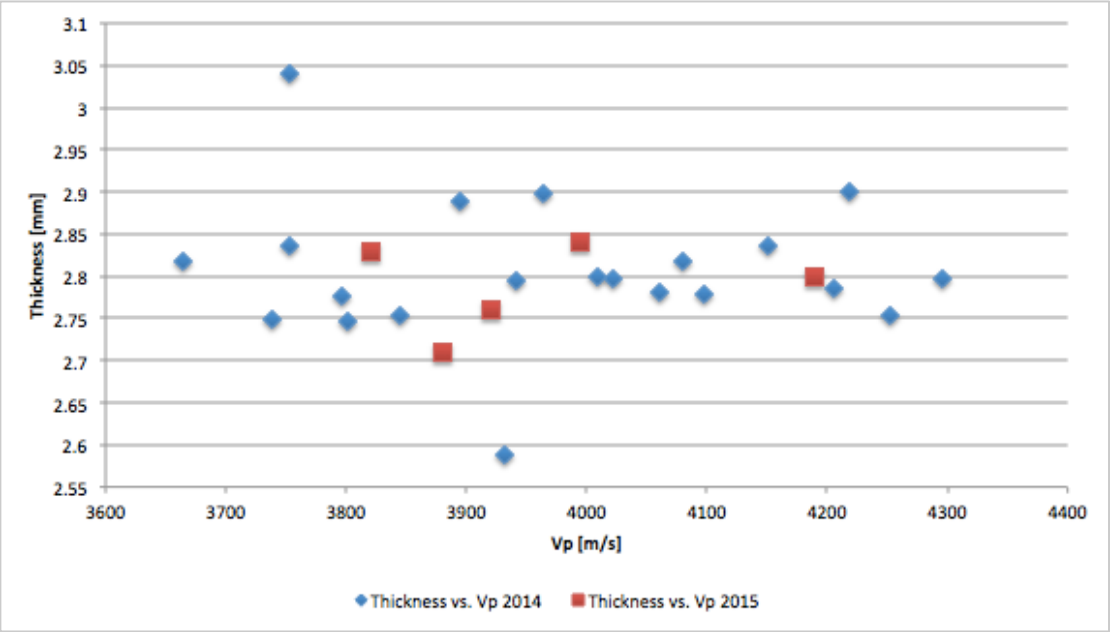

Figure 5-2 Mancos, Thickness vs. Vp. Blue squares are results from (Rugland 2014), and red squares are new results.

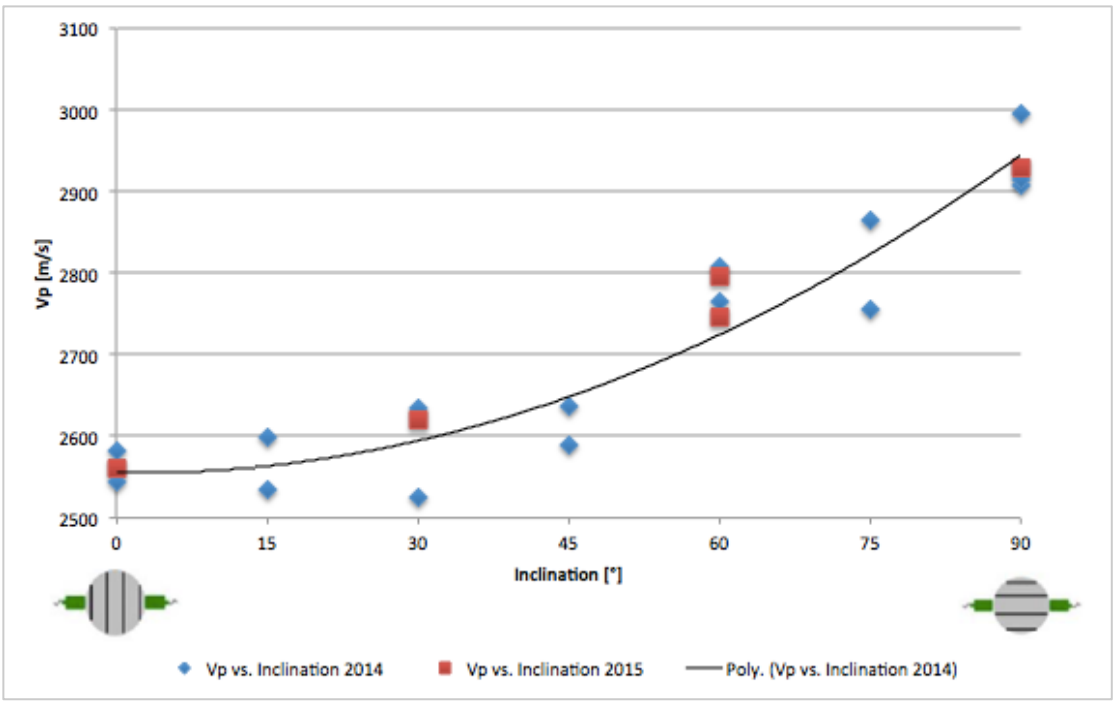

Figure 5-3 Pierre, Vp vs. Inclination. Blue squares are results from (Rugland 2014), and red squares are new results.

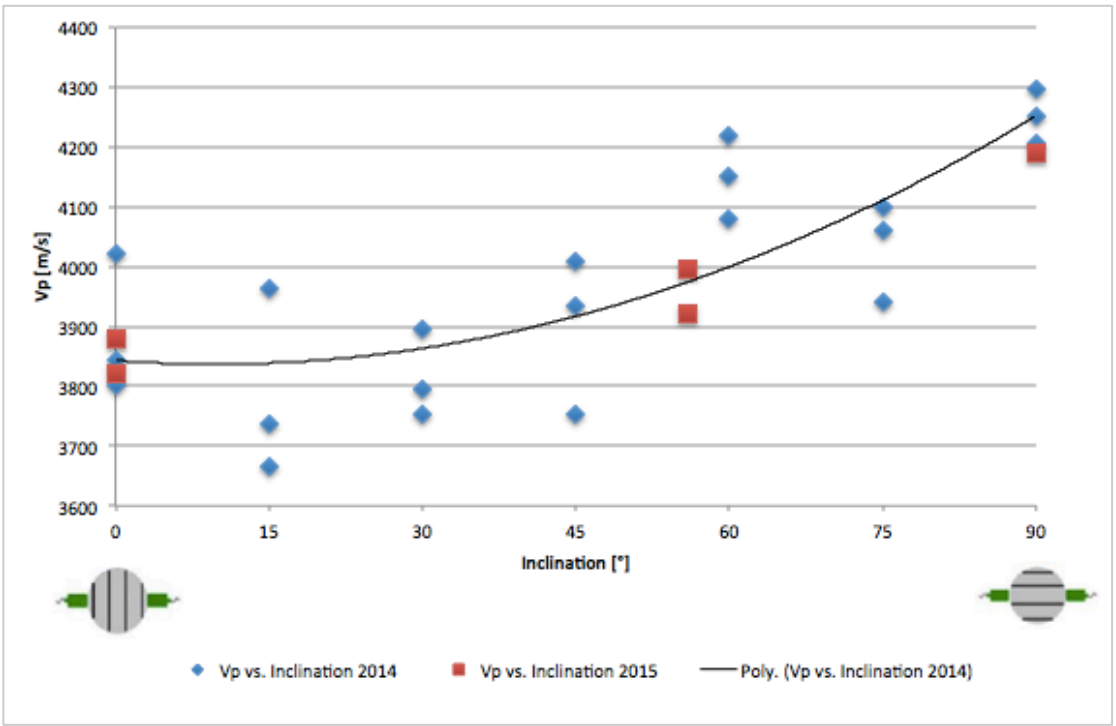

Figure 5-4 Mancos, Vp vs. Inclination. Blue squares are results from (Rugland 2014), and red squares are new results.

5.2 Shale Puncher Results

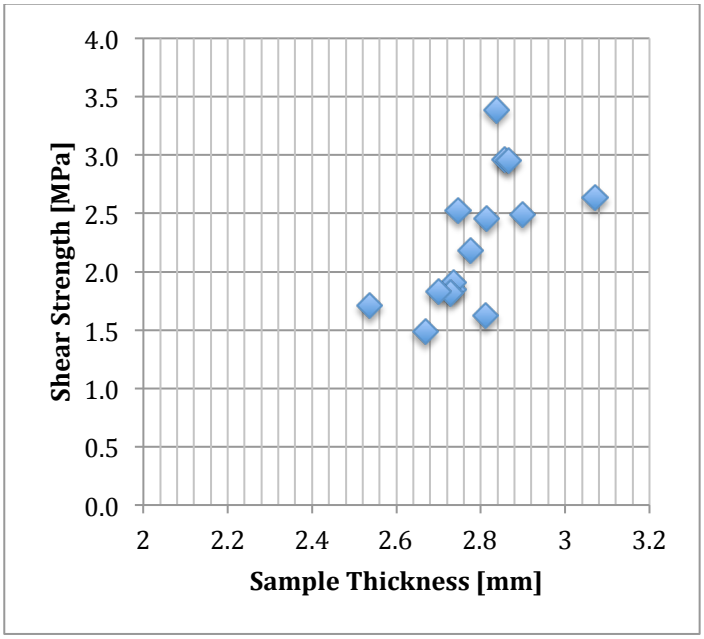

Figure 5-5 Pierre, Shear Strength vs. Sample Thickness (Rugland 2014).

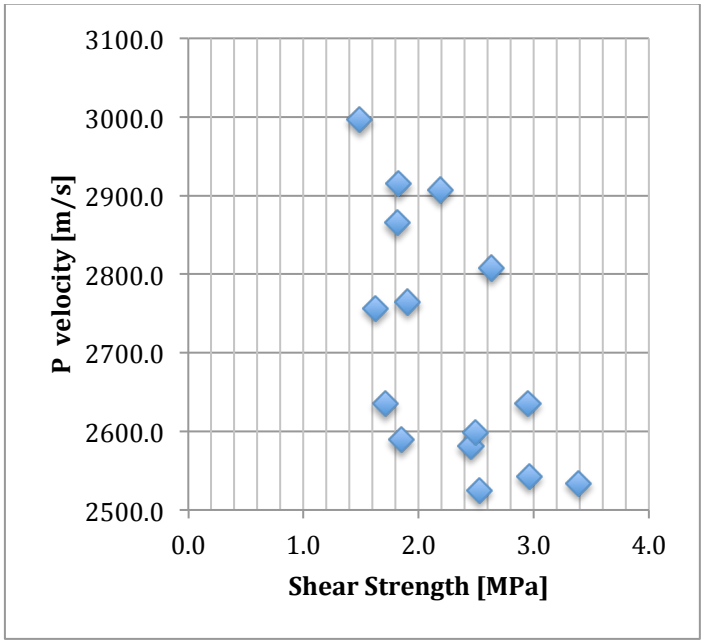

Figure 5-6 Pierre, Vp vs. Shear Strength (Rugland 2014).

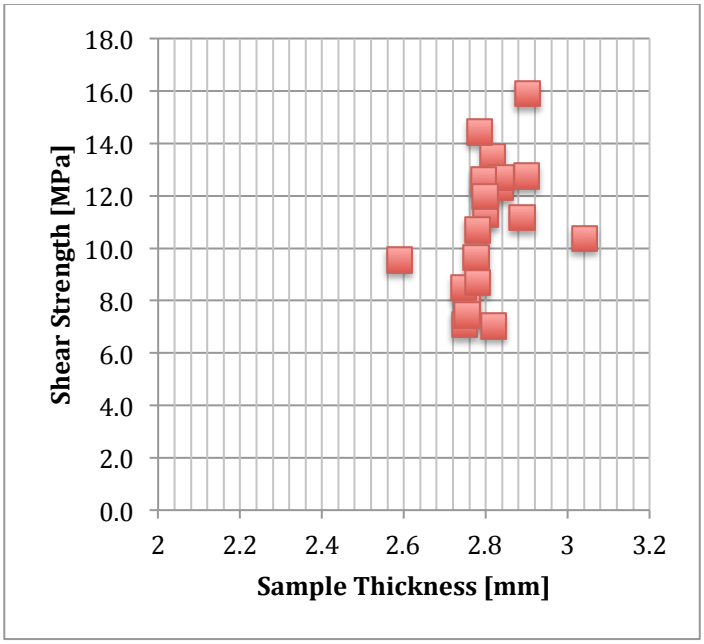

Figure 5-7 Mancos, Shear Strength vs. Sample Thickness (Rugland 2014).

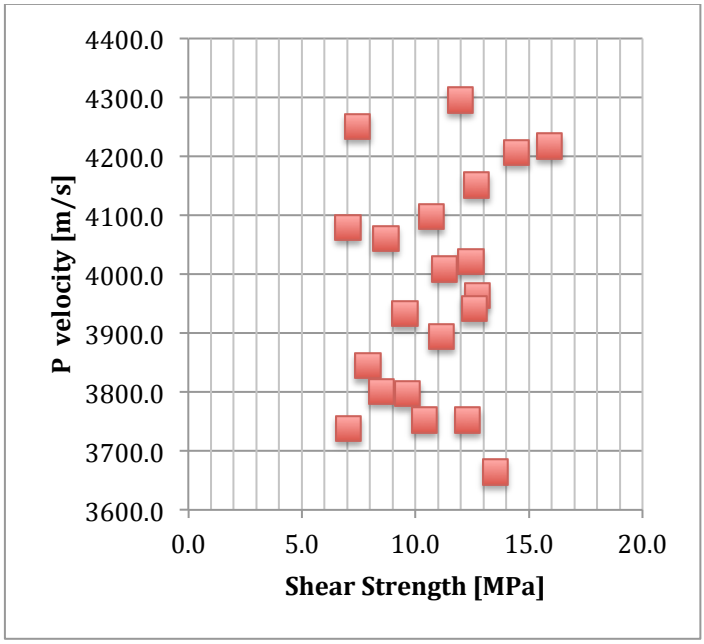

Figure 5-8 Mancos, Vp vs. Shear Strength (Rugland 2014).

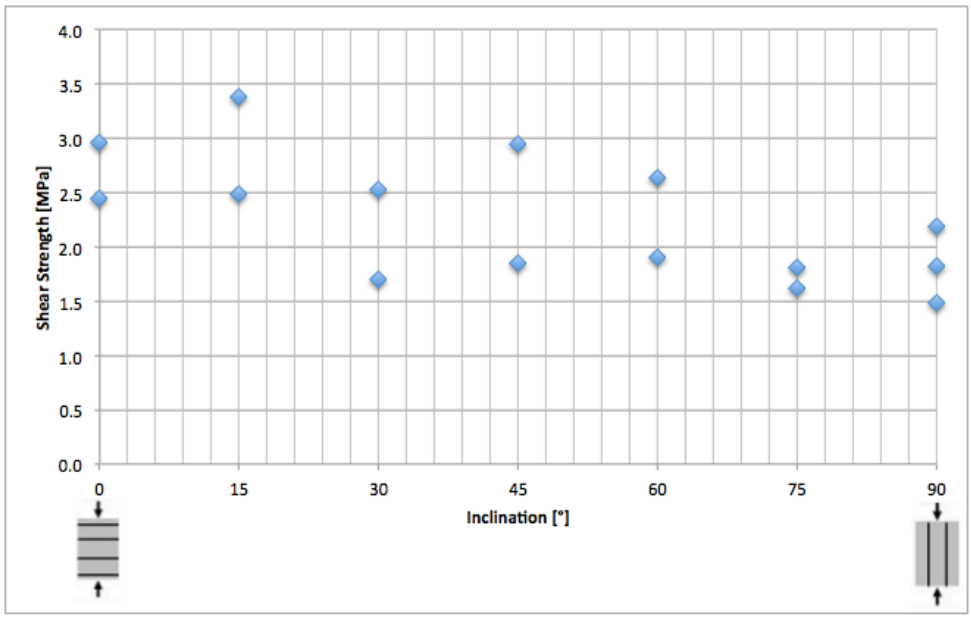

Figure 5-9 Pierre, Shear Strength vs. Inclination

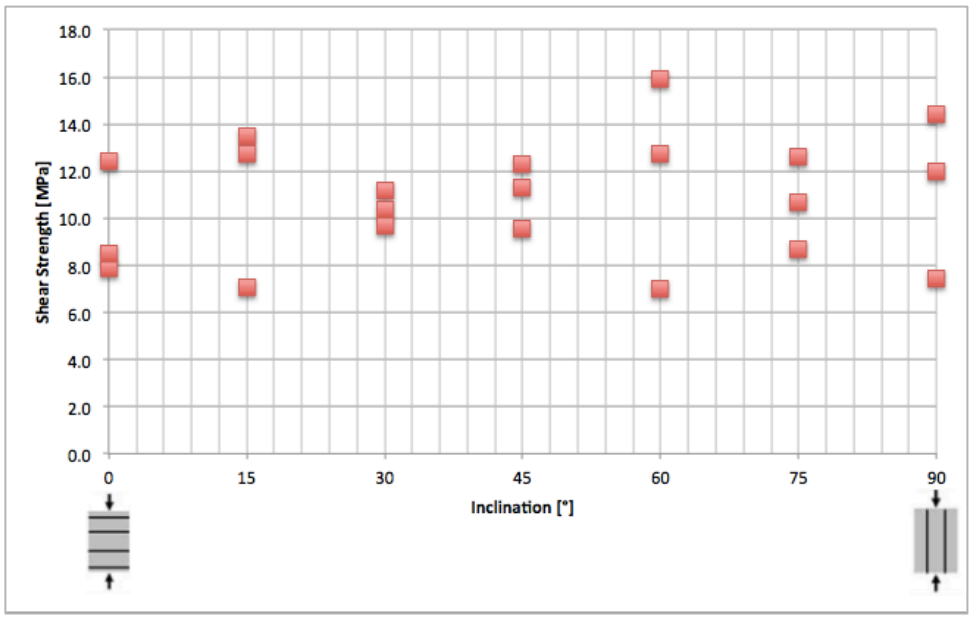

Figure 5-10 Mancos, Shear Strength vs. Inclination

Measurement Type Avg.	Pierre Cohesion, S_0 [MPa]	Mancos Cohesion, S_0 [MPa]
Punch Test	2,25	10,86
Punch Test, w phi	2,39	13,05

Table 5-1 Estimated Average Cohesion (Rugland 2014).

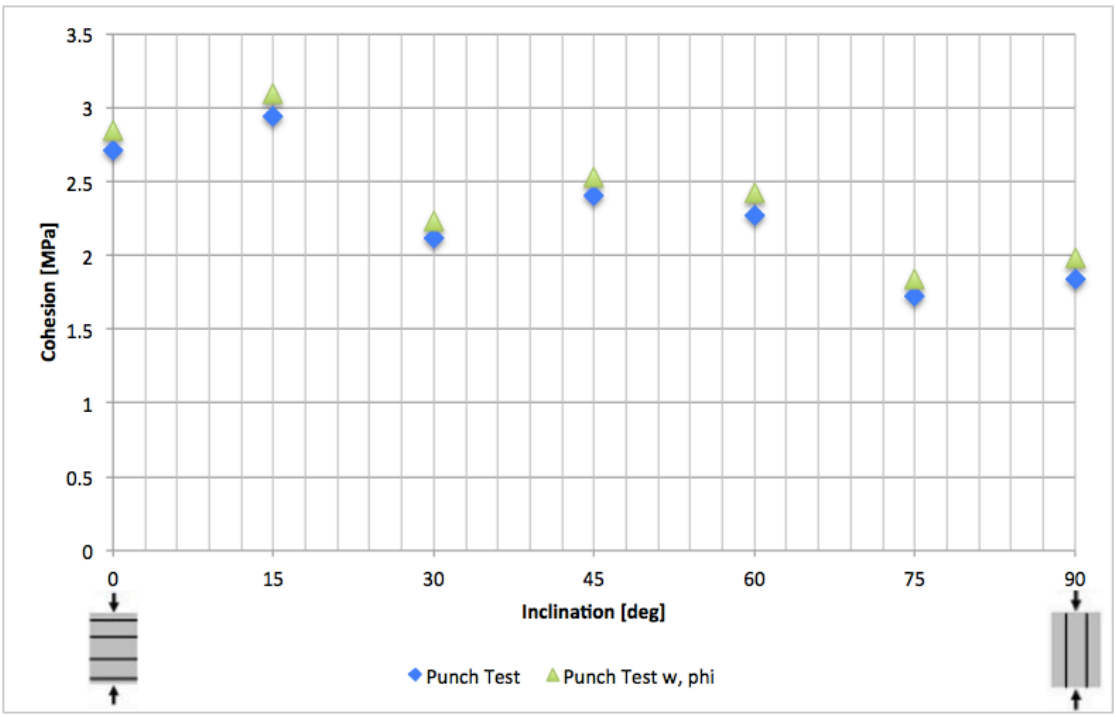

Figure 5-11 Pierre, Avg. Cohesion vs. Inclination

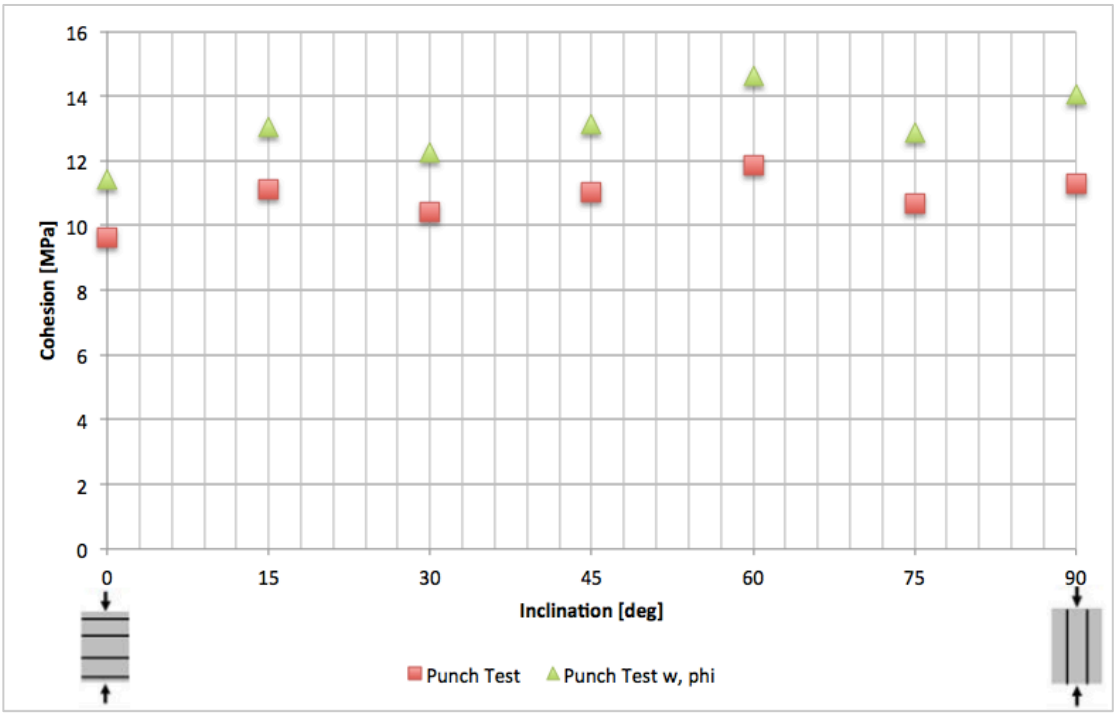

Figure 5-12 Mancos, Avg. Cohesion vs. Inclination

5.3 Scratch Results

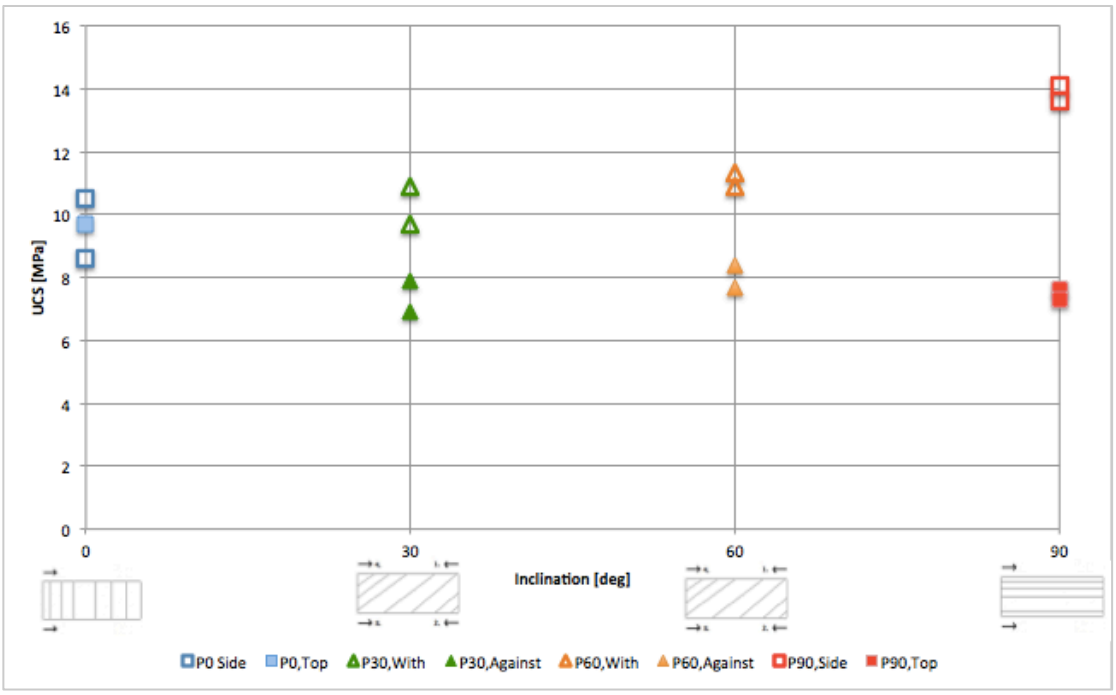

Figure 5-13 Pierre, UCS vs. Inclination. Note that for samples 0° and 90°, samples are turned and scratched for every 90°. See section 4.3.6 for definition of scratch direction.

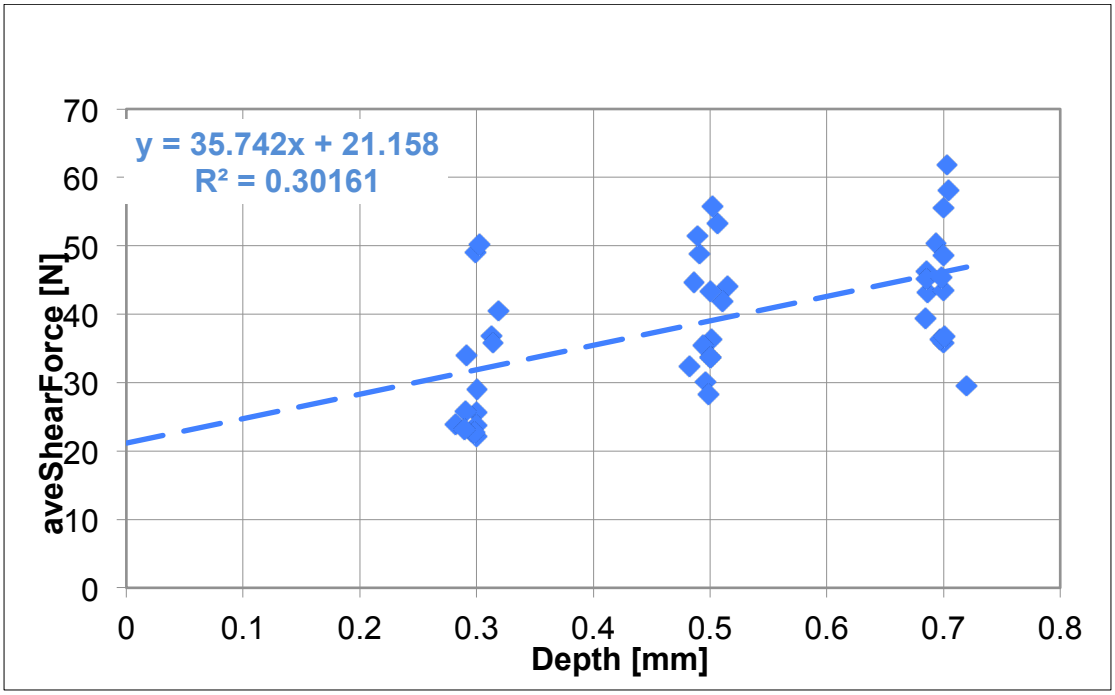

Figure 5-14 Pierre, average shear force vs. depth, for tested samples.

5.4 Brazilian Test Results

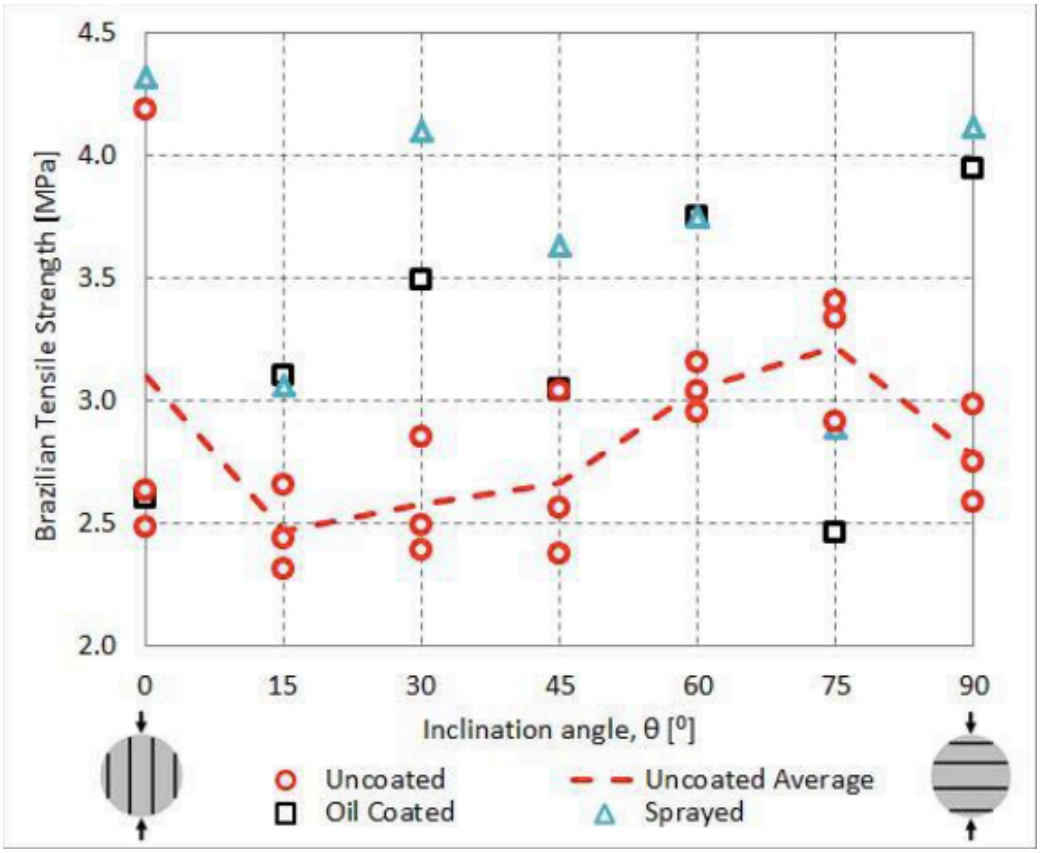

Figure 5-15 Brazilian Test Results presented in (Simpson, et al. 2014).

5.5 UCS

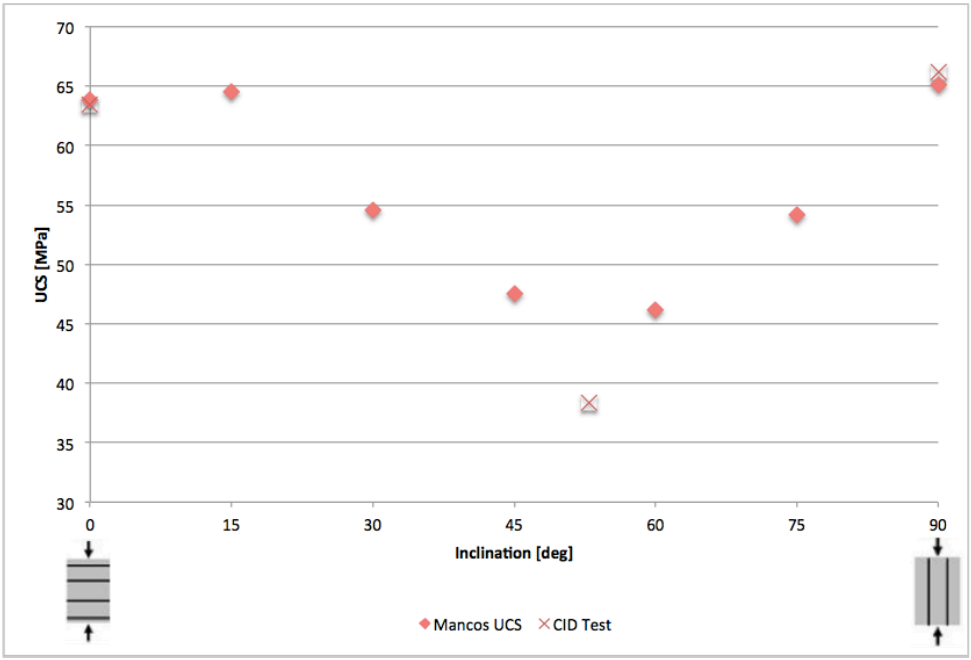

Figure 5-16 Mancos, UCS measurements recreated from (Fjær and Nes 2014). Red squares are results from UCS test, and red crosses are results extrapolated from CID test.

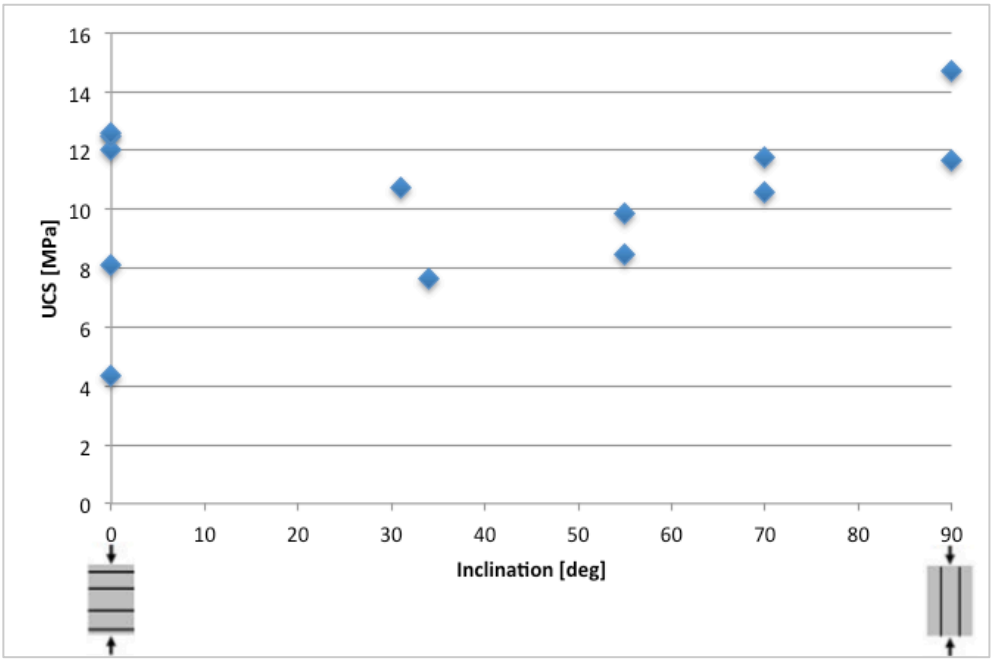

Figure 5-17 Pierre, UCS measurements, performed on small samples, recreated after SINTEF Petroleum, Erling Fjær.

6 Modelled Results

6.1 CWT Relation

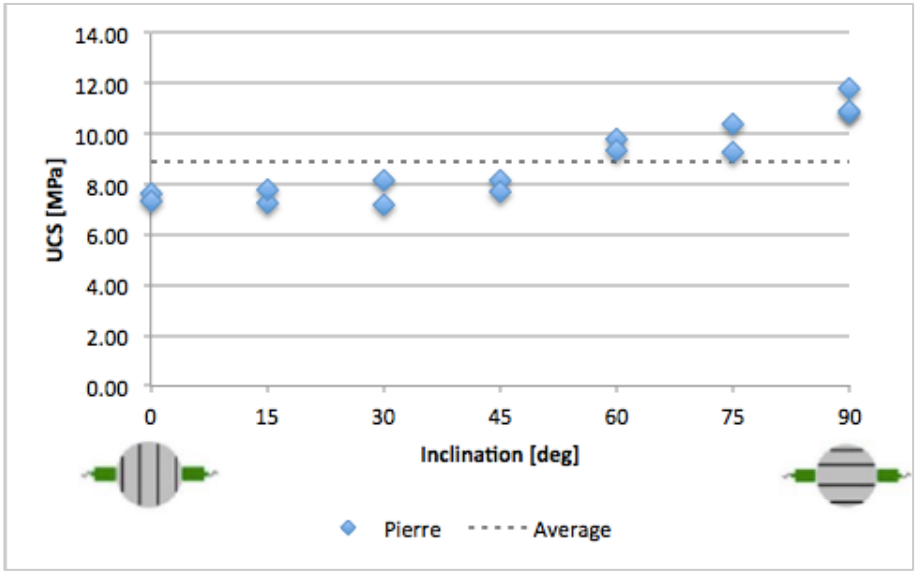

Figure 6-1 Pierre, UCS vs. inclination from CWT correlation.

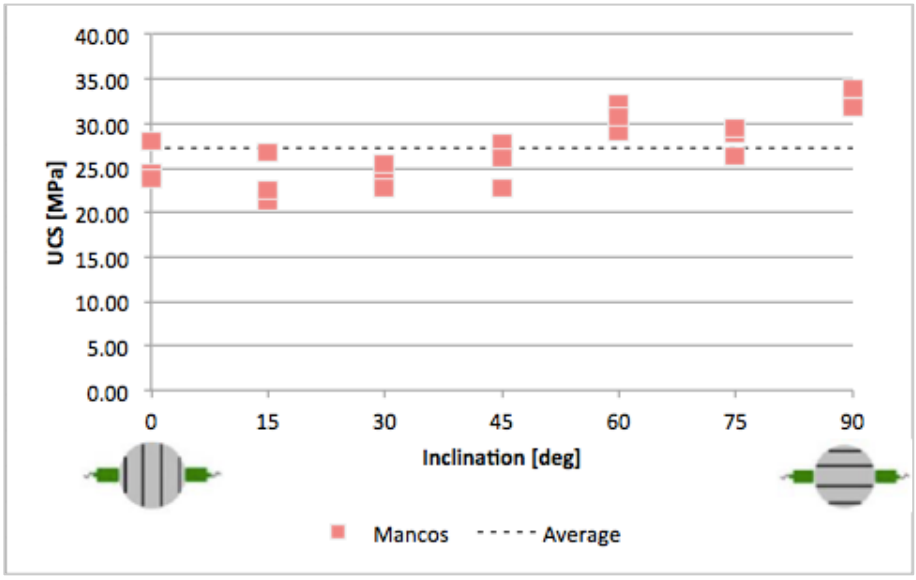

Figure 6-2 Mancos, UCS vs. inclination from CWT correlation.

6.2 Porosity Relation

Sample	Porosity [%]	UCS [MPa]
Mancos	6	25
Mancos	8	18
Pierre	19.2	6.65

Table 6-1 UCS calculated from porosity relation.

6.3 Patchy Weakness Model

6.3.1 Model sensitivity

Parameter	Value	Comment
S_0	2.39 [MPa]	From Punch Results
φ	19.6 [°]	From CWT Results
S_{0w}	1.195 [MPa]	Assumed 50% less than S_0
φ_w	16.66 [°]	Assumed 15% less than φ
η	0 [-]	

Table 6-2 Initial Input for sensitivity analysis.

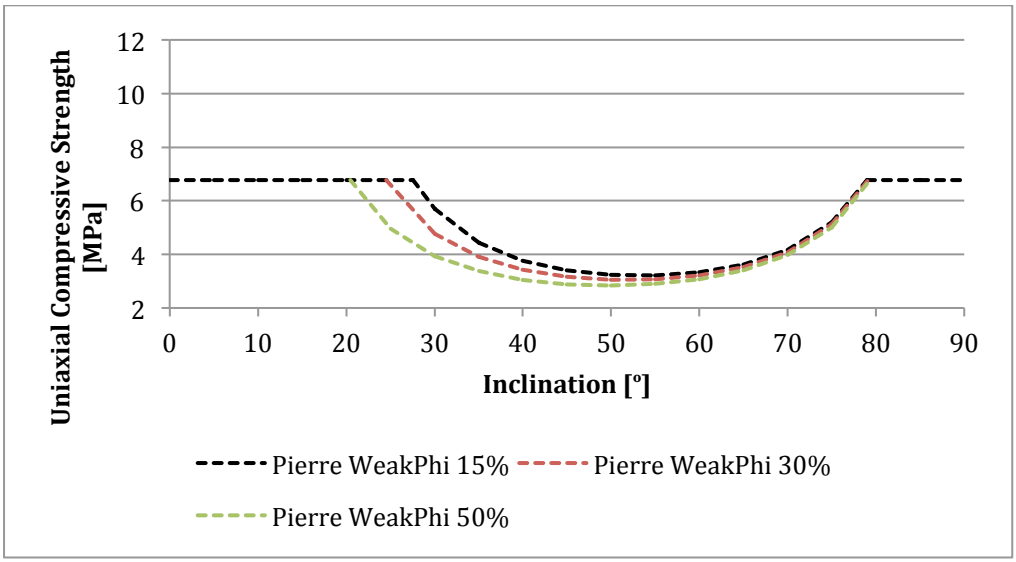

Figure 6-3 Patchy weakness model, Sensitivity analysis, with respect to WeakPhi

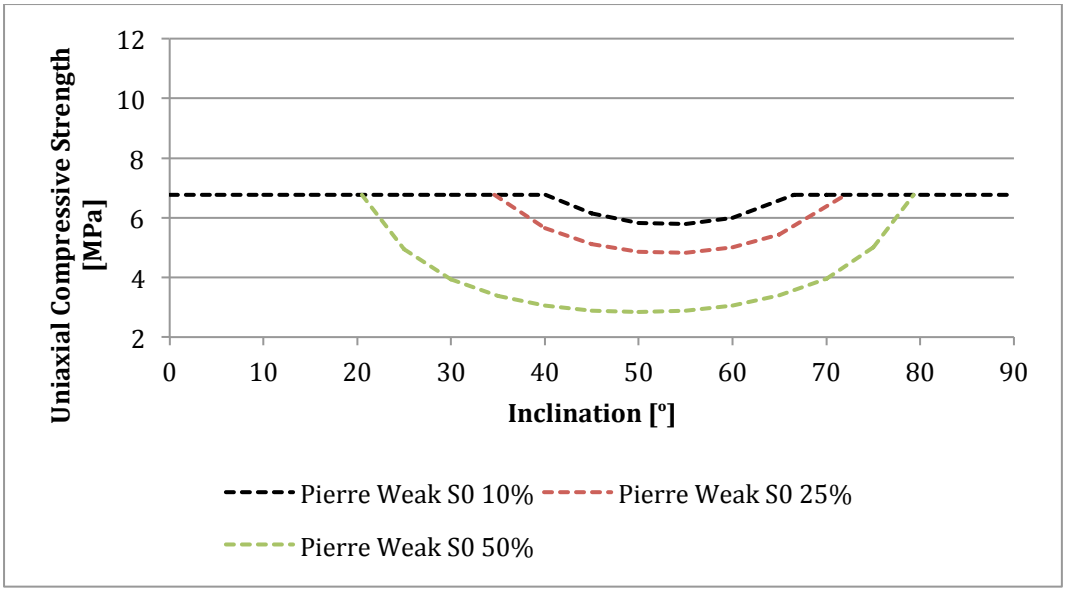

Figure 6-4 Patchy weakness model, Sensitivity analysis, with respect to WeakS0

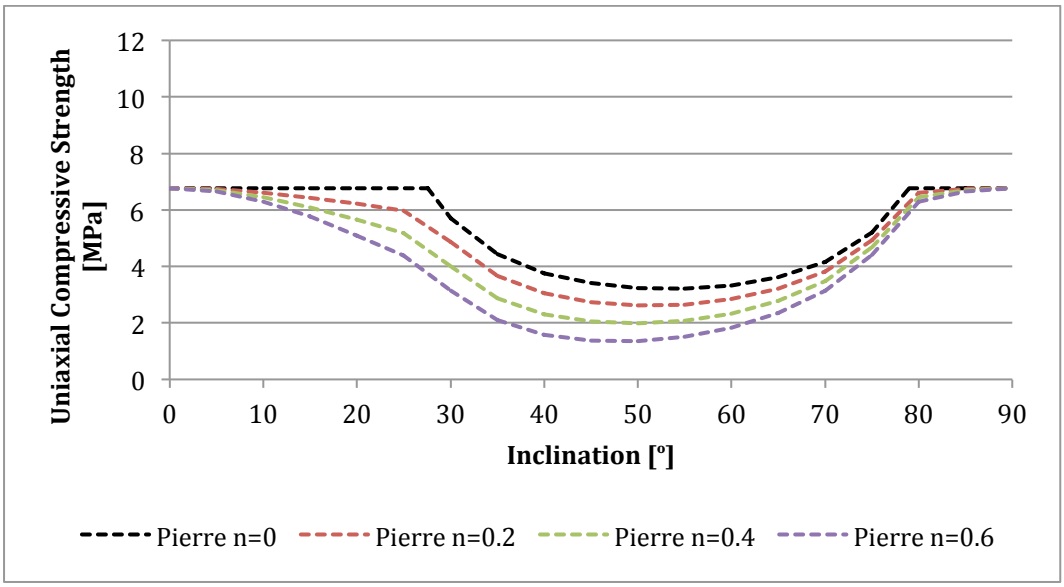

Figure 6-5 Patchy weakness model, Sensitivity analysis, with respect to n.

6.3.2 Pierre, Patchy Weakness Model, from Punch and CWT Results.

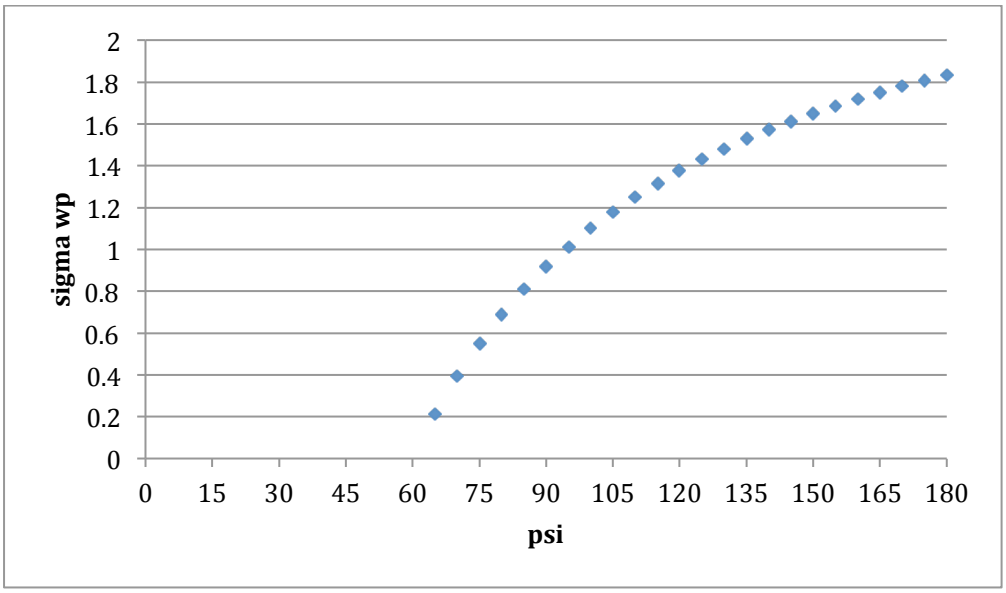

Figure 6-6 σ_{wp} vs. ψ, to determine S_{0w} in patchy weakness model

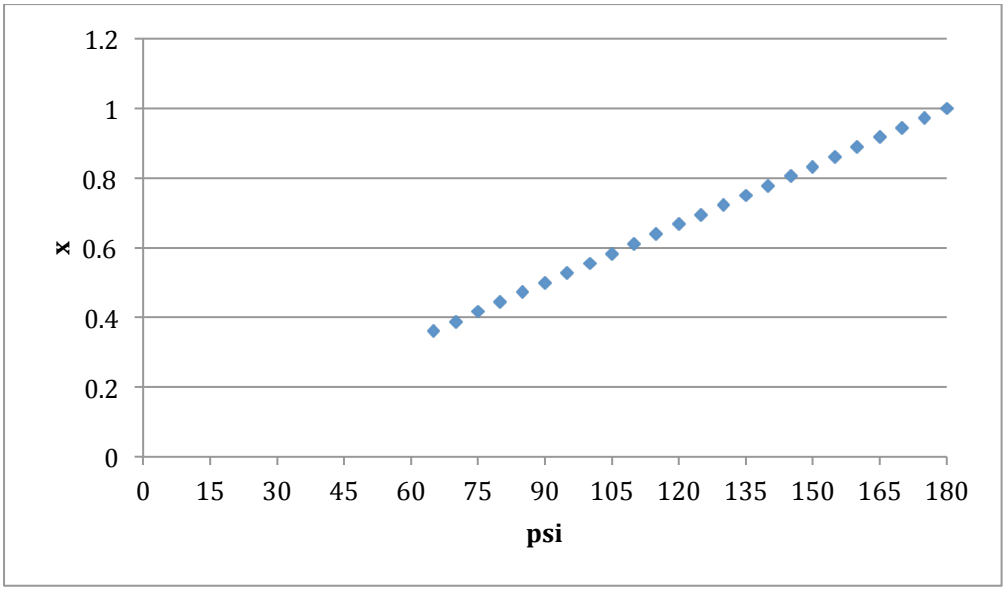

Figure 6-7 x vs. ψ, to determine S_{0w}in the patchy weakness model.

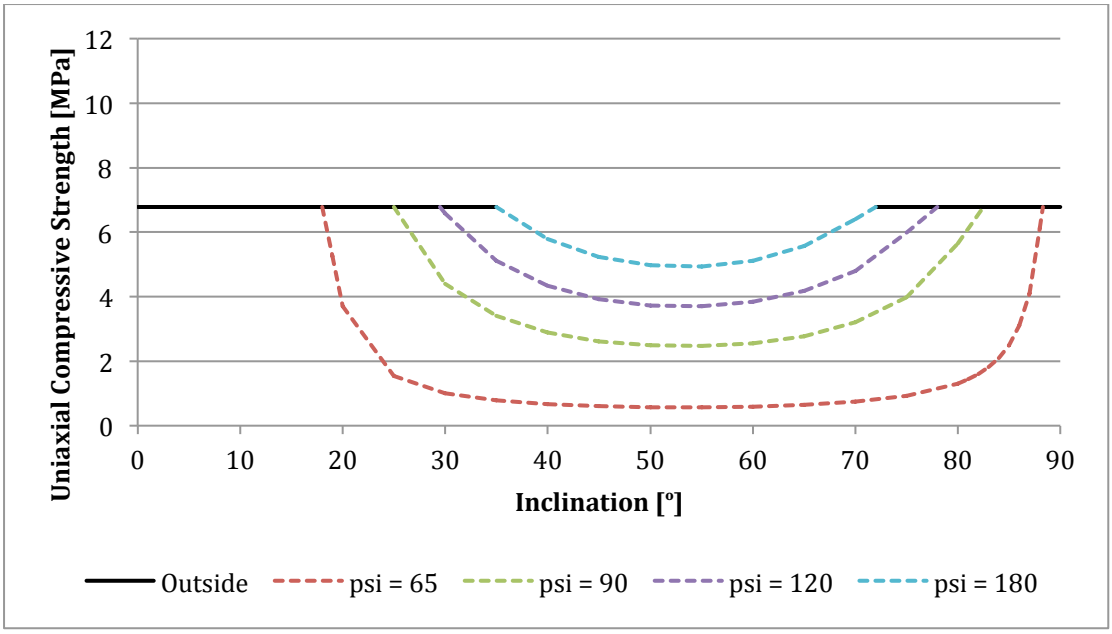

Figure 6-8 Patchy Weakness model for Pierre according to data from the Punch test and CWT results. Note n=0.

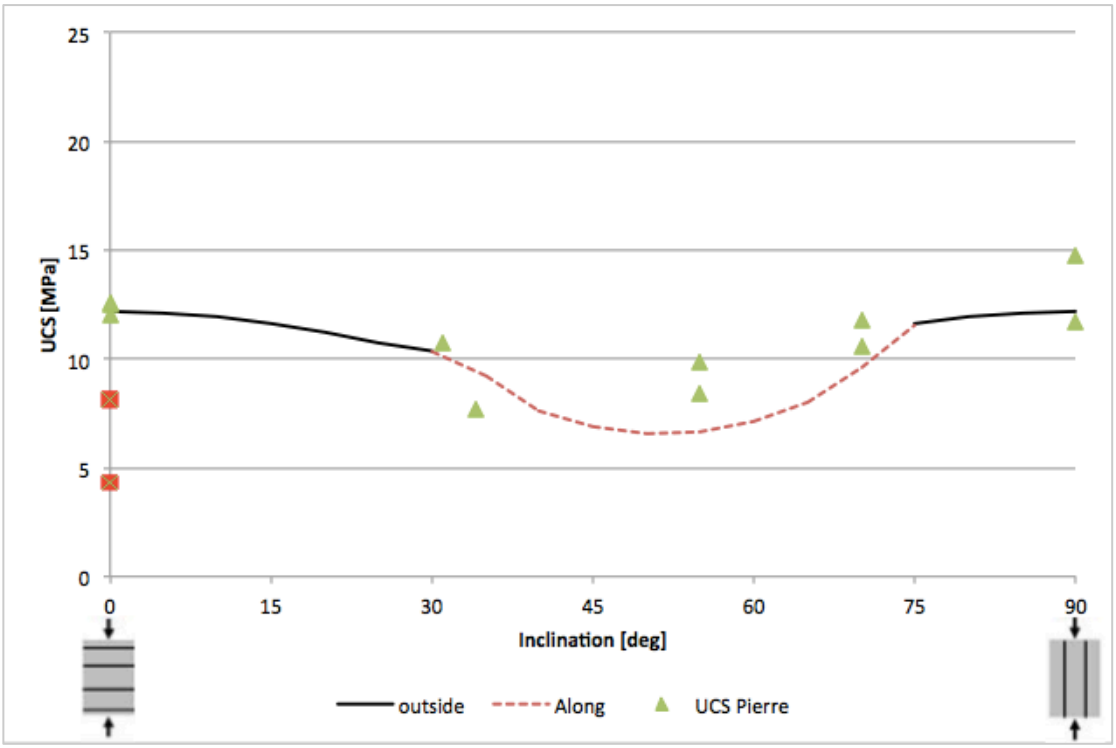

Figure 6-9 Patchy weakness model fitted to UCS datapoints for Pierre. Red squares are neglected measurements, and green squares are measured UCS results.

6.3.3 Mancos Patchy Weakness Model.

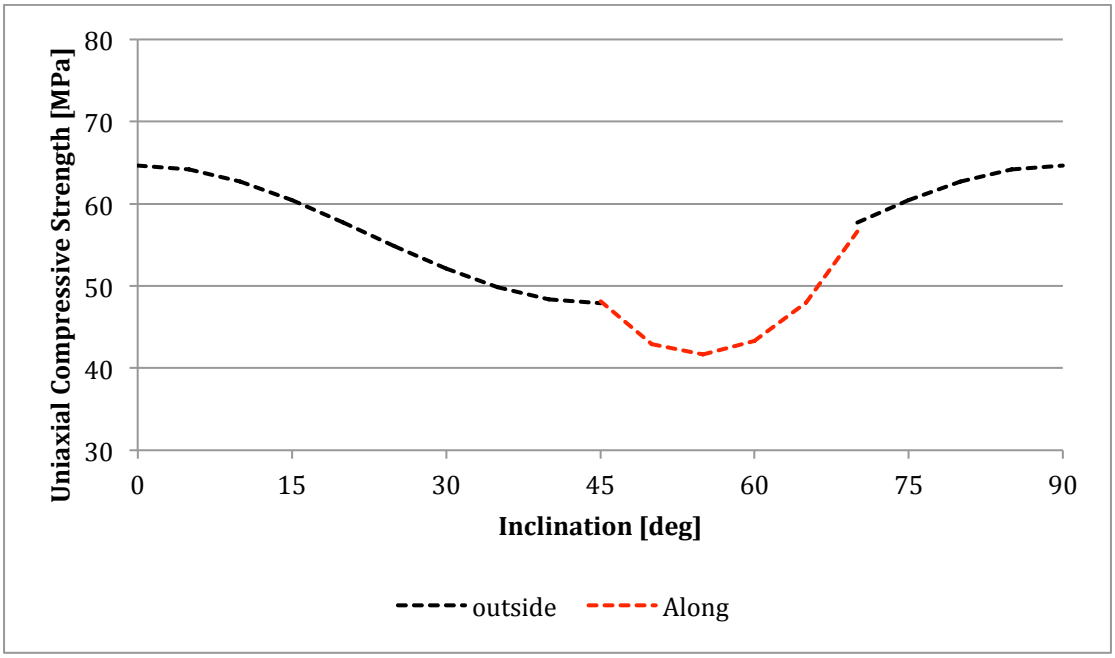

Figure 6-10 Mancos Patchy weakness model reproduced after data from (Fjær and Nes 2014).

Parameter	Value
S_0	18.3 [MPa]
φ	31 [°]
S_{0w}	16.8 [MPa]
φ_w	25.8 [°]
η	0.26 [-]

Table 6-3 Best fit parameters for Mancos after (Fjær and Nes, The impact of Heterogeneity on the Anisotropic Strength of an Outcrop Shale 2014)

7 Discussion of results

This chapter will discuss and explain the presented results from the previous chapter. Discussion of results is divided into different parts:

- A study of the actual results achieved from the tests and a comparison study between these to see if and how these results correlate.
- Use of the patchy weakness model, with a sensitivity analysis.
- A UCS comparison and expectation discussion. Including discussion on what information can be obtained by the test with respect to inclination, maximum and minimum measurements.
- An investigation concerning strength anisotropy and heterogeneity.

7.1 CWT

7.1.1 Validation of tested samples

The CWT measurement performed on the tested rocks was first used as an identification tool to compare the similarities from tested results from (Rugland 2014) and results with respect to the tested samples in this thesis. The CWT measurement a rock exhibit, may be compared to each other, and it is expected that similar or identical results may be used to tell at which degree an equality of the rocks presented is present. Pierre and Mancos samples from (Rugland 2014) are taken from the same block of rock as in this thesis. Therefore similarities are to expect. This is clearly the case and may be seen from Figure 5-1 and Figure 5-2. Where the same behaviour of the tested rocks is the situation. This indicates that comparing results from (Rugland 2014) and tested results may be continued. As it is the same block of rock, possible inequalities are expected to be due to local rock difference, concerning heterogeneity and anisotropy.

7.1.2 Thickness dependence

The acoustic wave velocity is calculated as a function of thickness of the presented sample. The measurement should therefore be independent of thickness. This is shown in (Stenebråten, et al. 2008). The results can be seen in Figure 7-1. Several materials were tested in order to justify this theory. The tested specimens for each series were cut with the same inclination to bedding.

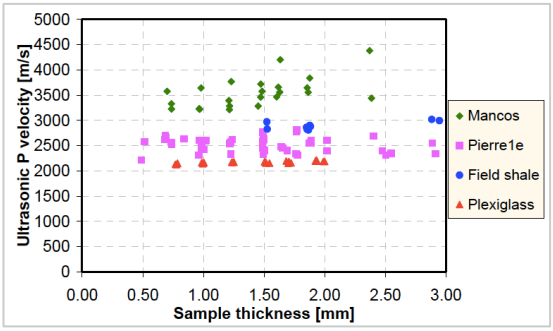

Figure 7-1 CWT independence of sample thickness (Stenebråten, et al. 2008).

Results presented for Pierre, sample thickness vs. V_p, in Figure 5-1 shows a scattering of data points along a thickness axis around 2.8mm. The same is seen for Mancos, sample thickness vs. V_p in Figure 5-2, but a lot more scattering is present. This may be referred to as the inclination effect. This effect is expected when measuring acoustic velocity in sedimentary-layered samples with respect to bedding inclination. Another reason of the scattering seen for Mancos is the consequence of local heterogeneity. Explained in 3.1.4, Mancos is highly heterogenic. This is also seen from the pictures presented in the same section. Mancos contains a lot of quartz, which enhance the velocity measurement. If quartz is present in the tested area (or parts of the area) between the two transducers higher readings will be recorded. Therefore the velocity measurement for Mancos also becomes a function of quartz content.

7.1.3 Inclination effect on velocity measurements

The inclination effect may be explained due to the angle of the layering of the rock relative to the transducers. Figure 5-3 and Figure 5-4 presents, respectively V_p vs. inclination for Pierre and Mancos samples. Clearly an increase in V_p from 0° to 90° can be spotted. This is the inclination effect. Figure 7-2 illustrates this effect. A layered rock sample is constructed of layers with different (small variations is

enough) properties. Only small property change will yield a difference in measurements. For a sample situated 0°, where P-wave velocity measurement is performed normal to the bedding, waves has to go through all the layers to reach the second transducer. Waves therefore arrive more or less at the same time. For the case of 90°, the P-wave velocity measurement is performed parallel to the layers. At some layers the waves travels faster, and other layers slower, this is indicated in the figure where the light grey layers are denoted V_p,1 and dark grey layers V_p,2 where V_p,1 > V_p,2. Waves traveling through layer V_p,1 will arrive at the second transducer before waves travelling in V_p,2. Hence the V_p from the fastest layers is reflected. Therefore this effect is expected for the measurement performed on shale. If a complete homogenous and isotropic material is tested, in theory velocity measurements should be the same independent of inclination.

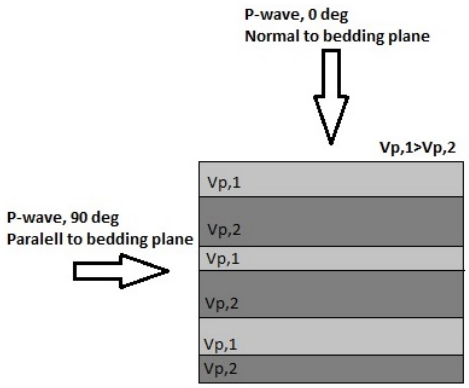

Figure 7-2 Inclination effect on CWT measurements (Rugland 2014).

CWT measurements on Mancos with respect to the inclination has been investigated in both (Simpson, et al. 2014) and (Torsæter, Nes and Rinna 2012). Velocity measurements compared to the obtained results in this thesis are almost identical. With a minimum measurement at 0°, at $3850 \pm 20\ m/s$ and a maximum at 90°, at $4190 \pm 50\ m/s$. Clearly results are highly comparable. Also confirming that previous tested rock may be compared to other results in this thesis.

7.2 Shale Puncher

7.2.1 Thickness dependence

Figure 5-5 and Figure 5-7 presents respectively shear strength vs. sample thickness for Pierre and Mancos samples. It is expected that the test is unaffected by the sample thickness. This is confirmed by the two figures. Data are scattered along thickness around 2.8mm. Only small variations of thickness in presented data are the case. Samples where prepared with a target thickness of 2.8mm, variations are therefore close to this value. This is also confirmed in (Stenebråten, et al. 2008). Scattering of data from the figures indicates that the punch test is in some degree affected by sample-inclination and/or local heterogeneity.

7.2.2 Strength dependence with respect to P-wave velocity

P-wave velocities presented in the previous section, are plotted against calculated shear strength from the shale puncher, for Pierre in Figure 5-6 and for Mancos in Figure 5-8. From the data shear strength do not seem to increase with increasing velocities. Each measurement for the shear strength is calculated from the measured peak force of that specific sample. Also explained in the previous section the inclination effect affects the CWT measurements. It is a reasonable assumption that the puncher is less affected by inclination than the CWT, yet it is assumed to some degree a minimum and maximum measurement of the shale puncher. The next paragraph will discuss the scattering of measured data.

7.2.3 Inclination and Heterogenic effect on measurements

With equations from 4.2.2, Figure 5-9 and Figure 5-10 presents shear strength vs. inclination for Pierre and Mancos. In the first figure, for Pierre, a small trend may be spotted. A maximum measurement obtained at 0° and a minimum value at 90°. This is as expected, and is previously explained in section 4.2.2.3. For inclinations between these two maximum and minimum, inclinations does not seem to affect the results at an abnormal degree. Especially for the Mancos case the data is strongly scattered, and measurements with respect to inclination does not seem to be affected at all. Two

explanations are the case. First investigating how the puncher breaks the rock sample. Figure 7-3 illustrates this, where light grey layers are stronger, and dark grey layers are weaker. For inclination 0°, bedding are normal to pistons. This means that for the sample to break all the layers has to be broken. Indicating a higher strength, intrinsic strength. For inclination 90°, the layers are parallel to the bedding. Pistons may therefore be situated between two layers, or at the edge of one, and break is affected by the positioning. A lower strength is expected parallel with the bedding.

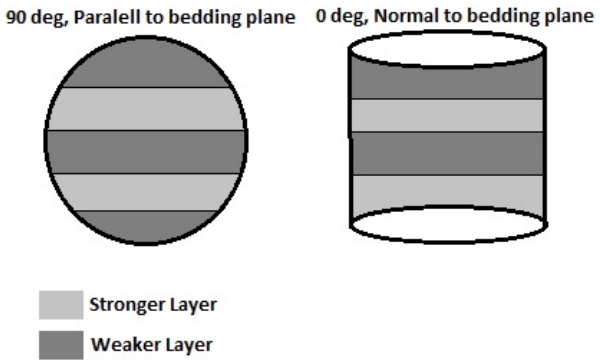

Figure 7-3 Layering of tested samples in the Shale Puncher (Rugland 2014)

In a standard uniaxial test the sample fails according to the weakest layer in the sample. Shear failure is initiated. For the puncher, all the layers have to be broken; hence it cannot choose which plane fails. This is a factor, which impact the scattering of the data seen in Figure 5-9 and Figure 5-10. From this discussion it can be concluded that drill cuttings, where inclination is unknown or cannot be determined, test result would still yield valuable information. This means that the test in conjunction with the CWT is useful in many areas. But then also reduce the ability to determine strength anisotropy of the sample. In some cases, as for Pierre, results from maximum and minimum measurements may be useful in modeling strength, but for other cases as for Mancos, results may not be used for strength modeling.

The second reason for strong scattering of Mancos results in Figure 5-10 is the degree of heterogeneity in Mancos. Pierre is a more homogeneous material, but it still contains some degree of local heterogeneity. As Mancos is highly heterogenic, shale puncher results are strongly affected by this. The quartz content in a small sample may be a lot, and quartz yield higher strength. As the puncher has to break all layers,

the degree of quartz content affects the measurements. This is the main reason the large scattering of data seen in Figure 5-10. Comparing the degree of scattering in Pierre and Mancos results, Pierre is in the range of $\approx 1Mpa$ for the maximum variation of data within an inclination step, while variation for Mancos ranges $\approx 10Mpa$. Clearly the degree of heterogeneity is strong in Mancos, and lower in Pierre.

7.2.4 Cohesion

Cohesion is as explained in section 4.2.2 calculated and presented in Figure 5-11 and Figure 5-12 for both Pierre and Mancos. Cohesion results are averaged from shear strength calculations, and plotted with inclination. Described in section 4.2.2, the friction angle φ is the difference from $\sigma_{measured}$ and the true cohesion point S_0. This friction angle may be estimated by use of the CWT measurements in accordance to equations presented in section 4.2.2.2. Using this relation a strong estimation of cohesion may be computed. Average cohesion for Pierre and Mancos including friction angle is presented in Table 5-1. Estimated cohesion correlates well with findings from (Rademakers 2010), where an extensive set of Pierre samples are tested. Cohesion results from (Stenebråten, et al. 2008) are too high concerning puncher results, but correlate with the CWT and triaxial compression test results. The cohesion calculations are in fact very sensitive to the geometry of the clamping and punching pistons presented in 4.2.2. A difference here may be the factor separating the other test results from the puncher.

By use of the theoretical assumption in 7.2.3 maximum (intrinsic) and minimum cohesion from Pierre results are calculated for further use in the patchy weakness model. This is calculated by use of the equations presented in 4.2.2.3.

7.3 Scratch Test

7.3.1 Performed measurements and typical test plots

Scratch measurements in this thesis are only performed for Pierre. Original plan was to investigate Mancos for the same scratch directions performed on Pierre to compare results. Unfortunately the scratch device was out of order due to worn bearings. Testing on Mancos was started, but already at the first scratch series measurements showed abnormal results. This can be seen in Figure 7-4. The scratch device at SINTEF Petroleum is the first model introduced by TerraTek, and new bearings would have to be ordered outside the country and time would not suffice. UCS comparison for Mancos is therefore performed without the Scratch results. Pierre was tested at an earlier stage and results are promising.

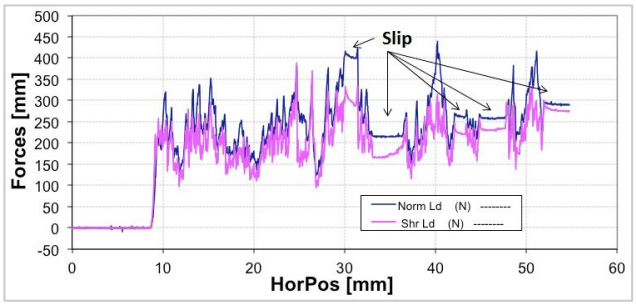

Figure 7-4 Scratch Mancos. Effect of worn bearings are indicated with black arrows, where the scratch device slips, meaning horizontal measurements continuous while scratch housing is stuck.

Typical test plots are presented in Figure 7-5 and Figure 7-6. Left plot is the shear force vs. horizontal position. Black solid lines are average values for each scratch depth. Measurements increase for increasing depths. This indicates the theory behind the scratch measurement, where UCS and specific energy is calculated. The right figure is the corresponding normal plot vs. horizontal position.

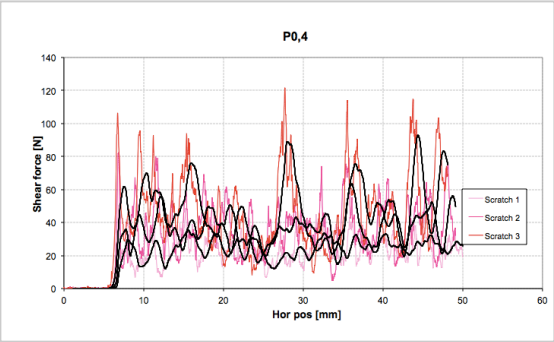

Figure 7-5 Typical test plot, shear force vs. horizontal position. Tested sample are Pierre 0°. Note the black solid lines are average.

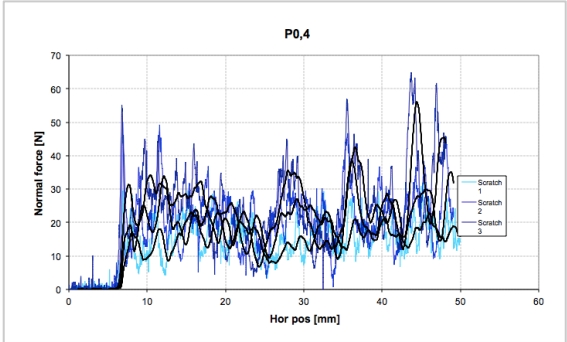

Figure 7-6 Typical test plot, normal force vs. horizontal position. Tested sample are Pierre 0°. Note the black solid lines are average.

7.3.2 Scratching as a function of inclination

Scratching was done as a function of direction as illustrated in 4.3.6. Results can be divided into three groups. 1. for 0° inclination. 2. between 0° and 90° inclination, in this case 30° and 60°. 3. for 90°. All scratch series consists of depths: 0.2, 0.3, 0.5, 0.7. Collected scratch data for all samples and directions, where shear force vs. depth is shown in Figure 5-14. Clearly similar depths are the case for all the samples. Scattering of data is explained by direction of scratch, and is further discussed in the next paragraphs. The raw data obtained from the test are further analysed in a pre-made excel sheet. Data are plotted for each depth, with corresponding normal, and shear force, and a linearization process determines the UCS. This is also explained by the equations presented in 4.3.4.5. This is assumed to be a good estimation of UCS as the measurement is a direct and continuous measurement of the rock presented.

For 0°, four scratch series were performed, turning the sample and measuring for every 90°. Only three of the series could be used in further analysis as sample fractured for the last test series. In Figure 5-13 scratch measurements at 0° are indicated by the blue squares, where open squares are the sides of the sample, and filled square are the top. Data point values are close to each other, and scattering is very small. Scratching on a sample where bedding is situated normal to the cutter, the knife has to scratch across the layers independently of direction of sample. Similarities in measurements are therefore as expected and results reflect the theoretical expectations.

The inclinations between 0° and 90°, are presented in Figure 5-13, where 30° correspond to the green triangles, where open triangles are scratching with bedding and closed triangles are scratching against bedding. 60° correspond to the orange triangles, where open triangles are scratching with bedding and closed triangles are scratching against bedding. For both 30° and 60°, a difference in estimated UCS values concerning scratch direction with or against bedding is seen. This may be explained by use of Figure 7-7 and Figure 7-8. First the case where scratch direction is situated with the bedding as seen in Figure 7-7 in the left illustration. The cutter can be divided into maximum and minimum principal stress. In 1. The largest arrow indicates the maximum, and the smaller arrow the minimum. The corresponding measurement in a UCS test would be the illustration 2. in the middle. Where measurement are performed normal to the bedding. Hence the resulting UCS value would be in the range marked by the red circle in illustration 3. in Figure 7-7, in the maximum range. For increasing inclination the corresponding UCS test would approach a situation where maximum principal stress is situated parallel to the bedding. Which equals the theoretical minimum in a scratch test, since scratching is performed parallel to the bedding in length direction.

For the situation where scratching is performed against bedding, the same explanation is applied by use of Figure 7-8. Illustration 1. indicates the maximum and minimum principal stress, where illustration 2. Is the corresponding UCS test. The corresponding UCS test is the situation where test direction is parallel to the bedding. Scratching against bedding would therefore yield a lower value according to illustration 3. This may be one explanation for the difference in measured results in Figure 5-13.

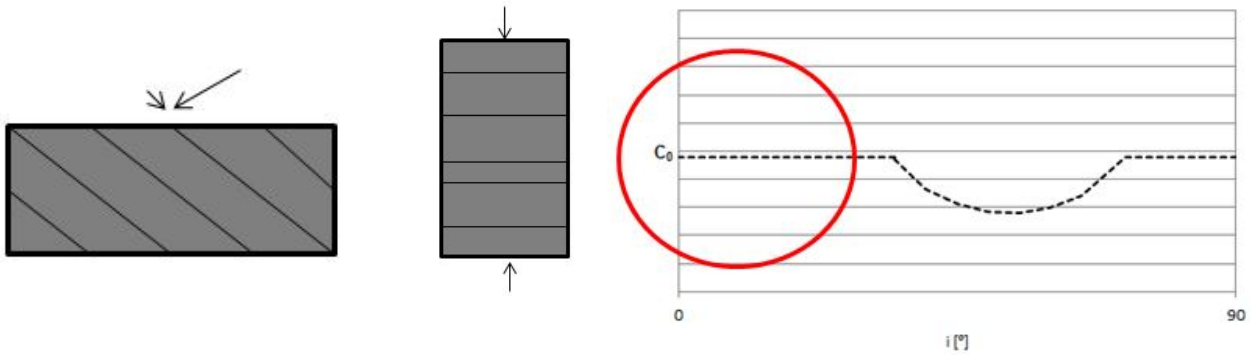

1. 2. 3.

Figure 7-7 Scratch with bedding, 1. Indicated the max and min principal stress. 2. The corresponding UCS test. 3. The corresponding characteristically UCS vs. inclination plot.

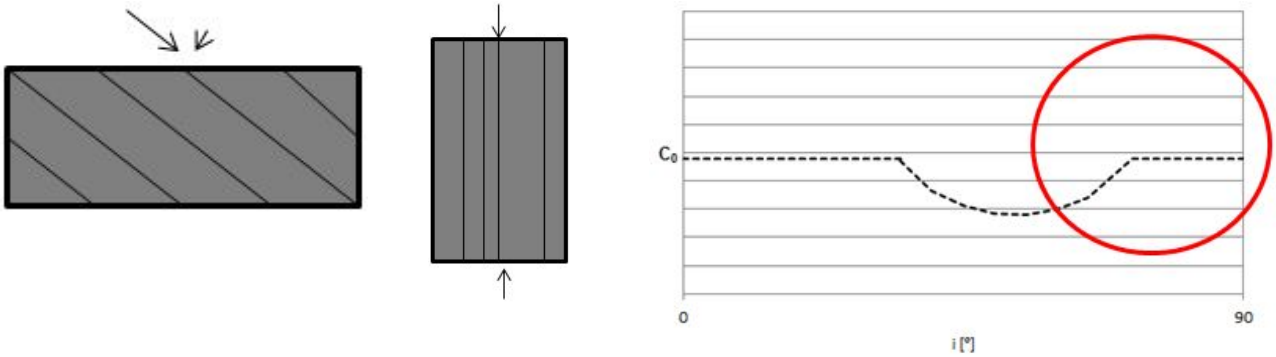

1. 2. 3.

Figure 7-8 Scratch against bedding, 1. Indicated the max and min principal stress. 2. The corresponding UCS test. 3. The corresponding characteristically UCS vs. inclination plot.

For 90° inclination, results in Figure 5-13 are indicated by the red squares, where open squares are the sides of the sample, and closed squares are respectively top and bottom. As shown in Figure 4-36. A difference in estimated UCS values as a function of direction is seen in the results. According to 4.3.4.2 this is expected, as scratching parallel to the bedding would yield a lower value, and across bedding lengthwise would yield a higher value. This measurement may be the best presented in this thesis concerning strength anisotropy. Scratching parallel to the bedding is seen as the weakest, or minimum reading in a theoretical aspect. This may indicate the minimum UCS estimate of the rock. While scratching across bedding lengthwise, would indicate the maximum. If this is assumed, it is possible to determine the degree of anisotropy by use of the scratch device where a sample is drilled parallel to the bedding, e.g. 90° inclination. The estimated difference is around 6MPa.

7.4 Brazilian Test

Results for the Brazilian test is reconstructed after (Simpson, et al. 2014). These results are presented in Figure 5-15. Data are divided into three groups, were tested specimens were either uncoated, sprayed or oil coated. Investigating all the data, inclination does not seem to affect the measurement. With this said for the oil coated samples (black open squares) and the sprayed (blue triangles) showing a higher value and more scattered than the uncoated. This may be explained as any type of coating will supress any flaws within the sample, not giving a realistic measurement of the actual situation in the sample.

Looking only at the uncoated samples, a possible trend within strength anisotropy can be seen. The red dashed line is an average of measurements at the different inclinations, and is seen similar to what would be expected theoretical. The variation of each sample for each inclination step is larger than the inclination effect itself; therefore further testing should be carried out, as more data would be required to draw any conclusions. But from the presented result, indications of the tensile strength anisotropy may be estimated.

7.5 Patchy Weakness model

7.5.1 Sensitivity

The Patchy Weakness model described in 3.2.1.3 is applied to measured data in this thesis. Before calculations were performed a sensitivity study of the model was carried out. Pierre parameters were used, as Mancos has already been modelled in several papers (Fjær and Nes 2013), (Fjær and Nes 2014) and (Fjær, Stenebråten, et al. 2014). The sensitivity analysis is presented throughout Figure 6-3 to Figure 6-5. Table 6-2 presents the initial input used as a standard for the sensitivity analysis. Cohesion, S_0, was estimated from the punch results as average, and cohesion for the weak planes was set to 50% of the initial value in this example. Friction angle, φ, was found from CWT correlations from equations in section 4.2.2.2. Friction angle for the weak planes were set to 85% of the initial value.

From the figures and also the initial equation regarding the patchy weakness model, initial cohesion and friction angle determines the limit of the maximum and minimum values in the model. In Figure 6-3 and Figure 6-4, η, the patchiness parameter is set to zero. The only thing changing as a function of S_{0w} and φ_w is the intersection points for the model along the planes and outside the planes. In Figure 6-3, the start of the characteristically minimum dip of the sample expands to the left (against inclination 0°) for decreasing friction angles. While in Figure 6-4 the weak plane cohesion affects the gap, or limits of the model.

The free parameter η, is somewhere between 0 and 1. And the effect of this is seen in Figure 6-5. UCS decreases with increasing η. This is to be expected as number of weak patches weakens the sample.

7.5.2 Pierre modelling

In the previous example, cohesion for the weak planes was set to a value of 50% of the initial value. By interpretation of the Punch results, both the “intrinsic” cohesion and the “weak” cohesion may be estimated. Within the tested sample in the puncher, it is assumed two symmetrical fractures with an angle ψ, according to Figure 4-15.

For an angle 180° this means a splitting of the sample. By using the equations presented in 4.2.2.3, x is a function of the angle ψ. How x varies with this angle is seen in Figure 6-7. For the case where x=0, $\sigma_{90} = \sigma_i$. As σ_{wp} is a function of x, at 60° σ_{wp} is zero. The fracture angle ψ, is therefore somewhere between 60° and 180°. This is shown in Figure 6-6.

Initial values are taken from Puncher Results presented in 5-11. Maximum cohesion or intrinsic cohesion at 0°, $\sigma_i = 2.75MPa$. Minimum cohesion, for the weak layers at 90°, $\sigma_{90} = 1.83MPa$. Friction angles are assumed from the CWT correlation in 4.2.2.2. Figure 6-8 shows the estimated UCS after the patchy weakness model (note that n=0), for the variations of ψ. Interpretation of the model may indicate that a ψ between 90° and 120° is sufficient, with corresponding x values of respectively 0.5 and 0.67. For $\eta = 0$, a minimum is seen around inclination 55°. With the limits of the characteristically dip at ~30° and ~80°. Assuming that η is small this interpretation may in fact be a respectable estimation of UCS variation with inclination for Pierre shale.

7.5.3 UCS test results for Pierre

In Figure 5-17 results from standard UCS testing are presented. Data are reproduced from SINTEF Petroleum after Erling Fjær. When first looking at the data, abnormalities may be spotted. At 0° inclination, two data points are off what would be expected. These are marked by red squares. By neglecting these points and averaging the measurement for each inclination step measured, a trend may be spotted (Figure 7-9). Results are scattered and may look inconsistent. This can be explained by tests are performed on relatively small samples. The black dashed line is the average.

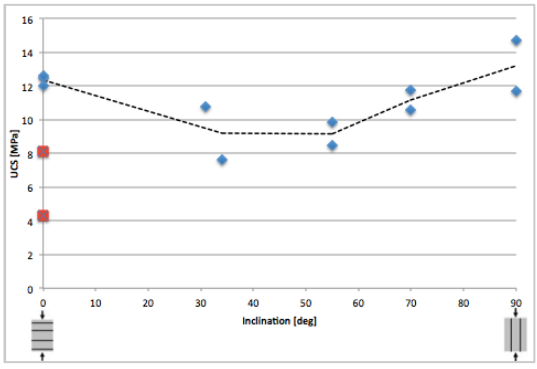

Figure 7-9 Pierre standard UCS data, remodelled and averaged.

By comparing the actual measured data with the modelled results in Figure 6-8 it is clear that the measured UCS is over the limits of the model. The assumption that the shale puncher results are estimated to low are therefore enhanced. This may be due to several reasons in combination. In section 7.2.4 it is explained that the punch results are sensitive to the geometry of the fracturing and punch pistons. Also estimated Pierre cohesion in (Stenebråten, et al. 2008) concluded with a higher cohesion than presented both in this thesis and in (Rademakers 2010). The measured punch results may therefore be within the range of acceptable values, but the interpretation concerning calculation of cohesion weakening the actual estimates.

Another reason why the results show a lower value may be due to the wettability in the samples. If the samples where not fully saturated when punched, micro-fractures or flaws within the samples may lead to lower strength. This may be expected as the samples are very small and dries out fast, and shale may exhibit irreversible property change due to evaporation. The same problem is assumed when testing in the CWT. Lower values are recorded if the sample is not 100% saturated. The degree of change is proportional with the size, meaning that smaller samples would exhibit a greater difference in measurements due to wettability change (Nes, et al. 1996). Considering the friction angle in this thesis is determined from the CWT measurements, this estimation may be to low. An increase in friction angle would increase the corresponding UCS estimation in the patchy weakness model.

In Figure 6-9 the patchy weakness model are fitted to the UCS measurements. In the presented figure an increase in estimated cohesion of 70% and a patchiness parameter of $\eta = 0.2$ is applied. The model fits well with the datapoints when neglected the two lowest points at 0° inclination.

7.6 UCS Comparison

In order to fully understand the effect of UCS measurement calculated from the test results, it is important to understand how the different tests and correlations would yield maximum and minimum readings for different inclinations for UCS estimates. Based on the theoretical background presented for each of the tests, and discussion of results, theoretical expectations are presented for each of the tests from Figure 7-10 to Figure 7-14. (Fjær 2015). The corresponding inclination definition and applied direction of measurement is indicated by the black arrows. Actual size of the dip, or depth of the minimum dip is not of great importance as this is a general presentation of what to expect from the measurements performed, and at which areas of inclinations a maximum and minimum value is seen. This section will also discuss what information of strength as a function of inclination may be obtained.

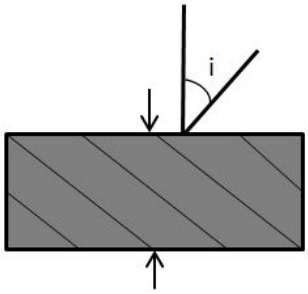

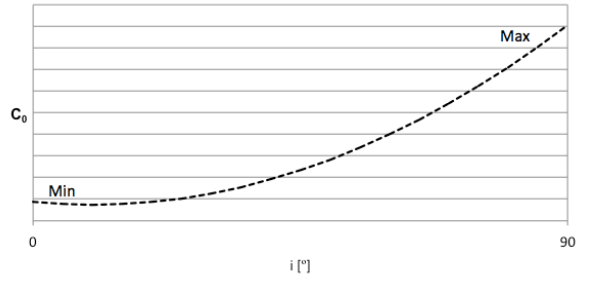

Figure 7-10 CWT expected trend with corresponding inclination definition.

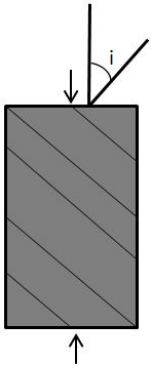

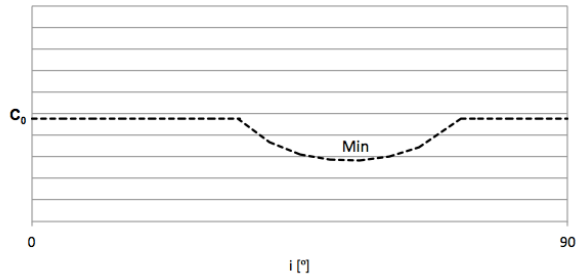

Figure 7-11 UCS expected trend with corresponding inclination definition.

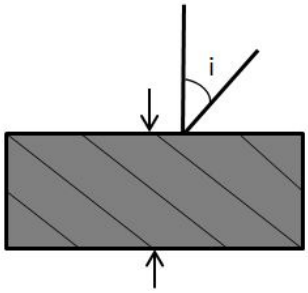

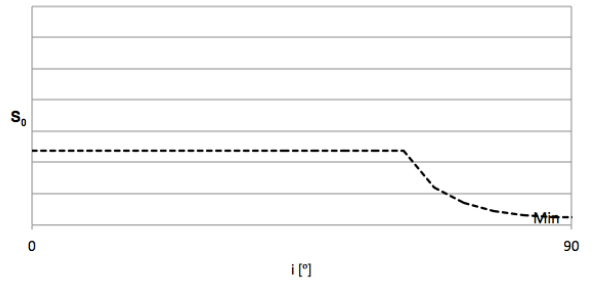

Figure 7-12 Punch test expected trend with corresponding inclination definition.

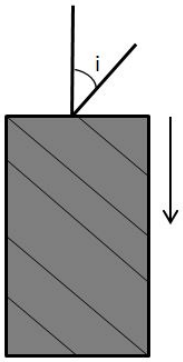

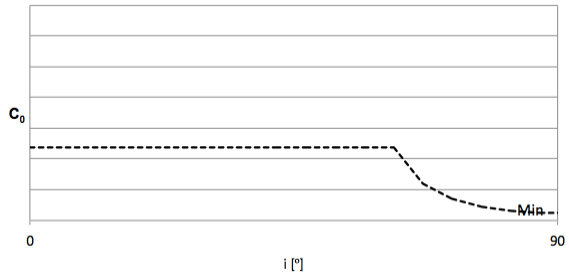

Figure 7-13 Scratch test expected trend with corresponding inclination definition.

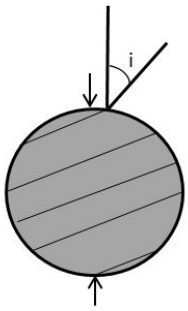

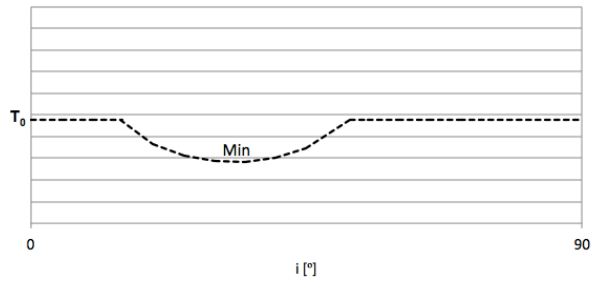

Figure 7-14 Brazilian test expected trend with corresponding inclination definition.

UCS estimates calculated by use of the CWT correlation presented in 4.1.4 is shown for Pierre and Mancos in Figure 6-1 and Figure 6-2. Expected trend illustrated in Figure 7-10 is clearly present. The inclination effect reflects the faster layers for the maximum value in the CWT correlation as explained in 7.1.3. The test itself may

therefore only provide information of maximum and minimum readings, and not describe strength as a function of inclination. Due to this inclination effect data should be considered as a general estimation for the rock, or formation. Using the average value independent of inclination gives a solid UCS estimation.

Mancos UCS results from standard uniaxial test are presented in Figure 5-16. Data show a great tendency of the expected trend in Figure 7-11. With a minimum around 55°. The limits of the characteristically dip is larger in the measured results than the one theoretical expected. This is explained by the patchiness parameter η. Weak patches along the planes are present and weaken the rock. This correlate well with compared data in Figure 3-14 where $\eta = 0.26$. This was first presented in (Fjær and Nes 2013). Standard UCS measurements for Pierre is presented in Figure 5-17. Looking at the average values discussed in section 7.5.3 measured results compare well with the other estimated results. UCS tests may be one of the best tests to provide information of strength as a function of inclination. This is clearly reflected in results both for Mancos and to some degree in Pierre. Thereby providing information concerninng at what inclination minimum reading is seen, and maximum and minimum readings.

As explained in 7.5.2, estimating UCS with use of the Punch results, the patchy weakness model is highly dependent of these results. As punch results are sensitive to heterogenic material (such as Mancos), results may not be used for all types of shale. And even if results are used it should be considered the degree of scattering of data. For the Pierre case, a trend as expected is the case. The difference between measurements at 0° and 90° might seem small, but Pierre is also a weak shale initially. Estimated UCS according to the patchy weakness model is therefore highly dependent of results from the puncher, meaning that to low cohesion measurements would yield to low UCS estimates than a realistic case. Looking at Punch results for both Pierre and Mancos in Figure 5-11 and Figure 5-12 scattering of results are the case, and strength as a function of inclination can not be extracted. For Pierre, already mentioned a maximum and minimum reading as illustrated in Figure 7-12 can be spotted. For Mancos scattering is too strong to provide any specific information concerning maximum and minimum readings. Due to the explanation in 7.2.3 this is also expected. The Punch test is yet very valuable in terms of cohesion estimates.

UCS calculated from the scratch test presented in Figure 5-13 shows the expected tendency when only looking at data from the defined inclination in Figure 7-13. A figure with only the data in this direction is shown in Figure 7-15. It can be seen that measured data correlate well with the expected tendency. Scratch test does not provide the same range of strength as a function of inclination as seen in std. UCS testing. But maximum and minimum readings are seen. The measurements on the sample situated parallel to scratch direction (90°) gives this estimation.

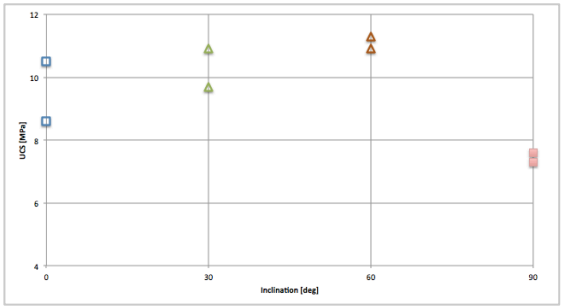

Figure 7-15 Scratch results in one direction

Data from the Brazilian test in Figure 5-15 correlate with the expected theoretical results when looking at uncoated sample results. This is also explained in 7.4. It is discussed that to some degree tensile strength as a function of inclination, similar to the std. UCS measurements can be spotted for the uncoated samples. There are still uncertainties concerning this matter, but more testing could enhance this theory.

Overall results correlate well. UCS estimations are within the same range, and it is clear that UCS estimation can be performed with use of index tests, standard uniaxial tests are necessarily not required to estimate UCS for the given rock or formation. Even the porosity correlation presented in Table 6-1 is within the range. Collecting UCS estimation from different sources, and investigate the degree of correlation strengthens the use of index testing. A direct strength measurement, which presents a full spectre of strength as a function of inclination is preferable. But as seen above, index tests provide information of maximum and minimum readings. This data can be used in conjunction with each other to provide estimates of the full description. This can be obtained by for example use of punch, CWT and patchy weakness model.

Two plots are presented with only the maximum and minimum reading for each measurement to compare data. Pierre is presented in Figure 7-16 and Mancos is presented in Figure 7-17. For Pierre it is clear that data correlate well for all the measurements. The CU test (from conversation with Idar Larsen at SINTEF Petroleum) and std. UCS test results represents the highest values. While patchy weakness model with data from the puncher represent the lowest. With the explanation of the low measurements in punch from 7.5.3 this is expected. In this case UCS estimates by use of index testing would give a solid estimation for further use.

For Mancos in Figure 7-17 results are more scattered. The maximum readings from std. UCS testing and patchy weakness model presented in (Fjær and Nes 2013) are a lot higher than other measured data presented in this thesis. These maximum readings are performed on another block of rock than in this thesis, and may be one of the reasons of the difference. Also considering the heterogeneity in mancos and the wettability effect explained in 7.5.3 may impact the test results from the index tests. Otherwise results fits well, and a respectable estimation of UCS is the case.

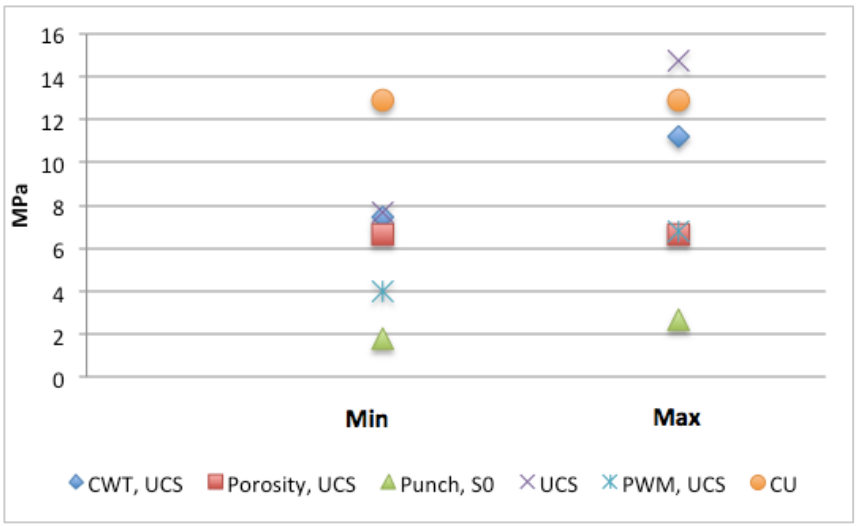

Figure 7-16 Collection of maximum and minimum results for Pierre

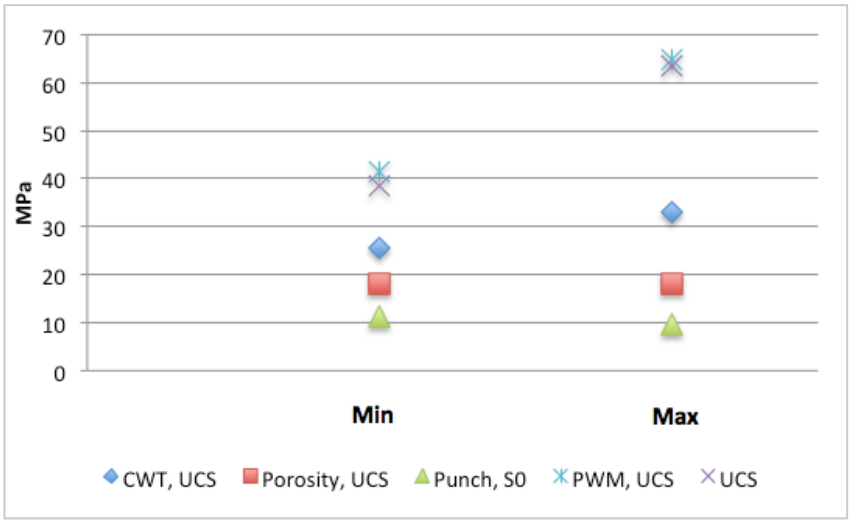

Figure 7-17 Collection of maximum and minimum results for Mancos

7.7 Determining strength anisotropy and heterogeneity

It has previously been discussed how the inclination affects the measurements, and what would be expected due to theoretical explanations. By use of the results from the index tests strength anisotropy may be estimated. This subchapter will discuss in what degree each test can provide information about this matter.

CWT is as explained very much affected by the inclination effect. Thus, it may be of interest concerning heterogeneity. Scattering of CWT results may be used as an indication, to determine the degree of heterogeneity.

The Punch test is as explained sensitive to local heterogeneity in samples. By investigating the scattering of data information about degree of heterogeneity may be determined. This correlates well with the results seen for Pierre and Mancos, where degree of scattering is larger for Mancos than Pierre.

Standard UCS testing may provide information about the strength anisotropy in a rock due to inclination. UCS results presented for Mancos in Figure 5-16 is clearly affected by inclination. The same test results for Pierre in Figure 5-17 is affected by inclination, but in a lower degree. Thus, getting a respectable measurement on strength anisotropy from std. UCS testing requires a lot of samples. Difference in maximum and minimum, respectively for Mancos and Pierre from the presented results are $\approx 20Mpa$ and $\approx 6Mpa$.

Determining strength anisotropy from Brazilian testing with respect to tensile strength might be possible from the results from Figure 5-15. A weak trend is the case, and an estimated value can be determined. A reliable measurement on strength anisotropy requires sensitive equipment and test results. The fact is that the Brazilian test is a very complex test regarding stress distribution in the sample. Strength anisotropy may therefore be difficult to estimate from this test.

The scratch test is in this thesis is investigated for several directions, and the application area of this test is extended. The major result from the test result is seen for the sample with 90° inclination, where scratching is performed both parallel to

bedding and across bedding lengthwise. All scratch results are well within the limits of the other measurements in Figure 7-16. A difference in maximum and minimum value of 6MPa is observed. By comparing this data to other test results in Figure 7-16 this value correlate well with the std. UCS measurements. This may indicate that estimation of strength anisotropy from the scratch test can be determined by testing only one sample plug at 90°. More testing should be performed to strengthen this theory, and the original plan of scratching Mancos in the same directions would provide more information. Results from the scratch test are promising as they correlate with the expected theoretical trend, other measured results and maximum/minimum values.

8 Further Work

As this thesis contains information from several tests, some further work on UCS testing should be done to finalize the comparison. UCS measurements are a valuable source of information as it provides data as a function of inclination. Std. UCS test on properly sized samples should be performed on Pierre to have a better reference to compare to other data. This already exists for Mancos, and is extremely valuable both concerning mathematical modelling and index testing. With the same data for Pierre, a more reliable comparison is the case and other results would be enhanced.

The unique finding in the scratch test should also be tested for more rock material to see how this correlate. Even though results are promising, more data are needed to strengthen the explained theory of strength anisotropy from the Scratch device. A start would be to perform this test on Mancos, which was the original plan before the device broke down. If a specific shale has previously been tested for UCS or other tests, only one sample, parallel to bedding is needed to investigate strength anisotropy. Therefore a lot of information is easily accessible for someone with the access to different shale material.

The new test technique explained in 4.5 could be further researched. Both conversations with Anna Stroiz and Alexandre Lavrov indicated interest of a study on this. The test technique represents valuable information concerning strength anisotropy and questions related to contact surface. It would also increase knowledge about the complexity in a Brazilian test.

9 Conclusion

Confirmed and discovered findings for each index test is shortly listed bellow:

CWT Results

- Applied sample preparation technique suitable.
- Consistent and comparable results, with respect to previous published results.
- Results are independent of sample thickness.
- Measurements are sensitive to local heterogeneity and wettability factors.
- Highly affected by sample inclination, due to faster and slower layers reflect the actual measured P-wave velocity.
- Provide information about maximum and minimum readings.

Shale Puncher

- Confirming previous findings, results are independent of sample thickness.
- Shear strength do not seem to increase with increasing velocities, as inclination effect is strong in CWT measurements.
- Results may be used to estimate UCS from mathematical models. Fits well in the Pierre case.
- Results used in conjunction with CWT and patchy weakness model may describe full description of strength as a function of inclination.
- Giving valuable information from samples where inclination is unknown, e.g. cuttings and cavings.
- Sensitive to sample heterogeneity, wettability and fracture geometry.

Scratch test

- Respectable UCS estimates, correlating with other measurements and published results.
- Direct and continuous rock measurements.
- May be the strongest test result to determine strength anisotropy. Easily performed on a core drilled parallel to bedding (90°), scratching along and across bedding (maximum and minimum measurements).
- Larger area of application than previously identified.

Brazilian Test

- Solid estimation of tensile strength, as expected.
- Complexity of the test makes it difficult to determine strength anisotropy, but a trend may be spotted for uncoated samples, providing a full description of strength as a function of inclination.
- Measurements affected by sample preparation, where coated (sprayed or oil coated) yield a higher tensile strength than uncoated samples, may be due to coating suppress existing flaws in the sample.

From comparison of results, and sensitivity analysis it is clear that Mancos is much more heterogenic than Pierre. All presented Pierre results correlate well, while Mancos is more scattered; yet Mancos results are of great interests as expected tendency of results explains difficulties in measurements. In both Pierre and Mancos case the estimated cohesion seems to low when looking at modeled results in the patchy weakness model. This may be due to sample wettability change and geometrical difficulties. Compared UCS data for Pierre fits well for both obtained and previous results. While for Mancos a difference is seen for previous results compared to new data presented. This difference is not extreme, and new results still possess important value. Explanations may be different tested rock and heterogeneity and wettability impact on index test measurements.

The unique strength anisotropy results from the scratch test are promising as an actual value may be determined, and results are confirmed by both UCS and other index test maximum and minimum measurements. More testing should be carried out to enhance this finding. By use of information in conjunction with several index tests, a full description of strength as a function of inclination may be provided.

Results form index tests are promising, and may in fact replace some of the conventional laboratory tests. The same information can be obtained cheaper, faster and easier by use of Index testing.

10 Works Cited

Bøe, Reidar. *Mineralogical and petrophysical charaterization of Pierre 1 shale.* Trondheim: SINTEF Petroleum Research, 2005.

Broadhead, Ron. *San Juan Basin Energy Conference.* New Mexico Bureau of Geology and Mineral Resources. 3 2013. https://geoinfo.nmt.edu/staff/broadhead/documents/MancosShaleslideset.pdf (accessed 03.2014).

Claesson, J, and B Bohloli. "Brazilian test: stress field and tensile strength of anisotropic rocks using an analytical solution." *International Journal of Rock Mechanics and Mining Sciences*, 2002.

Fjær, Erling "Personal communication: Theoretical expectations discussion" May 2015.

Fjær, E, R.M Holt, P Horsrud, A.M Raaen, and R Risnes. *Petroleum Related Rock Mechanics.* 2nd Edition. Elsevier B.V, 2008.

Fjær, Erling, and Olav Magnar Nes. *Strength anisotropy of Mancos shale.* ARMA 13-519, 2013.

Fjær, Erling, and Olav Magnar Nes. *The impact of Heterogeneity on the Anisotropic Strength of an Outcrop Shale.* Springer, RMRE 47:1603-1611, 2014.

Fjær, Erling, Jørn F Stenebråten, Rune M Holt, Andreas Bauer, Per Horsrud, and Olav Magnar Nes. *Modeling strength anisotropy.* ISRM, 2014.

Holt, R. M., E. F. Sønstebø, and P. Horsrud. "acoustic Velocities of North Sea Shales." 1996.

Horsrud, Per. "Estimating Mechanical Properties of Shale From Emperical Correlations." Sci. Paper, 2001.

Larsen, I. "Personal communication: CU Test result Pierre from SINTEF Petroleum AS", April 2015.

Khan, Safdar, Sajjad Ansari, Hongue Han, and Nader Khosravi. *Understanding Shale Heterogeneity - Key to Minimizing Drilling Problems in Horn River Basin.* SPE, IADC/SPE 151752, 2012.

Nes, O.-M, et al. *Rig-site and Laboratory use of CWT Acoustic Velocity Measurements on Cuttings.* Sci. paper, SPE 36854, 1996.

Rademakers, Frederik. "Shale punching and acoustic wave velocity measurements for the evaluation of fluid exposure effects on small shale samples." 2010.

Ringstad, C, E.B Lofthus, E.F Sønstebø, and E Fjær. *Prediction of Rock Parameters from Micro-Indentation Measurements: The Effect of Sample Size.* Sci. paper, SPE/ISRM 47313, 1998.

Rugland, T.A. *Index Testing, A study of the effect of inclination in relation to bedding on rock mechanical parameters.* NTNU, 2014.

Schei, G, E Fjær, E Detournay, C.J Kenter, G.F Fuh, and F Zausa. *The Scratch Test: An Attractive Technique for Determining Strength and Elastic Properties of Sedimentary Rocks.* Sci. paper, SPE 63255, 2000.

Schlumberger Oilfield Glossary.
http://www.glossary.oilfield.slb.com/en/Terms.aspx?LookIn=term%20name&filter=Young's%20modulus (accessed November 10, 2014).

Schultz, L.G, A Harry, J.R Tourtelot, Gill, and J.G Boerngen. *Composition and properties of the Pierre shale and equivalent rocks, northern great plains region.* 1980. http://pubs.usgs.gov/pp/1064b/report.pdf (accessed 12 2014).

Simpson, N.D.J, A Stroisz, A Bauer, A Vervoort, and R.M Holt. *Failure Mechanics of Anisotropic Shale during Brazilian Tests.* ARMA 14-7399, 2014.

SINTEFPetroleum. "Orientation." 2014.

SINTEF Petroleum, Erling Fjær. *UCS Pierre data*, 2015

Skalle, Pål. *Drilling Fluid Engineering.* 5th Edition. Bookboon, 2014.

Stenebråten, J.F, E Fjær, S Haaland, A.V Lavrov, and E.F Sønstebø. *The shale puncher - a compact tool for fast testing of small shale samples.* Sci. paper, ARMA 08-227, 2008.

TerraTek. "TerraPROFILE Operations Manual ." 2005.

The James Hutton Institute. 2006. http://www.claysandminerals.com/materials/shales.

Torsæter, M, O.M Nes, and J Rinna. "Nanostructure vs Macroscopic Properties of Mancos Shale." SPE 162737, 2012.